EXPERIMENTAL INVESTIGATION OF THE HYDRO-MECHANICAL EFFECTS OF HEATING ON KAOLIN AND MICROPLASTIC CONTAMINATION USING GEOPHYSICAL METHODS

A Thesis

Presented to

The Faculty of the Department of Civil Engineering

California State University, Los Angeles

In Partial Fulfillment

of the Requirements for the Degree

Master of Science

in

Civil Engineering

By

Elizabeth Rosario Nunez

May 2025

© 2025

Elizabeth Rosario Nunez

ALL RIGHTS RESERVED

The thesis of Elizabeth Rosario Nunez is approved.

Professor Wing Shun Kwan, Committee Chair

Professor Idil Akin (University of California, Los Angeles), Committee Member

Professor Mark Tufenkjian, Committee Member

Professor Joseph Lucey, Committee Member

Professor Yixian Wang, Committee Member

Professor Gustavo Menezes, Department Chair

California State University, Los Angeles

May 2025

TABLE OF CONTENTS

ABSTRACT

Experimental Investigation of the Hydro-Mechanical Effects of Heating on Kaolin and Microplastic Contamination Using Geophysical Methods

By

Elizabeth Rosario Nunez

This research utilizes two geophysical methods, a bender element and an electrical resistivity meter, to study the mechanical and hydraulic behavior of Kaolin clay under the combined influence of heat and microplastic contamination. As extreme heat waves become more frequent due to global warming, and microplastics emerge as a growing environmental concern, it is essential to understand how these factors alter the stiffness and hydraulic conductivity of soil. Reconstituted pure Kaolin and Kaolin mixed with microplastics were heated to 60 °C in a controlled laboratory setting. The bender element and resistivity meter were used to determine the maximum shear modulus (G_{max}) and electrical resistivity (ρ), respectively. These non-destructive tools enabled real-time measurements of a single sample at various temperatures (20–60 °C). Results show that heat exposure alone reduced both G_{max} and electrical resistivity in Kaolin samples. When only microplastics were added, G_{max} also decreased, while electrical resistivity increased—likely due to the non-conductive nature of microplastics affecting current flow. Because electrical resistivity is material-dependent, pure and microplastic-mixed samples cannot be directly compared. When both heat and microplastics were present, G_{max} decreased and resistivity increased. Lower stiffness may lead to greater surface soil detachment, potentially affecting slope stability and erosion; and decreased hydraulic conductivity may hinder groundwater recharge, potentially stressing water resources in

areas vulnerable to climate change such as Southern California. This study demonstrates how geophysical testing in laboratories can reveal early-stage changes in soil behavior caused by emerging environmental stressors.

ACKNOWLEDGMENTS

I would first like to thank Dr. Kwan for all the guidance and support he has given me throughout these years. If he had not asked me to join the Geotech Research Team back in 2020, I would not be where I am today and I will forever be grateful. I am very fortunate to have had Dr. Kwan as an advisor but especially as a professor. I would also like to thank my thesis committee for their support and valuable insight they have given me for this research. Their presence at my thesis defense meant a lot to me. I want to give gratitude to the Geotech Research Team for their support, help, and for being such a great group of people. I wish them continued success for their futures. I would also not be where I am today without my family and loved ones. Their support and unconditional love have pushed me to be the best version of myself I can possibly be. I would like to thank my significant other for his support and for being by my side along the way. I especially cannot thank my parents and Godparents enough for all their sacrifices and for always being there for me when I needed them. I am grateful to have them in my life and for them to be able to see what I have accomplished throughout these years. Los amo mucho.

Lastly, I would like to dedicate my thesis to all four of my grandparents who I lost during my academic journey: Jose Matuz, Esperanza Tejeda, Jesus Nunez, and Rosario Nunez. I hope to have made them proud.

This work has been supported by the NSF grant: CREST Center for Advancement towards Sustainable Urban Systems at California State University, Los Angeles (Award No. HRD-2112554).

LIST OF TABLES

Table

LIST OF FIGURES

Figure

CHAPTER 1

Introduction

Heat waves are a frequent occurrence in California and are becoming more common due to the extreme weather conditions driven by climate change. Temperatures can reach up to 109 degrees Fahrenheit (~43 ˚C) in Southern California (NOAA 2024). In some deserts, such as Death Valley, the ground can reach temperatures as high as 160°F (~70 ˚C) (National Park Service n.d.). At the same time, microplastic pollution continues to rise as the production of polymer-based products accelerates. This research paper explores how heat and microplastic contamination independently and simultaneously affect the hydraulic conductivity and soil strength of Kaolin clay by using geophysical methods. Additionally, the effects of heat and microplastic contamination are also studied simultaneously to see how the hydraulic conductivity and soil strength change to showcase a scenario of a heatwave taking place in a high microplastic-polluted area. These results provide insight into soil detachment and ground water recharge when soils experience heat and microplastic contamination.

This Master's thesis is organized into nine chapters, beginning with an Introduction (Chapter 1) that outlines the motivation, objectives, and scope of the study, followed by a Background chapter (Chapter 2) that reviews relevant literature and sets the scientific context. The Testing Program (Chapter 3) is detailed in four sub-sections, covering the materials used, sample preparation procedures, equipment, and experimental setup, providing a comprehensive overview of the methodology employed in the research.

Subsequent chapters present and analyze the experimental findings. Chapter 4 focuses on data collection procedures, while Chapters 5 through 7 explore the effects of heat, mechanical pressure (MP), and their combined influence on kaolin clay, respectively. Chapter 8 investigates the behavior of G_{max} (shear modulus) versus normalized water content in both heated and controlled conditions, emphasizing the role of enclosed testing environments. The thesis concludes with Chapter 9, summarizing key findings and offering recommendations for future work.

CHAPTER 2

Background

Geophysics is the study of the Earth's subsurface that utilizes non-invasive methods that can characterize it without having to disturb the soil. The growing use of geophysical techniques is driven by their ability to provide fast, cost-effective alternatives for field investigations, potentially saving time and resources in the future, making it one of the key aspects of this research. This research utilizes two geophysical methods: bender element and resistance meter. Which allows for finding the shear modulus (G_{max}) and electrical resistivity (ρ) respectively of reconstituted Kaolin clay samples.

The second key aspect of this research is heat. Heatwaves are a natural and inevitable phenomenon that will continue to occur in the future due to global warming. Heat can potentially alter the soil's chemical and physical properties, putting infrastructure and lives at risk.

The third key aspect is microplastic contamination. Due to the high production rate of plastics and their slow degradation, microplastics are increasingly being introduced into soils (Ng and Obbard, 2006). There has been previous research that has investigated detention and extraction techniques for microplastics, however there is still not a finite solution for a removal process (Fan et. al, 2023). The presence of microplastics can potentially change the soil's porosity, ultimately affecting water infiltration rate and cohesiveness, and with the combination of wildfires, the microplastics will be burned and broken down, potentially damaging the soil's integrity even further. Understanding how heat and microplastic contamination affect soil strength

is crucial for applications such as slope stability and groundwater recharge after the event of a wildfire.

From my knowledge and at the time of writing this Thesis, there have been limited studies that have used geophysical methods with the combination of heat and microplastic contamination. However, there have been past research who have explored the effect of heat and microplastic contamination independently. For instance, Doerr et al. (2004) heated field-sampled soft soils, from an Australian eucalypt forest, in a furnace before testing them using the water drop penetration method. Temperatures ranged from 250˚C to 400˚C, resulting that heated samples had an increase in water repellency in comparison to samples that were not heated. Additionally, Jaradat and Abdelaziz have tested remolded EPK samples by using a heated triaxial cell. Two samples were sheared at 0.5 %/hr, however, for one of the samples, prior to shearing, it was heated to 70 degrees Celsius and cooled to 10 degrees Celsius before returning to 20 degrees. Results showed that the sample that was induced with heating and cooling showed a lower shear strength compared to the controlled sample.

The effects of microplastics have also been looked upon; Dike and Apte (2024) have researched how Low-Density Polyethylene (LPD), High-Density Polyethylene (HDPE), and Polyvinyl Chloride (PVC) affect the parameters of clayey soil, sandy soil, and silty soil. Various concentrations of MPs, ranging from 2-6% by weight, were manually added to the different soil types and were tested om multiple days for various parameters. As a result, the higher the concentration of MPs were added to the soil, the soil's ability to retain water decreases causing the water content to decrease at a faster

rate in comparison to soils without MP contamination. It was also observed that in all soil types and all levels of MPs, there was an overall decrease in the soil's shear strength.

CHAPTER 3

Testing Program

3.1 Materials

This study focuses on Kaolinite Clay from R.T. Vanderbitt Holding Company, Inc. and is in the CH group for USCS. In general, Kaolin particles have a size of 0.2 to 210 μm, Liquid Limit (LL) range of 30 to 110, and Plastic Limit (PL) range of 25 to 40 (Kam et al. 2020). The microplastics used for contamination are Ultrafine Polyethylene Terephthalate from NANOCHEMAZONE, with particle size ranging from 1-5 micrometers. Figure 1 shows the product information of the microplastics used for contamination. Figure 2 showcases the microplastics at a naked-eye view and at a microscopic view, which was taken by the Keyence VHX-7000 4K High Accuracy Digital Microscope at Cal State LA. Figure 3 shows the Kaolin clay used for the samples along with a microscopic view. Table 1 summarizes the LL and PL values that were measured from a previous study (Kwan et al. 2019) on the same Kaolin used.

Figure 1: Product Information for Ultrafine Polyethylene Terephthalate

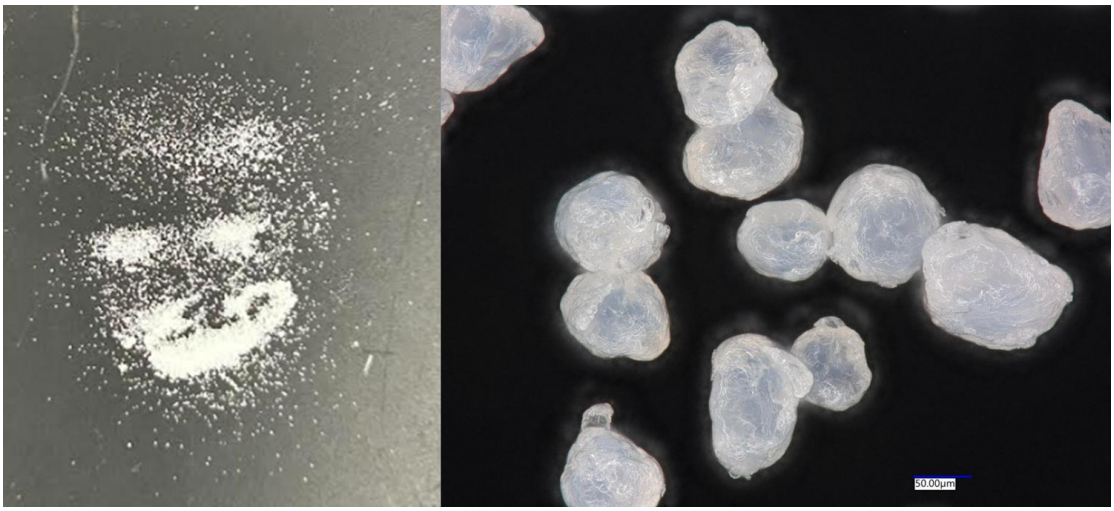

Figure 2: Ultrafine Polyethylene Terephthalate

Table 1: Kaolinite Characteristics (Kwan et al. 2019)

LL	**PL**
60	25-30

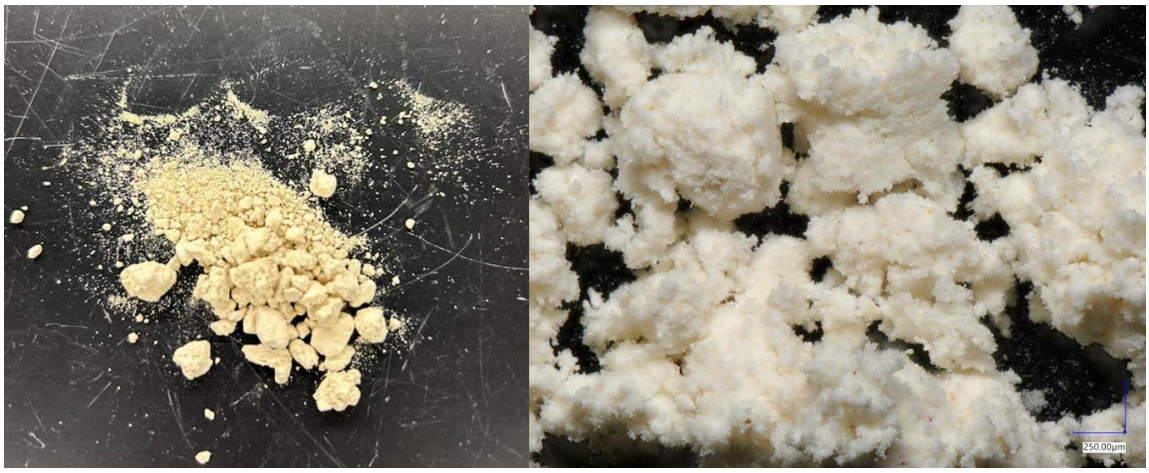

Figure 3: Kaolin Clay

3.2 Sample Preparation

To create the pure clay samples, the slurry-based clay reconstitution method was used (Suzuki and Dyvik, 2017; Kam et. al. 2020). A mixture of 9 kg of Kaolin Clay and 10 kg of distilled water were mixed thoroughly with an industrial hand-held mixer as shown in Figure 4.

Figure 4: Kaolin and Distilled Water Mixter

Once the mixture was fully mixed, it was poured into a 5-gallon bucket and covered with plastic wrap before the lid was placed. The mixture was left overnight. The next day, the mixture was poured into a metal consolidation box and was consolidated in four stages: 5 kPa, 12.5 kPa, 25 kPa, and 50 kPa. To better mimic shallow surface conditions, 50 kPa was the minimum stress level required for the clay to maintain its integrity. If a lower stress level than 50 kPa was used, the sample would not have been able to hold itself together. Once the last stage of consolidation was completed, Shelby

tubes, with a height of 153mm and a diameter of 62mm were inserted into the mixture. The box was taken apart to expose the consolidated clay with the now-inserted tubes, as shown in Figure 5.

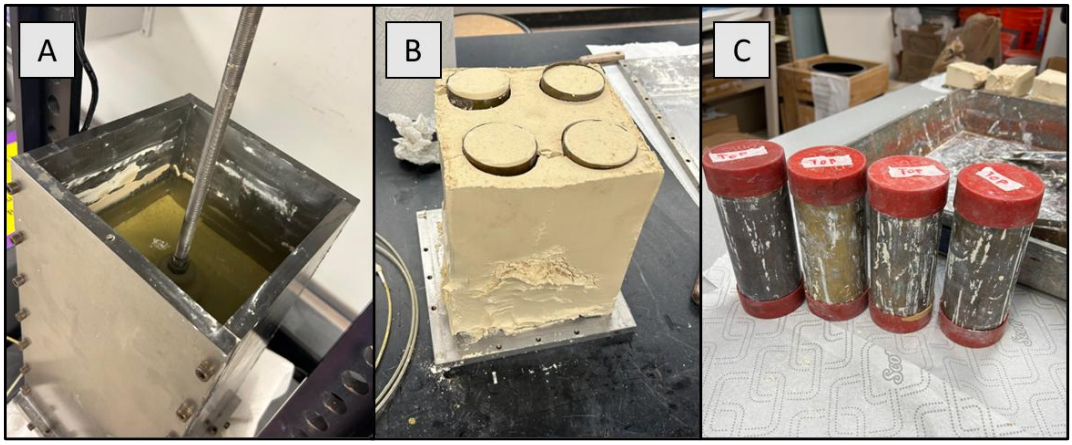

Figure 5: Process of Sample Preparation (Nunez et al. 2025)

The excess clay surrounding the Shelby tubes was carefully cut away so that the tubes could be removed, capped, and stored in a moisture-controlled environment.

For the samples containing microplastics, the same process used for the pure Kaolin samples was followed. However, to minimize the amount of microplastics required, the Shelby tubes were cut in half. This reduction in size ensured that when 10% microplastic by mass (relative to the Kaolin clay) was added, the total amount needed was significantly less compared to using full-sized Shelby tubes.

To determine the appropriate masses of Kaolin clay and distilled water, a trial-and-error approach was employed. Initially, both the Kaolin clay and distilled water masses were halved to match the reduced size of the Shelby tubes. After mixing 4.5 kg of Kaolin with 5 kg of distilled water and consolidating the mixture as previously described, it became apparent that once the halved Shelby tubes were inserted, the clay and water masses could be further reduced. The goal was to have just enough to fill the half-sized

Shelby tubes. Leading to the final masses of the clay and water were 35% of their original amount. As a result, the final mixture consisted of 3.15 kg of Kaolin clay and 3.5 kg of distilled water, combined with 315 g of microplastics. The microplastics were added and mixed the following day once the mixture was left covered with the plastic wrap and lid. This helped to reduce the amount of microplastics that sank to the bottom.

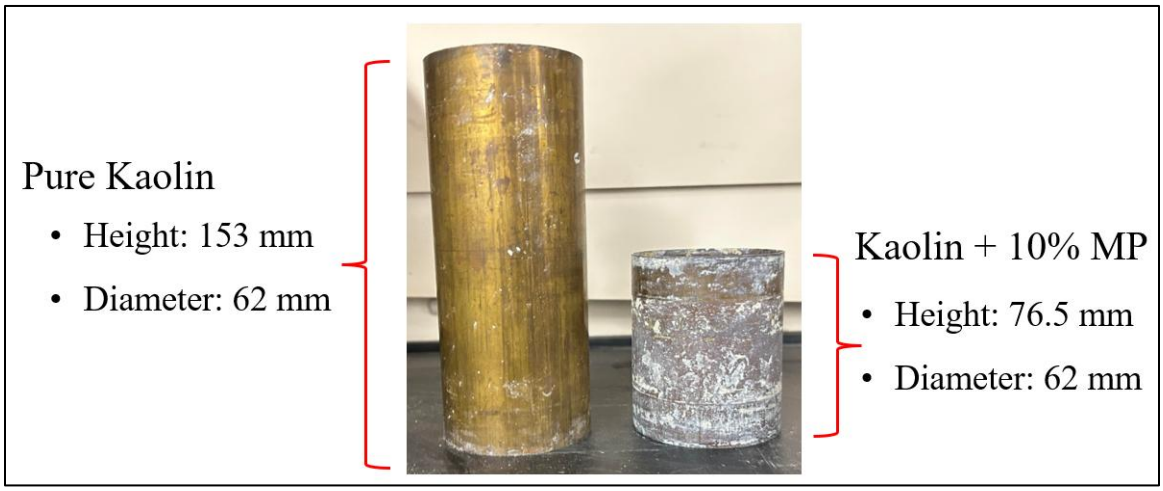

Figure 6: Dimensions of Samples

3.3 Equipment

Table 2 shows the equipment used along with the range, precision, and units of measurements.

Table 2: Equipment Precision and Measurement Capabilities

Equipment Name	Range	Precision	Unit
Resistivity Meter Miller 400A	0 to 11,000	0.1	Ω
P&S Wave Measurement System	0.1 to 50 kHz	0.01	ms
Dial Gauge	0 to 1	0.001	mm
Scale	0 to 32,000	0.1	g
Digital Thermocouple Thermometer	-50 to 300	0.1	˚C
Wagner FURNO 700 Heat Gun	125 to 1,300	10	˚F

3.3.1 Resistance Meter

Both sample types were tested using the Resistance meter box (Miller 400A from Geocomp) shown in Figure 7b for resistance and the setup can be shown in Figure 7a. The resistance meter box consists of two caps that measure resistance directly. Before any tests were conducted, the resistance meter was calibrated to ensure accurate readings. This was done by using an RS-200 resistance substitute (Figure 8). The RS-200 is connected to the input terminals of the resistance meter and is set to various specific resistances, if the resistance meter matches the specific expected value, then it is working how it is supposed to. If the reading does not match, the calibration knobs on the resistance meter are adjusted so that the reading matches the expected value. After calibration was completed, the resistance meter was ready to be used. Using the resistance measured, the electrical resistivity can be calculated with the following:

$$\rho = R \times \frac{A}{L}$$

ρ = Resistivity

R = Resistance

A = Area of sample

L = Length of sample

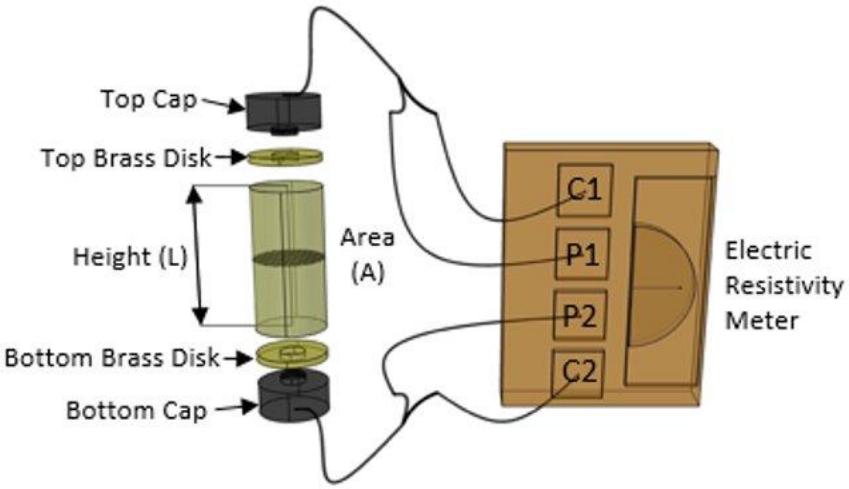

Figure 7a: Setup of Resistance Measurement Using the Electrical Resistivity Caps (Kwan et al. 2019)

Figure 7b: Miller 400 A Resistance Meter and Electrical Resistivity Caps

Figure 8: RS-200 Resistance Substituter

3.3.2 Bender Element

The bender element caps and wave generator used are from Geocomp (P&S Wave Measure System) [Geocomp, 2024]. The caps consist of 5.5 mm long protruding electrodes that are inserted into the sample where the bottom electrode produces the sine wave, and the top electrode receives the wave. The WaVeMe software from Geocomp is used to measure the travel time it took for the wave to travel to one electrode to the other as shown in Figure 10. Peak-to-peak travel time was used based on ASTM D8295-19. The software allows for the adjustment of the amplitude and frequency of the waves so that the period of the output wave matches the period of the input wave. The frequency

used for testing ranged from 2000 to 5000 Hz. The settings shown in Table 3 were utilized for all tests.

Table 3: Settings for WaVeMe Software

Parameter	**Setting**
Amplitude	100
Trigger Mode	Normal
Waveform Generator Trigger Form	Free Running
Waveform Generator Output Form	Tone Burst
Trigger Source	Manual
Trigger Cycles	
- On	1
- Off	100
- Repeat	3
Setup Mode	Logarithmic

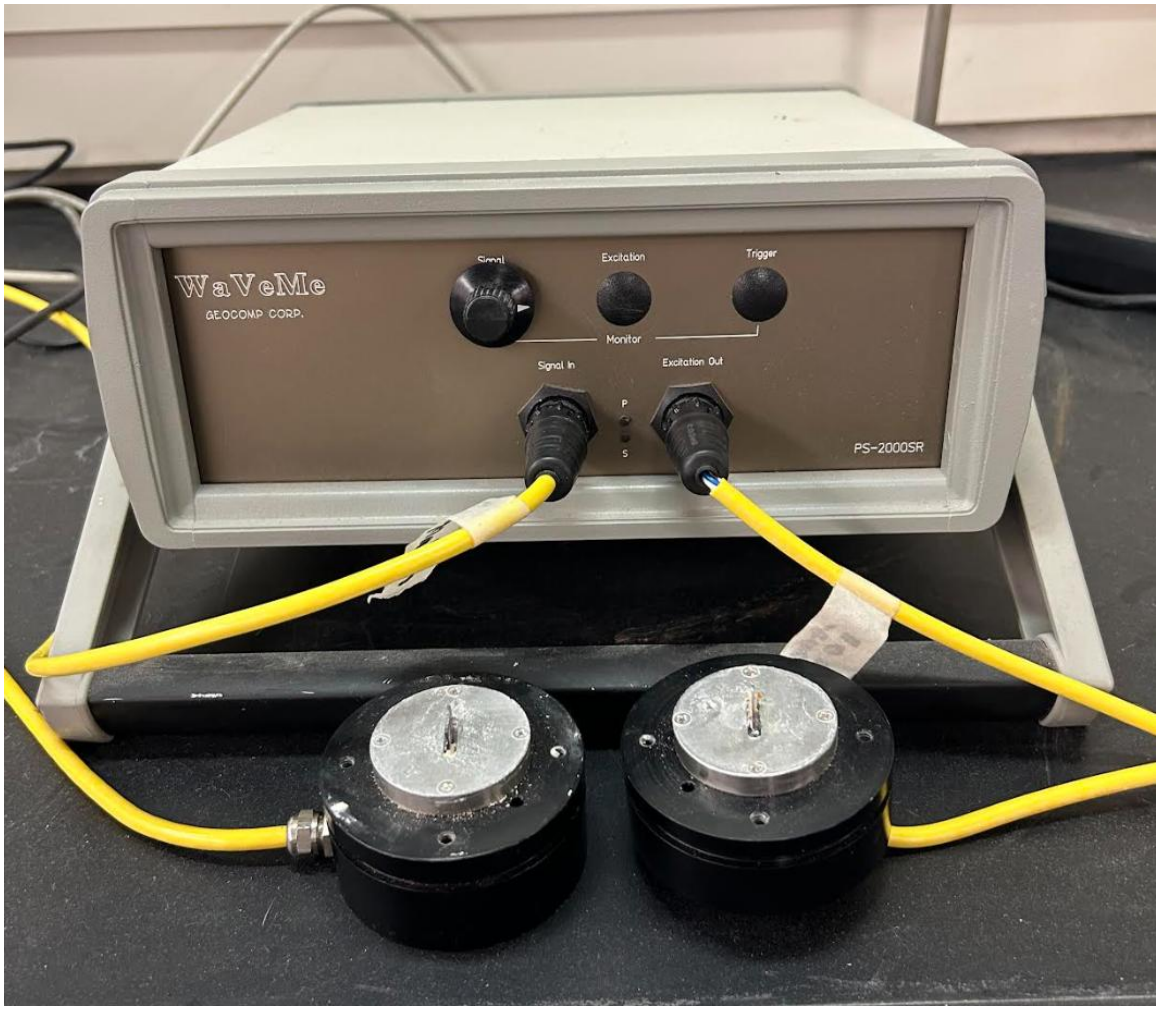

Figure 9: Wave Generator and Caps

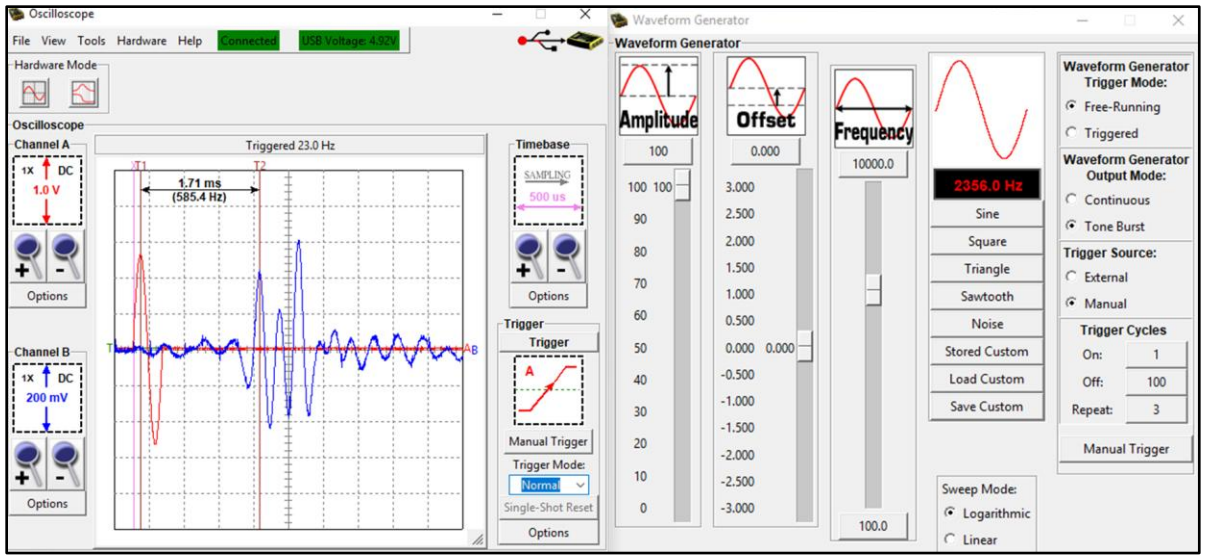

Figure 10: WaVeMe Software

The shear wave velocity was found using the following.

$$V_s = \frac{L}{\Delta t}\ , G_{max} = \rho V_s^2$$

V_s= Shear wave velocity

L = sample length

Δt= travel time

G_{max}= Shear wave velocity

ρ = density

3.3.3 Heat Gun

For this study, two heat guns were used to heat samples as they are tested using the resistance meter and bender element. The heat guns used are FURNO 700 Heat Guns from WAGNER capable of heating from 125 to 1300 degrees Fahrenheit. The portable heat guns allowed the samples to be heated in a controlled setting that was done by placing the samples in a room temperature environment and having the samples experience heat only from the heat guns. Which enabled the user to adjust the temperature as needed, making it a key component to determine if heat had any effect on the pure Kaolin and Kaolin mixed with microplastic samples.

Figure 11: Wagner FURNO 700 Heat Gun

3.3.4 Dial Gauge

A dial gauge is incorporated into the setup to keep track of the change in height as samples lose their moisture and shrink. This was essential to correct for the travel distance when calculating the shear wave velocity as mentioned in 3.3.2. Additionally, it was used to keep track of the change of height of the sample. The load from the plunger exerts a small amount of mass which was found by measuring the mass at various displacements. The results are shown in Figure 13.

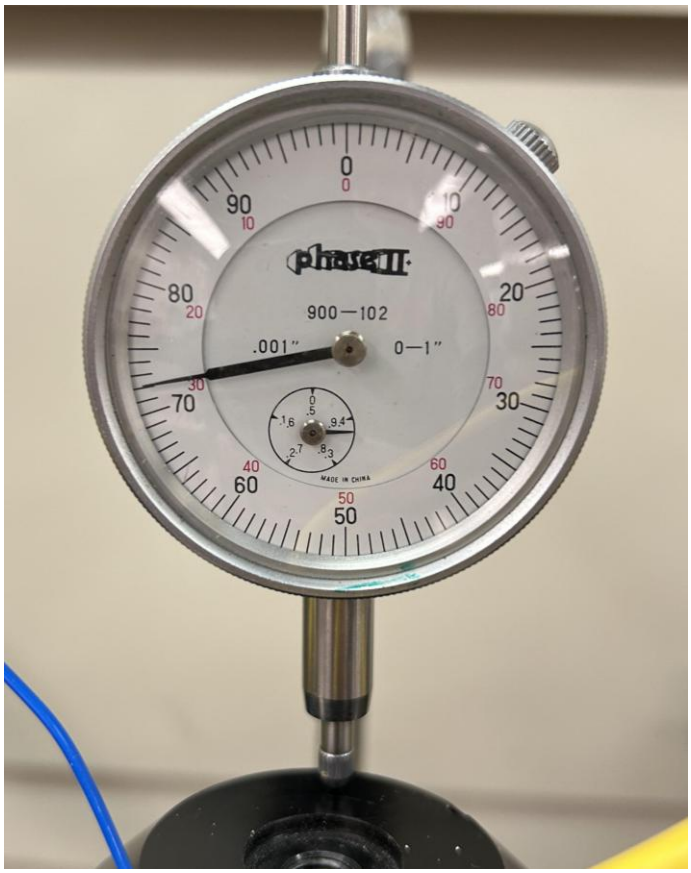

Figure 12: One-inch range Dial Gauge with a Measurement Precision of 0.001 inch.

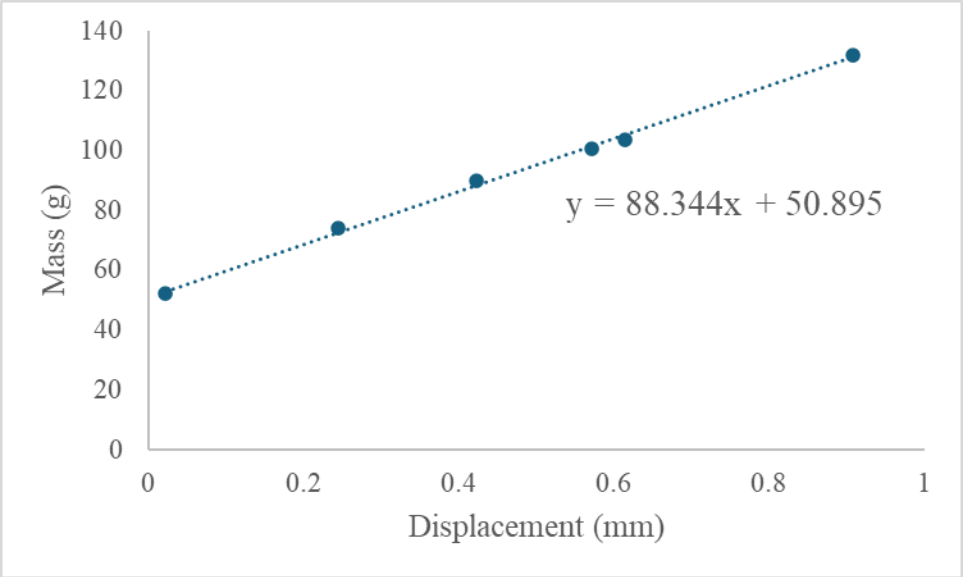

Figure 13: Mass Exerted from Dial Gauge Plunger

3.3.5 Scale

As samples lose their moisture, they don't only decrease in height but in mass as well. A scale from ExplorerPro (Figure 14) was used to keep track of the water that is being lost. This helped to calculate the water content throughout the test. At the end of each test, a final water content is taken by using the entire sample for more accurate measurement. Using the final water content, the water content at any point during the test can be found using the following:

$$WC_i = \frac{WC_{final} + \sum \Delta M - \Delta M_i}{W_s}$$

WC_i = Water content at selected time

WC_{final} = Final water content (measured at the end of test)

$\sum \Delta M$ = Total accumulated change in mass at end of test

ΔM_i= Accumulated change in mass at that point

W_s = Weight of solids

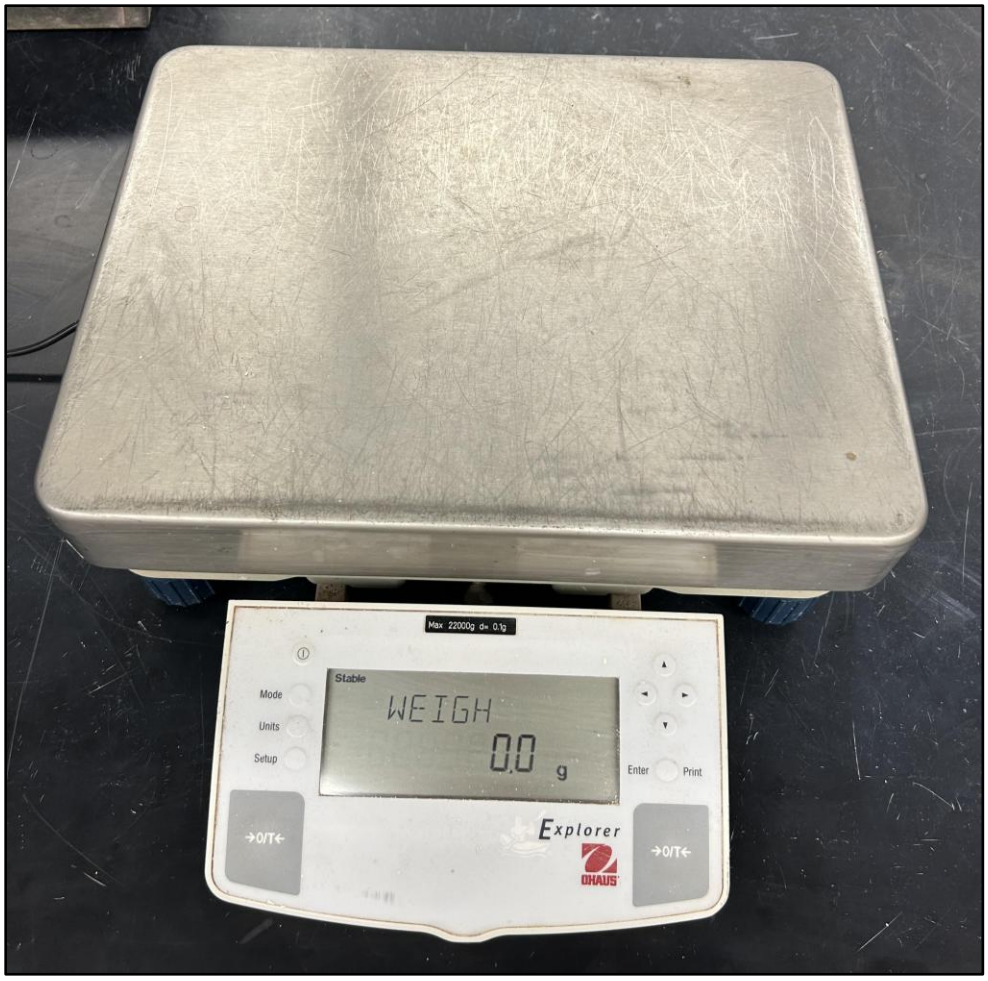

Figure 14: ExplorerPro Scale

3.3.6 Thermometer

Lastly, a digital thermocouple thermometer from G-TECH was used to keep track of the temperature inside of the samples. The thermometer consisted of thin wires that made it easy to insert to the top and bottom of the sample and is capable of reading of temperatures ranging from – 50 to 300 degrees Celsius. However, temperatures inside the samples only ranged from about 22 to 60 degrees Celsius due to the resistance and bender element caps not being heat proof. To prevent noisy and unreliable readings from the caps, temperatures had to be kept to a minimum. Through various trials, it had resulted that 60 degrees Celsius would be the maximum value to reach.

Figure 15: Digital Thermocouple Thermometer

3.4 Setup for Heated Samples

3.4.1 Resistance Meter

To understand the effects of heat, samples were heated in a controlled setting while various measurements were being taken. The setup for the heated samples tested using the resistance meter included a sample placed on the bottom cap, which rested on a supporting frame. A rod, screwed into the top cap, was held in place by the frame. The frame was placed on top of a scale to keep of any water that is being lost to back track the water content from the final water content measurement.

Due to the flat contact surfaces of the resistivity caps, sufficient seating pressure is necessary to maintain consistent contact with the soil. This was done by placing a dead weight on the rod. The dead weight weighed 583 grams and exerted a sitting pressure of

approximately 5 kPa. On top of the dead weight was a dial gauge to keep track of the change in height. It was taken into consideration that the plunger from the dial gauge adds a small amount of pressure to the sample. However, due to the dial gauge being placed on top of the scale and being a part of the entire system, the mass produced from the plunger (Figure 13) was not used in any calculations.

To heat the samples, two heat guns were placed on opposite sides pointing to the center of the sample. The heat guns were roughly 18 mm away from the Shelby tube. It was discovered that the further the heat guns were from the sample, the longer and more difficult it was for the temperature inside the sample to increase. Although sometimes it was difficult to increase the temperature inside the sample, using the heat guns were essential to allow the other equipment to be used as the sample was being heated.

Figure 16: Distance from Heat Gun to Shelby Tube

Lastly, a thermocouple is also used to take measurements of the temperature inside the sample. Wires were inserted into the top and bottom of the sample, approximately 10 mm, for temperature measurements. The entire setup is shown in Figure 17.

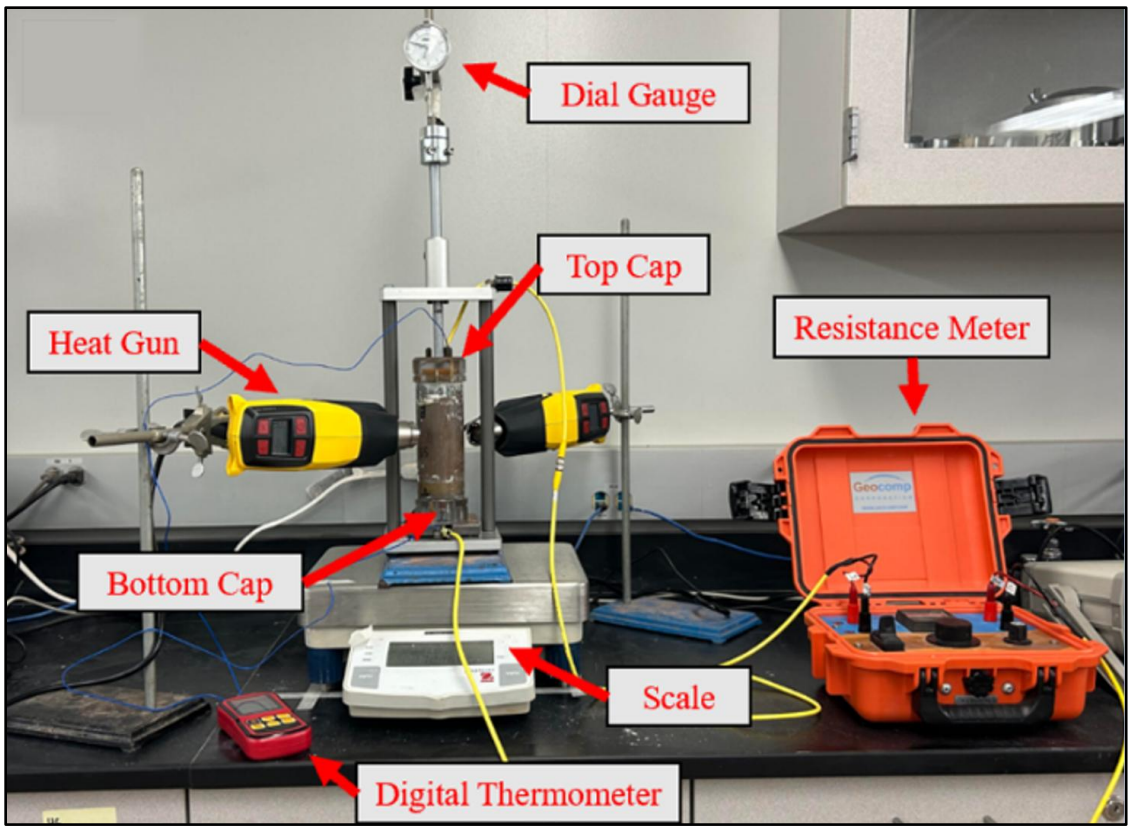

Figure 17: Setup for Heated Samples Tested By the Resistance Meter (Nunez et al. 2025)

The samples were heated in the setup shown in Figure 17 until the internal temperature reached 60 degrees Celsius and were left to cool down back to, if not close to, room temperature. It would be ideal for the temperature to have gone beyond 60 degrees Celsius, however, due to the equipment not being heat proof, temperatures had to remain below 60 degrees Celsius to prevent unreliable measurements. Measurements of weight, displacement, temperature, and resistance were taken when there was a noticeable change in resistance. This process took 6-8 hours and concluded when the resistivity caps were close to losing contact with the sample as shown in Figure 18. The last step would be to carefully remove the sample along with the Shelby tube from the setup and place them both on an oven-safe pan to conduct a final water content test. This

was essential to determine the water content throughout each reading by using the change in weight to add to the water weight from the water content test as shown in section 3.3.5.

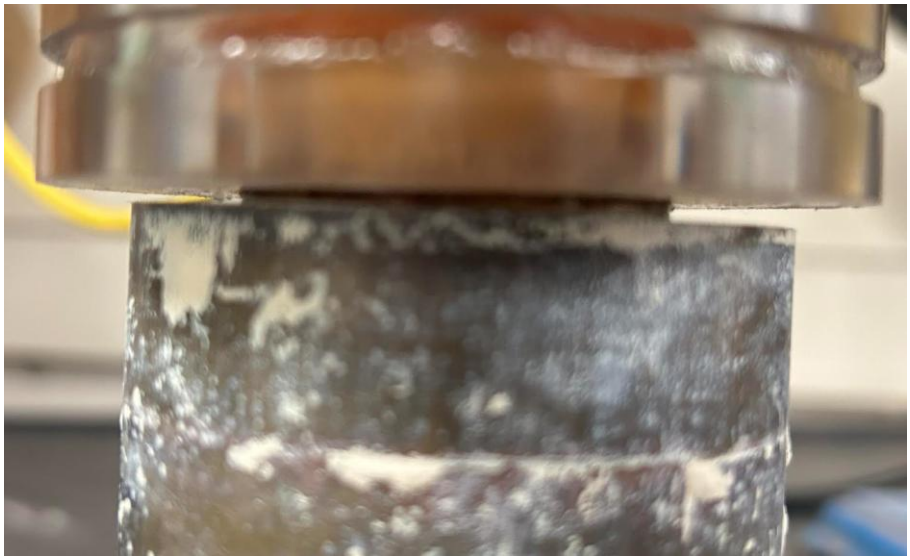

Figure 18: Distance Between Resistance Caps and Shelby Tube at End of Test

3.4.2 Bender Element

The second testing method used was the bender element. The exact same process for the heated tests was taken into practice. However, for the setup, the resistance meter box is replaced by a wave generator, and the resistivity caps are switched to the bender element caps. The testing setup for the heated test using the bender element is shown in Figure 19. The software mentioned in section 3.3.2 is also used during this setup but is not shown.

Figure 20 showcases a sample reading that was taken using the bender element caps when temperatures did not go beyond 60 degrees Celsius. Figure 21 illustrates how the readings are affected when temperatures exceed 60 °C. As the temperature within the sample increases, the receiver wave becomes more unstable and harder to read due to the excessive demand on the equipment, making it difficult to generate the receiving wave

and resulting in unreliable results. To avoid that, temperatures were kept below 60 degrees Celsius. As mentioned previously, the bottom cap triggers the wave, and the top cap receives the wave and can be presented in red and blue respectively in Figures 20 and 21.

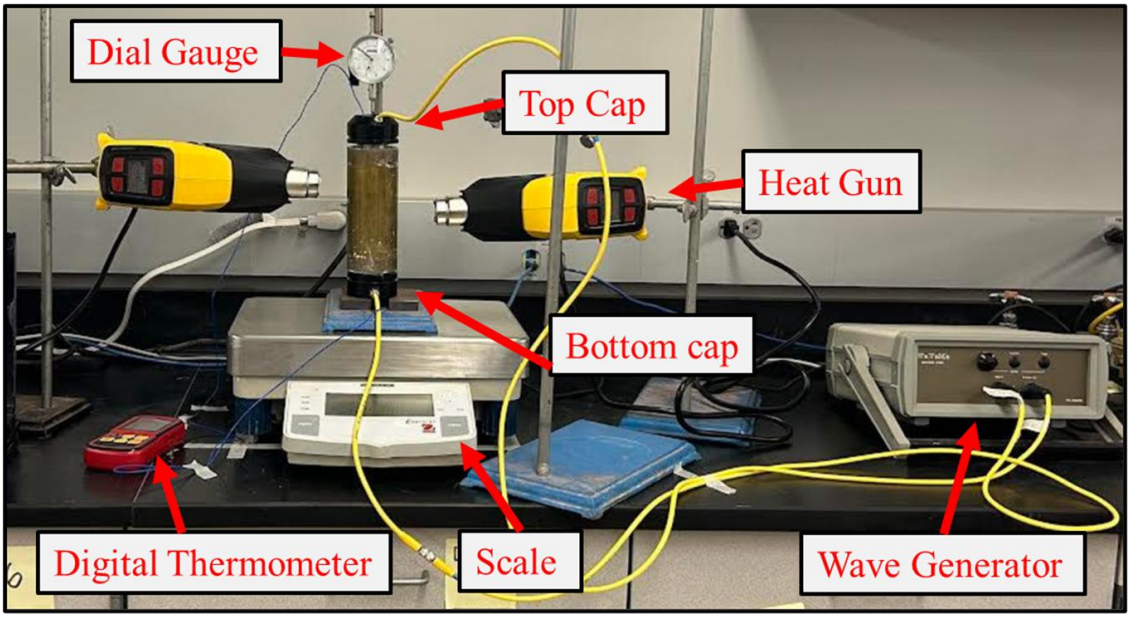

Figure 19: Setup for Heated Samples Tested By the Bender Element (Nunez et al. 2025)

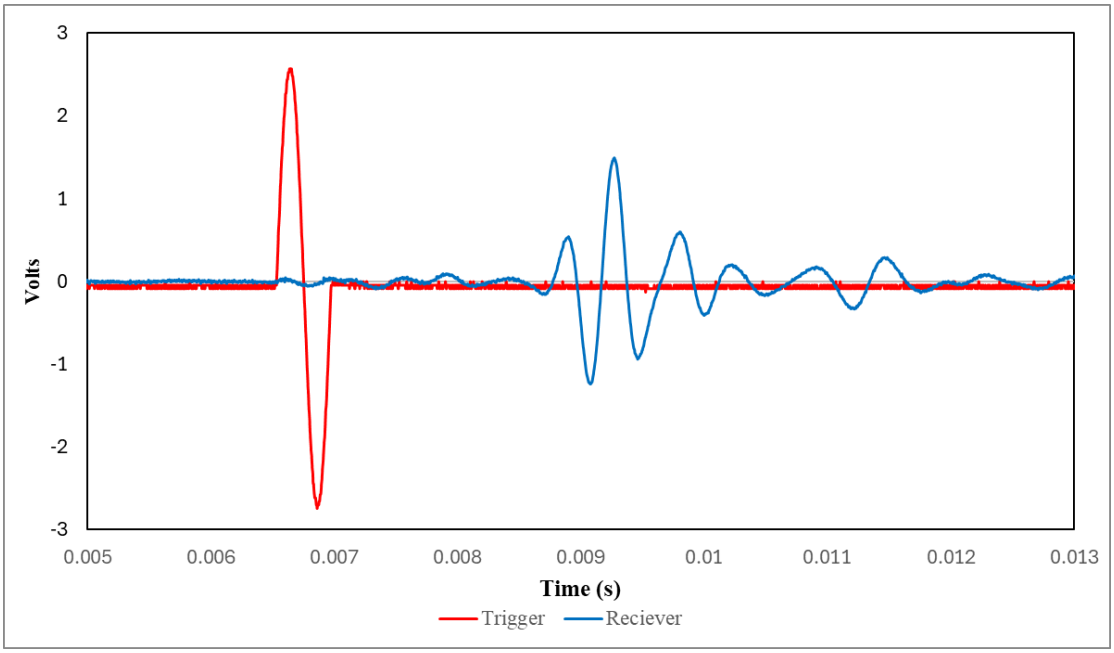

Figure 20: Sample Reading when Sample is Below 60 Degrees Celsius

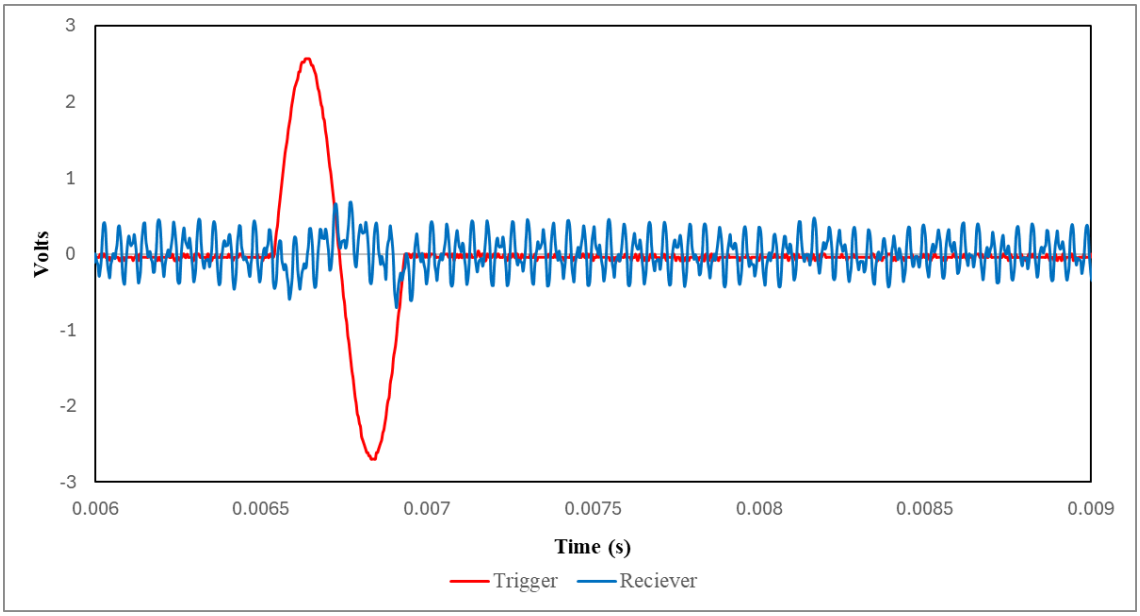

Figure 21: Sample Reading when Sample is Above 60 Degrees Celsius

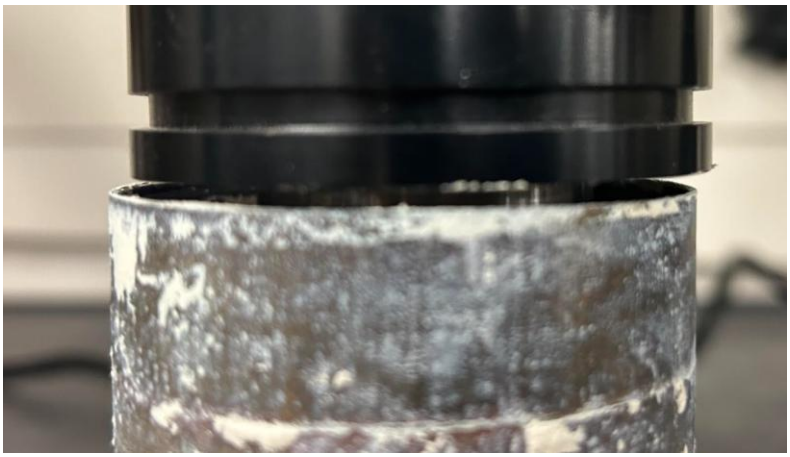

Figure 22: Distance Between Bender Element Caps and Shelby Tube at End of Test

3.5 Setup for Controlled Samples

To determine how heat affects the Kaolin samples, heated samples had to be compared to non-heated samples which will be referred to as controlled samples. Controlled samples had the same setup as the heated samples that were tested using the resistance meter and bender element. However, the heat guns are not used at all, and the samples are kept in that setup for 3-4 weeks to allow the specimen to dry out naturally at room temperature and measurements would be taken as days go by. Figures 23 and 24 demonstrate how the two setups were the same as for the heated samples, but the heat guns were not utilized.

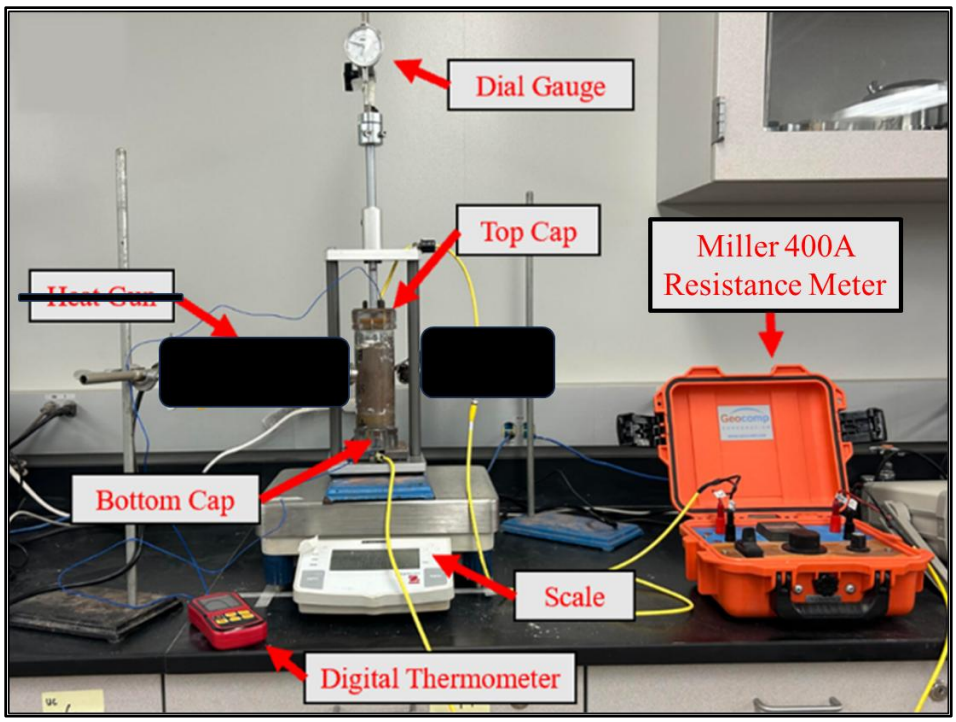

Figure 23: Setup for Controlled Samples Tested by the Resistance Meter

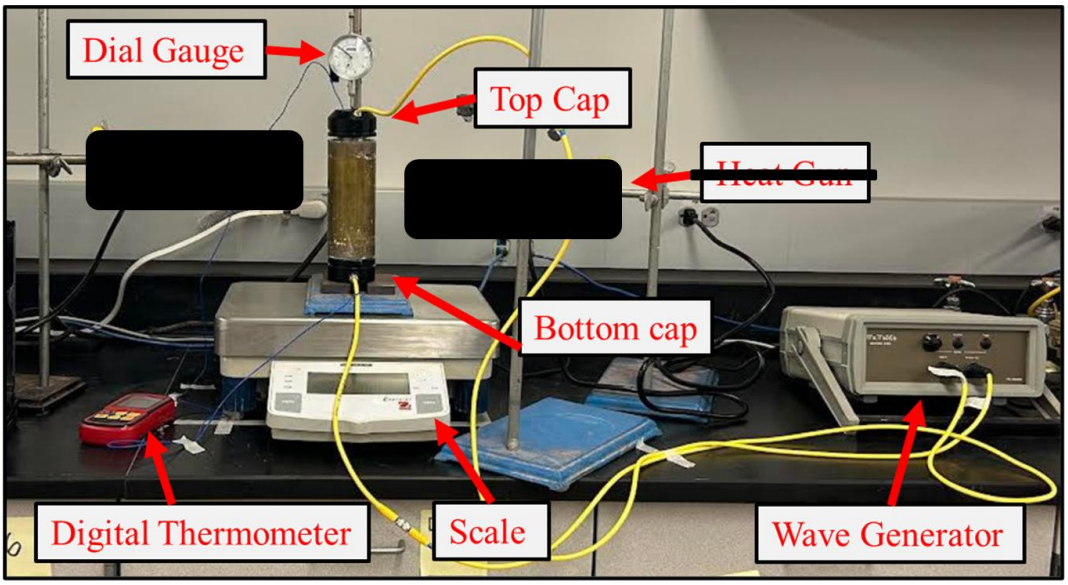

Figure 24: Setup for Controlled Samples Tested by the Bender Element

CHAPTER 4

Data Collection

As mentioned in sections 3.4 and 3.5, heated samples were heated using heat guns while measurements for electrical resistance (or shear wave travel time), weight, displacement and temperature were taken when there was a noticeable change in the resistance (or travel time). Similarly, controlled samples were left to dry on their own for 3-4 weeks while the same measurements would be taken as days go. These measurements were used to calculate the updated sample height, volume, density, water content, and mass, as well as electrical resistivity and G_{max}, incorporating the updated sample dimensions and mass. The following presents the fundamental measurements obtained from the instrumentation, which form the basis for the parameters used in the analyses in Chapters 3.3.1 to 3.3.5.

- Thermometer: Temperature
- Scale: Mass → Water Content (W.C.)
  → Density
- Dial Gauge: Displacement → Sample Height → Volume (V) → Density
  → Electrical Resistivity (ρ)
  → Shear Modulus (G_{max})
- Resistance Meter: Resistance → Electrical Resistivity (ρ)
- Bender Element: Travel Time → (Shear Velocity) V_s → Shear Modulus (G_{max})

Figures 25-28 showcase all the raw data collected during all tests using the dial gauge, thermometer, scale, resistance meter and bender element. A total of 11 tests were

conducted. Six tests involved using pure Kaolin samples and five tests involved using Kaolin mixed with microplastics (MP). The test and sample types are listed in Table 4.

Table 4: Overview of Tests Conducted

Test ID	Material	Description	Test Type	Trial	Color
R-CON	Pure Kaolin	Controlled	Resistance Meter	1	Dark Blue
R-HC1	Pure Kaolin	Heat + Cool	Resistance Meter	1	Blue
R-HC2	Pure Kaolin	Heat + Cool	Resistance Meter	2	Teal
B-CON	Pure Kaolin	Controlled	Bender Element	1	Purple
B-HC1	Pure Kaolin	Heat + Cool	Bender Element	1	Light Purple
B-HC2	Pure Kaolin	Heat + Cool	Bender Element	2	Pink
MP-R-CON	Kaolin + MP	Controlled	Resistance Meter	1	Dark Green
MP-R-HC1	Kaolin + MP	Heat + Cool	Resistance Meter	1	Light Green
MP-B-CON	Kaolin + MP	Controlled	Bender Element	1	Orange
MP-B-HC1	Kaolin + MP	Heat + Cool	Bender Element	1	Yellow
MP-B-HC2	Kaolin + MP	Heat + Cool	Bender Element	2	Red

The marker shapes in the plots presented in Chapters 4–7 indicate the type and stage of each sample. Triangular markers represent control samples that were not exposed to heat. Closed-circle markers indicate measurements taken during the heating stage, while open-circle markers signify that the sample was in the cooling stage at the time of measurement.

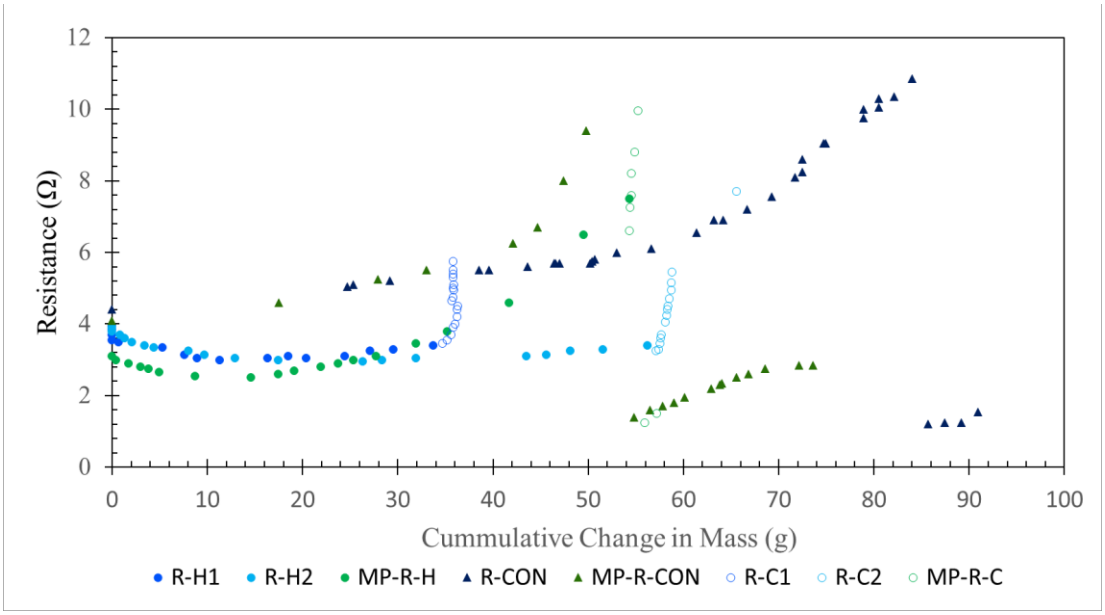

Figure 25: Raw Measurements of Resistance and Change of Mass of Samples Tested by Resistance Meter

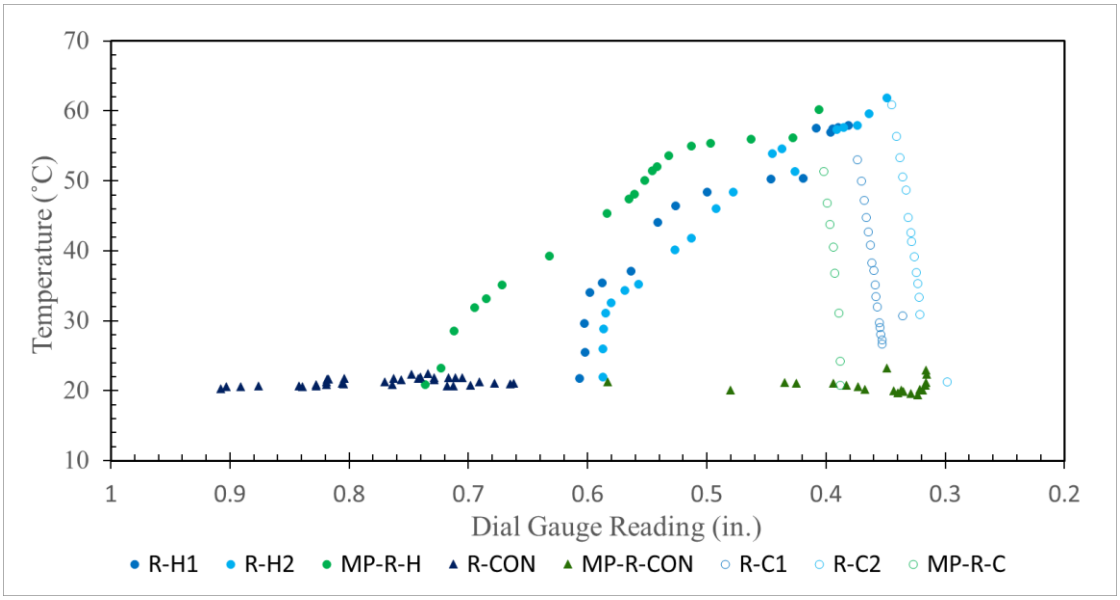

Figure 26: Raw Measurements of Temperature and Dial Gauge Reading of Samples Tested by Resistance Meter

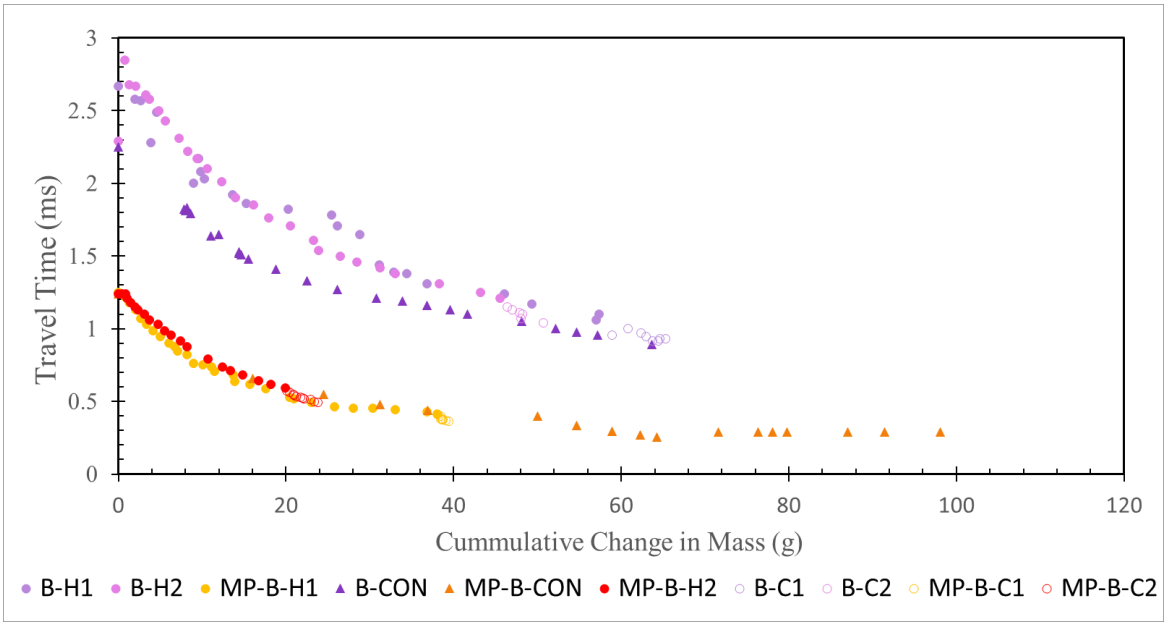

Figure 27: Raw Measurements of Travel Time and Change of Mass of Samples Tested by Bender Element

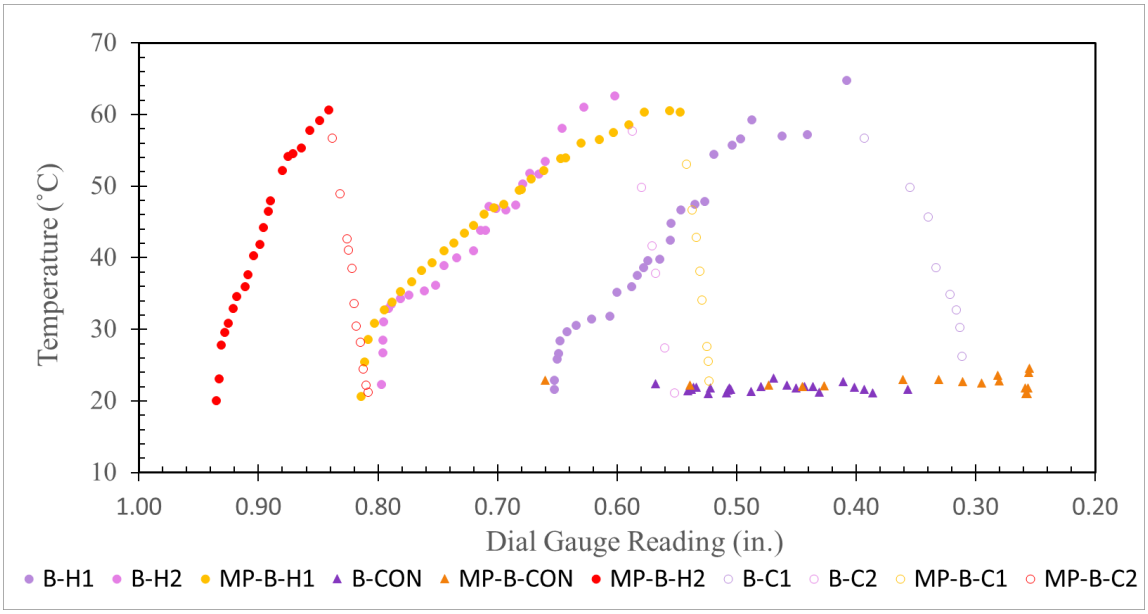

Figure 28: Raw Measurements of Temperature and Dial Gauge Reading of Samples Tested by Bender Element

CHAPTER 5

The Effects of Heat on Kaolin

Pure Kaolin Clay

This research aimed to investigate the effects of both heat and microplastic contamination. To isolate the impact of heat alone, the results from the pure clay samples were examined first in this chapter. All measurements, as well as the calculated electrical resistivity and G_{max} for the pure clay samples are shown in Appendix A. A total of six samples of pure clay were tested, three were tested using the resistance meter: one controlled test (R-CON) and two heating and cooling tests (R-HC1 and R-HC2). The remaining three were tested using the bender element: one controlled test (B-CON) and two heating and cooling tests (B-HC1 and B-HC2).

Figure 29 shows the behavior of electrical resistivity in response to the change in water content. The data starts from left to right to showcase that the water content decreases overtime due to heating or self-drying at the room temperature. For R-CON, electrical resistivity increases at a non-steady rate, where the electrical resistivity increases faster as water content decreases, reaching a final value of 319 Ωm. Alternatively, for the heating stages for R-HC1 and R-HC2, there is little to no change to the electrical resistivity as water content decreases. However, when the cooling stage starts for R-HC1 and R-HC2, a different behavior is shown where electrical resistivity increases while water content remains mostly constant reaching a final value of 167 and 177 Ωm respectively. It should be noted that the water content for the controlled test started at a different percentage compared to the other two tests. To better compare all three tests, Figure 30 also shows electrical resistivity but with the water content

normalized. The water content was normalized by dividing each water content measurement by the initial water content of the respective sample. This was done to ensure that the tests being compared started from a common reference point, since the samples did not all begin with the same water content.

Figure 31 also showcases R-CON, R-HC1, and R-HC2 but with electrical resistivity in relation to temperature. R-CON can be shown with an average temperature of around 22 degrees Celsius with the electrical resistivity increasing, data starting from bottom to top. For R-HC1 and R-HC2, temperatures start at around 22 degrees Celsius (data starting on the lower left side). Samples are heated to only 60 degrees Celsius (due to the equipment not being heatproof) and after reaching 60 degrees Celsius, samples are left to cool down to room temperature (~20 ˚C). For the cooling stage for both samples, we can see a gradual increase in electrical resistivity as temperatures decrease from 60 degrees Celsius. It is important to note that the last point for the cooling stage of R-HC2 is completely at its original temperature, whereas R-HC1 did not fully return to 22 degrees Celsius. This is due to sample R-HC2 being left overnight, giving it more time to cool down completely, resulting in the extra data point. As mentioned previously, samples R-CON, R-HC1, and R-HC2 had final electrical resistivity values of 319, 167, and 177 Ωm respectively. Showcasing that heat significantly decreased the electrical resistance in the two heated samples, about 50 percent decrease on average due to heat provided by the heat guns.

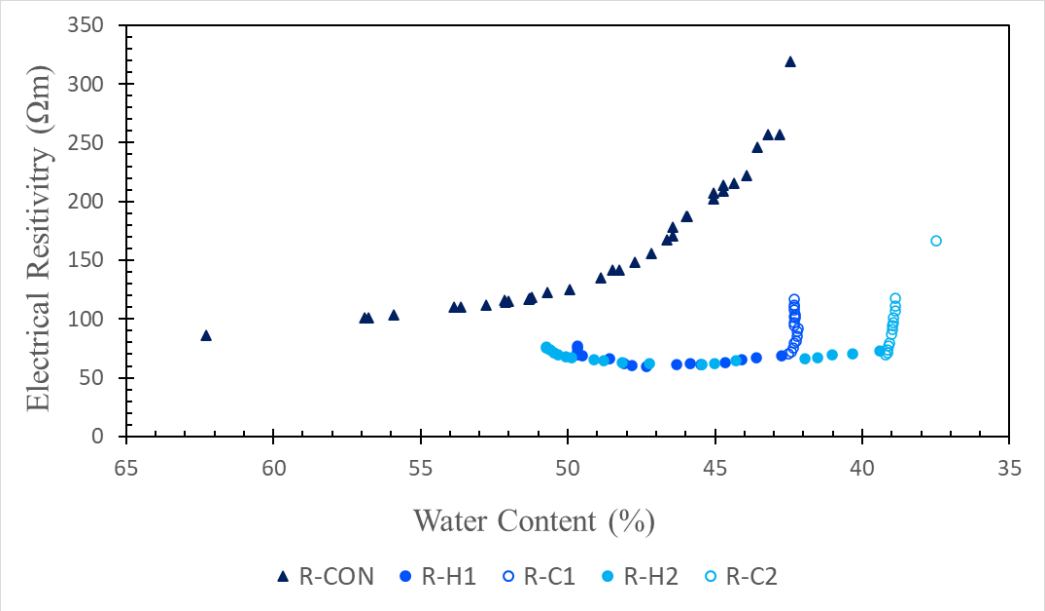

Figure 29: Electrical Resistivity vs. Water Content for Pure Kaolin

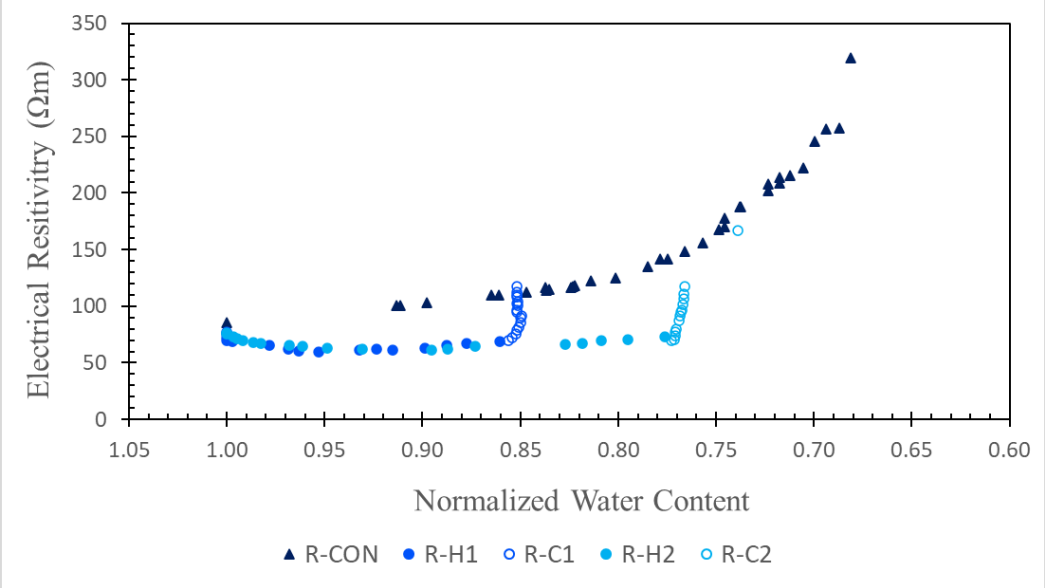

Figure 30: Electrical Resistivity vs. Normalized Water Content for Pure Kaolin

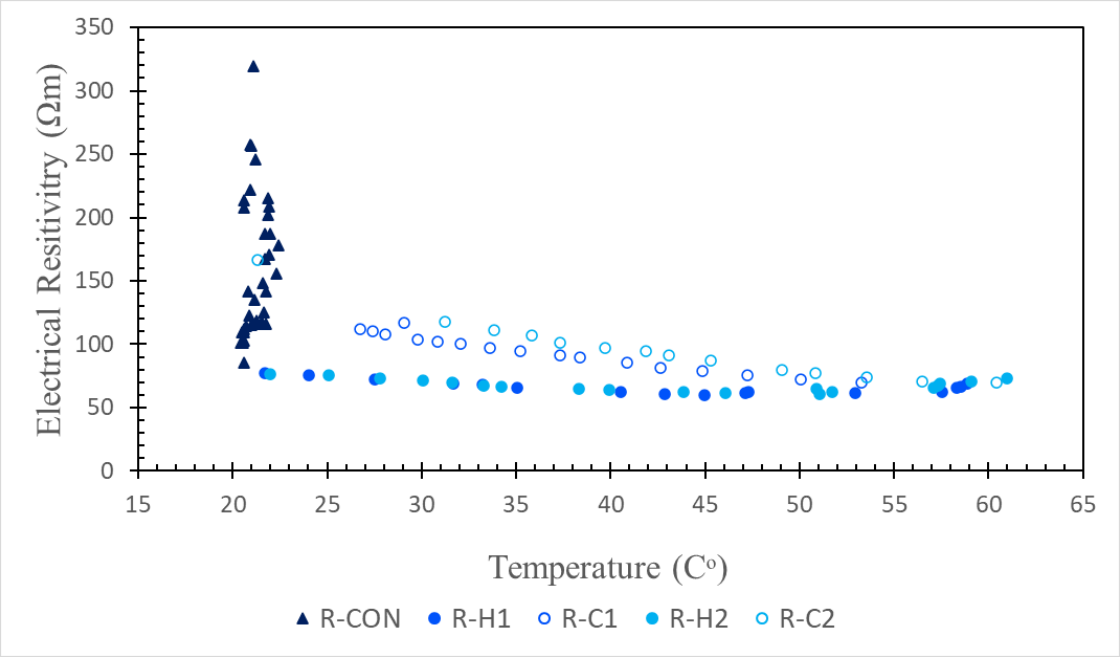

Figure 31: Electrical Resistivity vs. Temperature for Pure Kaolin

Pure Kaolin Clay (Bender Element)

Figure 32 demonstrates G_{max} in respect to water content for the three-remainder pure clay kaolin samples that were tested using the bender element. The dark purple triangles represent the controlled sample (B-CON), the light purple and pink filled circles represent the heating stages for B-HC1 and B-HC2 respectively, and the non-filled light purple and pink circles represent the cooling stages for B-HC1 and B-HC2 respectively. On Figure 30, it is apparent that for B-HC1 and B-HC2 during the heating stage, G_{max} increases at a slightly slower rate when comparing it to the cooling stage. Once reaching the cooling stage, the G_{max} for B-HC1 and B-HC2 increased at a slightly faster rate reaching a final G_{max} value of 32.8 and 27.1 MPa respectively. Whereas for B-CON, the G_{max} increases at a mostly constant rate as water content decreases reaching a final value of 36.7 MPa. With B-HC1 starting at a very similar water content as B-CON, it can be

shown that the G_{max} for B-HC1 increases at a slower rate as water content decreases in comparison to the controlled sample. It was taken into consideration that sample B-HC2 started at a higher water content percentage in comparison to B-CON and B-HC1, therefore the water content was normalized as shown in Figure 33. Figure 33 highlights the similarities in behavior for the two heated samples throughout the test, especially the heating stage.

Figure 34 shows the G_{max} in respect to temperature. Sample B-HC2 was given an extra day to completely cool back down hence the final data point reaching its starting temperature. During the temperature rise and drop of B-HC1 and B-HC2 G_{max} increases regardless of the stage. It is important to highlight the B-HC1 and B-HC2 reached final G_{max} values of 32.8 and 27.1 MPa (about an 18% decrease on average) whereas B-CON reached a final G_{max} 36.7 MPa. Meaning that the two heated samples were not able to fully recover in stiffness even after giving them a chance to cooldown.

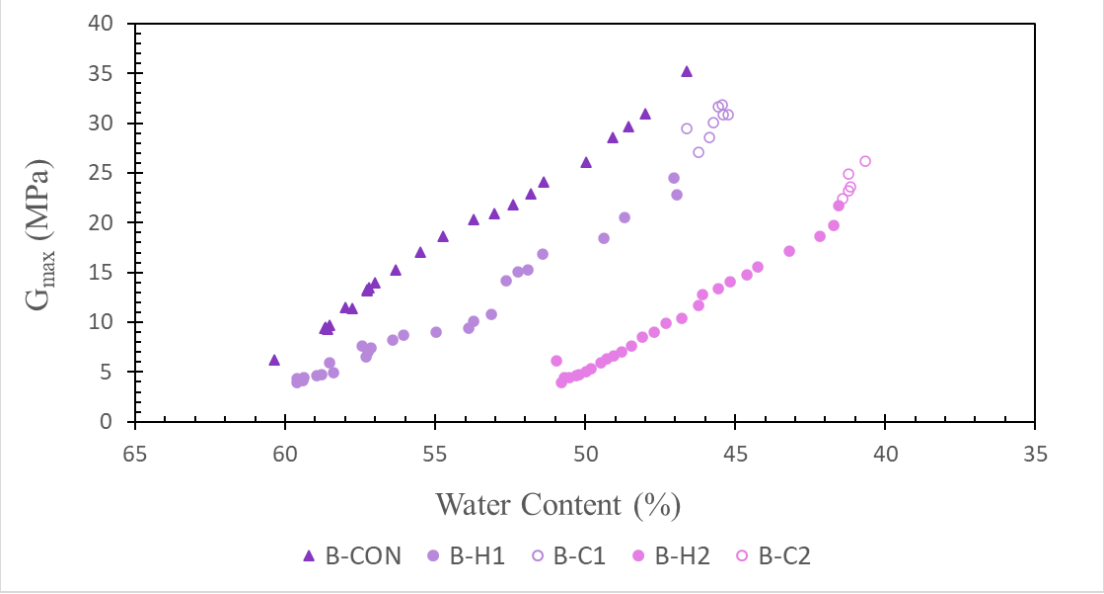

Figure 32: G_{max} vs. Water Content for Pure Kaolin

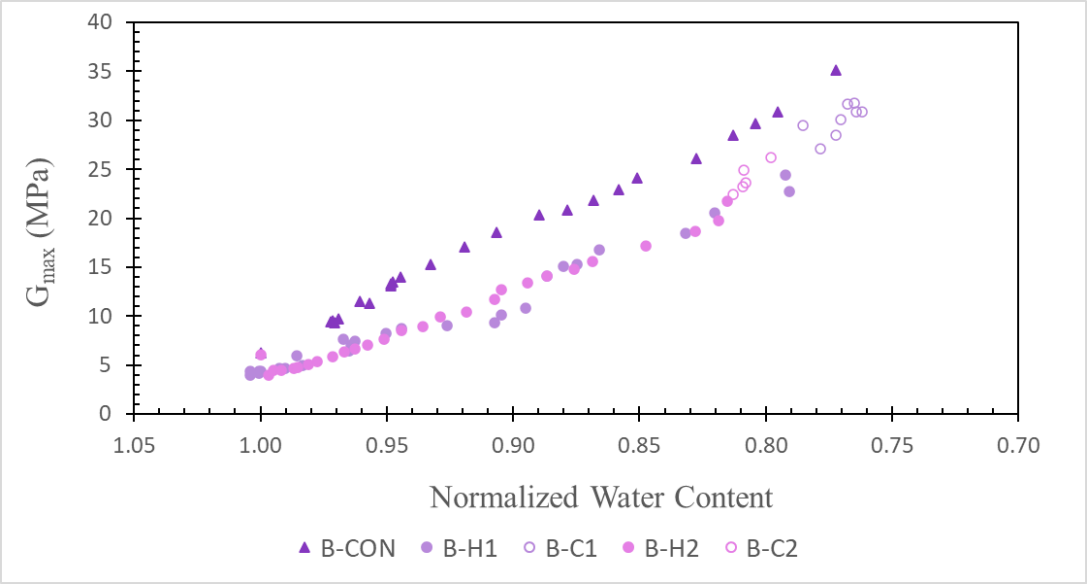

Figure 33: G_{max} vs. Normalized Water Content for Pure Kaolin

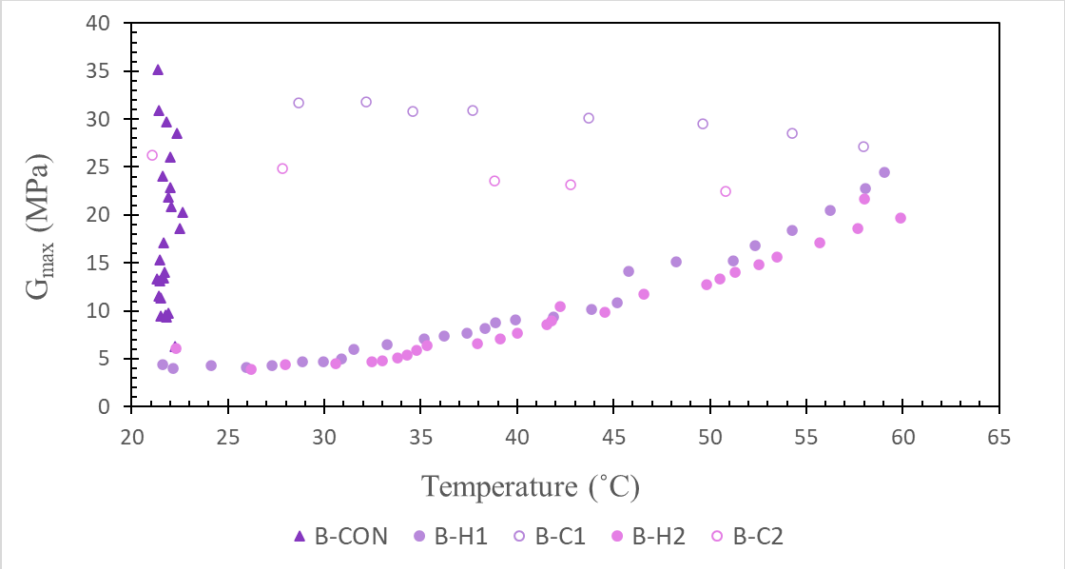

Figure 34: G_{max} vs. Temperature for Pure Kaolin

CHAPTER 6

The Effects of MP on Kaolin

Before looking at the effects from both heat and microplastics, it is essential to first determine the effects of microplastics. To see how microplastics affect electrical resistivity and shear modulus, the controlled tests from the pure kaolin will be compared to the controlled test with microplastics. As mentioned previously, the Kaolin + MP samples are half the size of the pure Kaolin samples. However, for both the calculation for the electrical resistivity and G_{max} the height and travel distance of the sample are considered which allows for comparable data even though the samples are different lengths.

Resistance Meter

Figure 35 showcases the controlled pure kaolin sample (R-CON) and the controlled Kaolin mixed with microplastics (MP-R-CON). The sample with microplastics has a much higher electrical resistivity than the pure Kaolin sample. As mentioned earlier, MP-R-CON has a final value of 1363 Ωm whereas R-CON has a final value of 319 Ωm, which is over a 300 percent increase due to the microplastics added. It was concluded that due to the non-conductive nature of microplastics, the readings from the resistance meter would be highly influenced, unfortunately causing a bias in the readings when compared with the kaolin-only samples. For this research, the results are still included but it is important to note that microplastics restrict electrical current. In can also be shown that sample MP-R-CON lost more water in comparison to R-CON; MP-R-CON decreased 30% in water content while R-CON decreased 20% in water content.

Which can be expected due to the non-absorbent behavior of microplastics, making it easier for the moisture to escape from the sample.

Figure 37 plots the electrical resistivity against temperature for R-CON and MP-R-CON. When it comes to the samples at room temperature, there is little to no correlation between electrical resistivity and temperature as shown by the low R squared values (0.0247 and0.0564) in Figure 37.

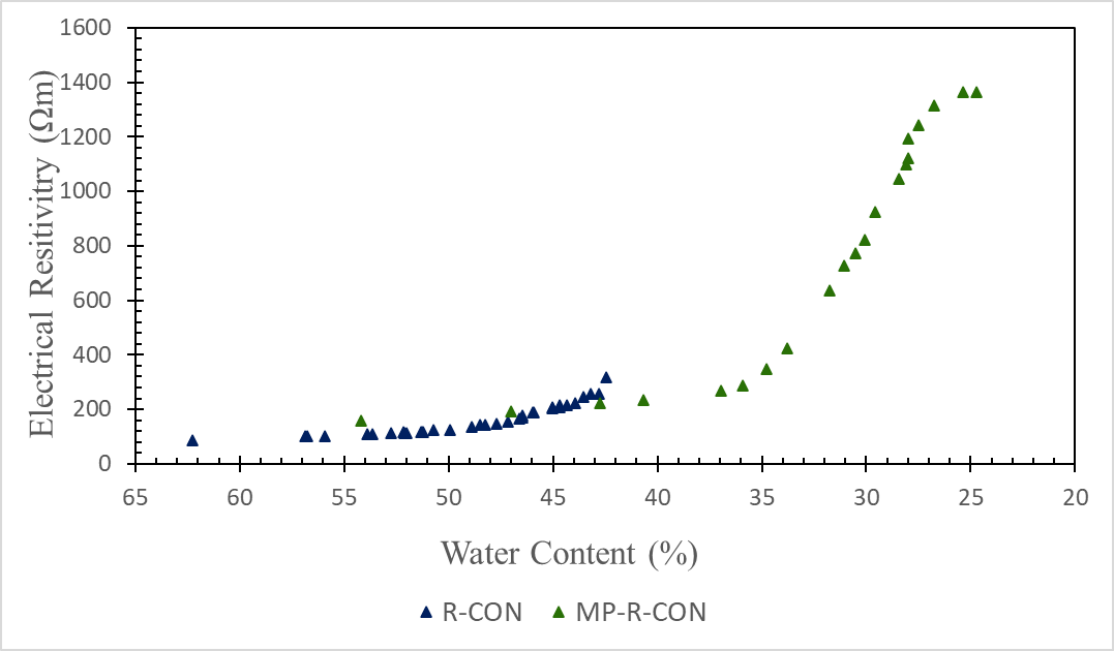

Figure 35: Electrical Resistivity vs. Water Content for Controlled Samples

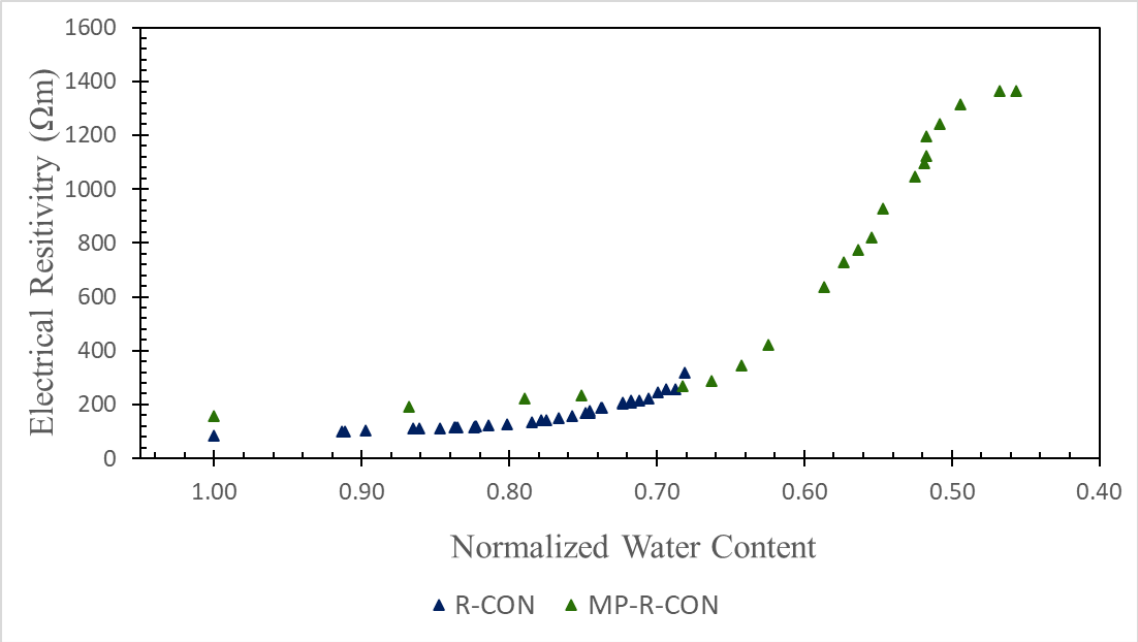

Figure 36: Electrical Resistivity vs. Normalized Water Content for Controlled Samples

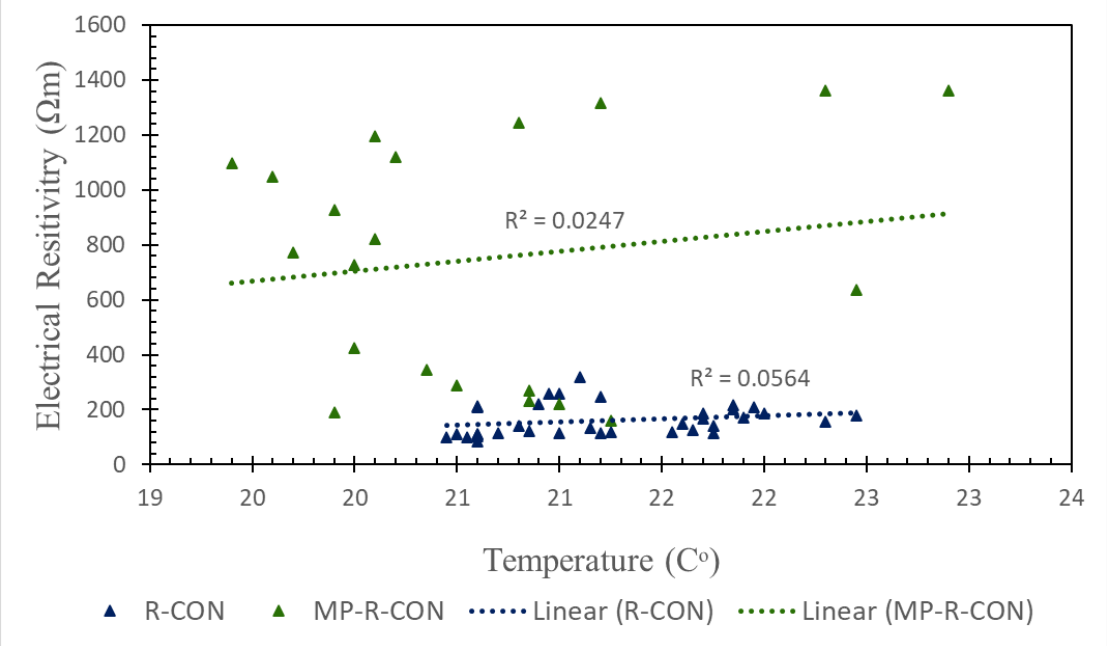

Figure 37: Electrical Resistivity vs. Temperature for Controlled Samples

Bender Element

Figures 38 and 39 show how the G_{max} changes in respect to water content and normalized water content, respectively, in our controlled and contaminated sample. In the first few measurements, the G_{max} of B-CON was greater than the G_{max} of MP-B-CON. It was not until MP-B-CON reached a water content of 37% where the G_{max} begins to increase more rapidly reaching a value of 74 MPa. Whereas B-CON had only reached 37 MPa, resulting that microplastics increases G_{max} by 100%. Similarly to MP-R-CON, MP-B-CON decreases much lower in water content compared to B-CON. B-CON decreased 14% in water content and MP-B-CON decreased 26%. Which can be expected since microplastics are repellent to water.

Figure 40 showcases how G_{max} changes at room temperature for B-CON and MP-B-CON. When samples are at room temperature, there is not much correlation between temperature and G_{max} (R^2 = 0.2685 and 0.0065).

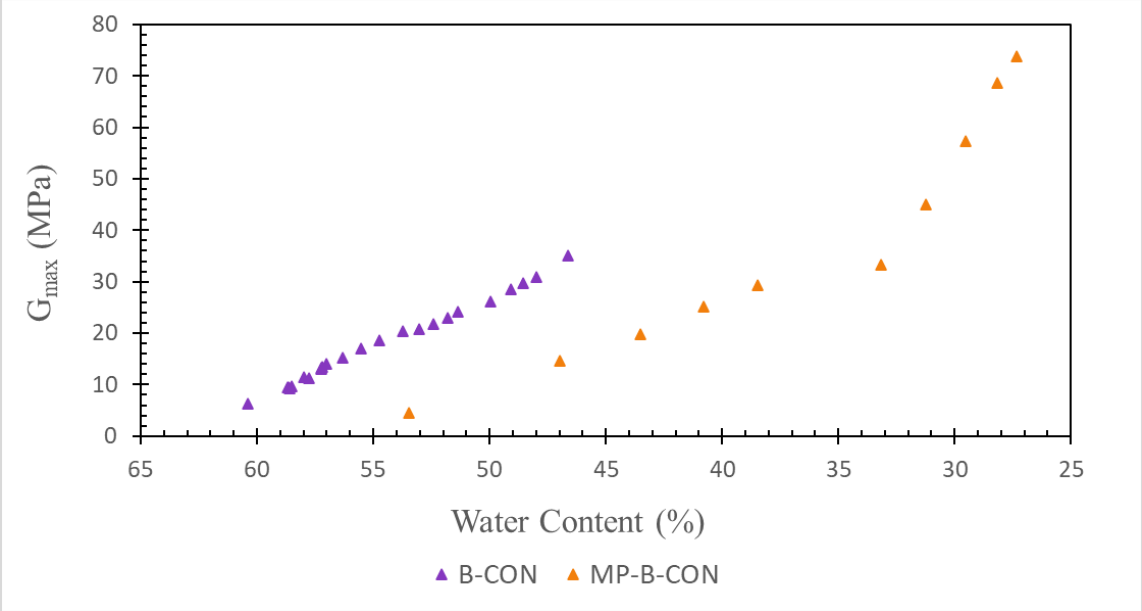

Figure 38: G_{max} vs. Water Content for Controlled Samples

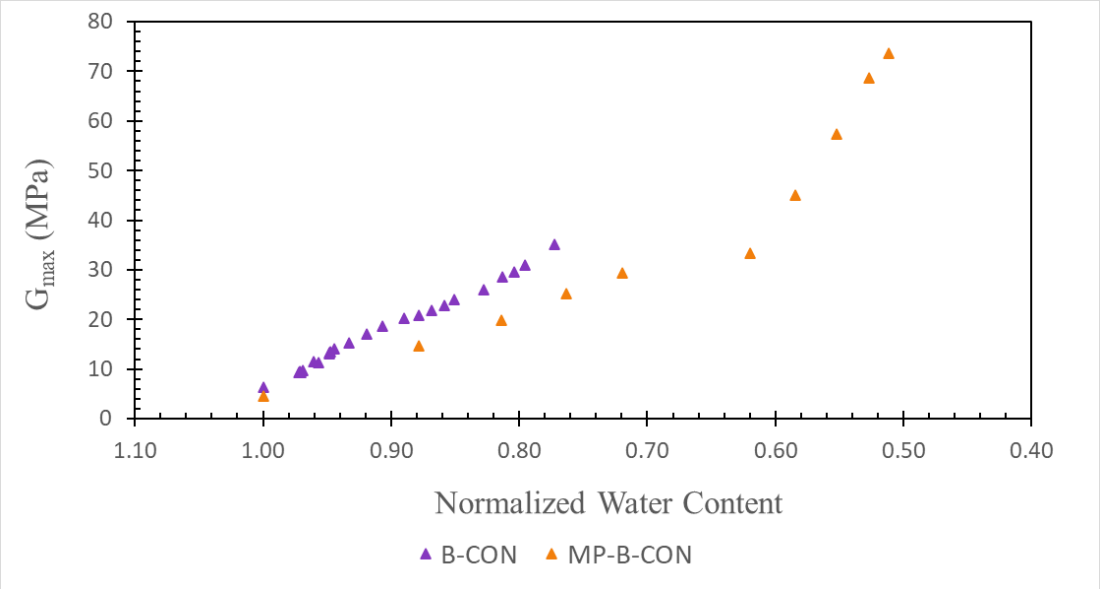

Figure 39: G_{max} vs. Normalized Water Content for Controlled Samples

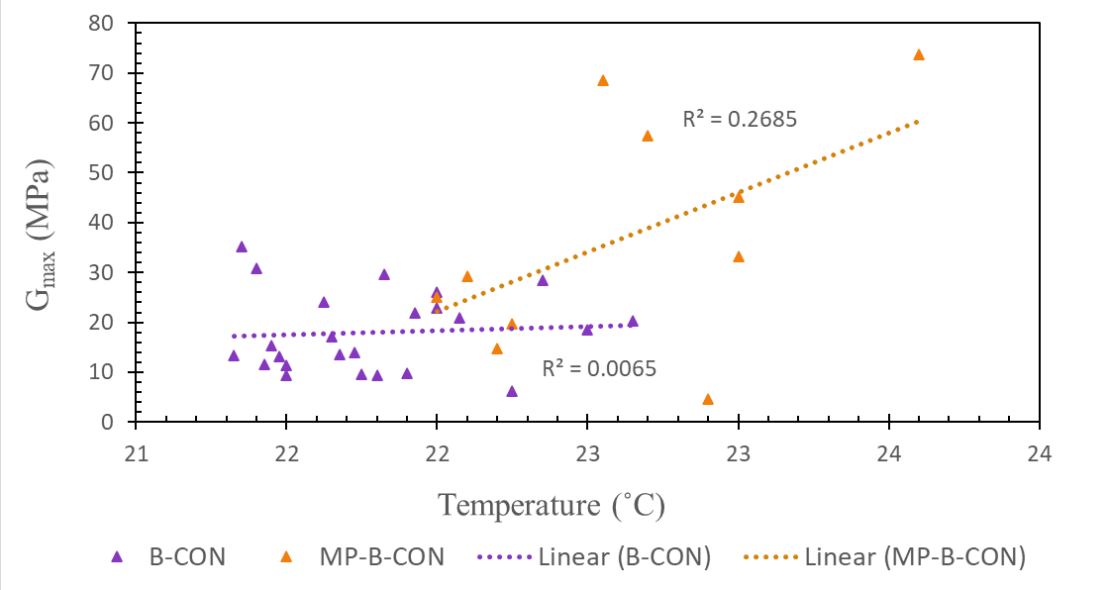

Figure 40: G_{max} vs. Temperature for Controlled Samples

CHAPTER 7

The Effects of Heat and MP on Kaolin

In Chapter 5 the effects of heat were explored in pure Kaolin samples. Additionally, in Chapter 6 the effect of only microplastics on pure Kaolin samples was observed. For this chapter, controlled pure Kaoin samples are compared to heated Kaolin + MP samples to see how both heat and microplastics affect the electrical resistivity and G_{max} of Kaolin clay.

Figures 41 and 42 illustrate how heating and the addition of 10% microplastics affect electrical resistivity as the water content changes in the sample. In the heating stage for MP-R-HC, the electrical resistivity behaves very similar to R-CON. The data points follow the same path and can be easier seen in Figure 42 up until the heating stage starts for MP-R-HC. Once the cooling stage starts for MP-R-HC, the electricity resistivity increases rapidly. Although in previous chapters it was discovered that heat lowers the electrical resistivity of samples, the non-conductive behavior of the microplastics has a much larger effect. Resulting in the final value of MP-R-HC to be 742 Ωm, which is 132% larger than the final value for R-CON. However, as mentioned previously, these results cannot be relied on due to the heavy influence microplastics have on electrical resistivity.

Figure 43 shows the heating and cooling path for MP-R-HC as R-CON stays at a constant temperature. The electrical resistivity of MP-R-HC during the heating stage behaves very similarly to the heating stage of the pure Kaolin samples, where there is not much change in the electrical resistivity. However, towards the end of the heating stage

the electrical resistivity begins to increase and at the start of the cooling stage we still that shift in behavior where the electrical resistivity increases at a much faster rate.

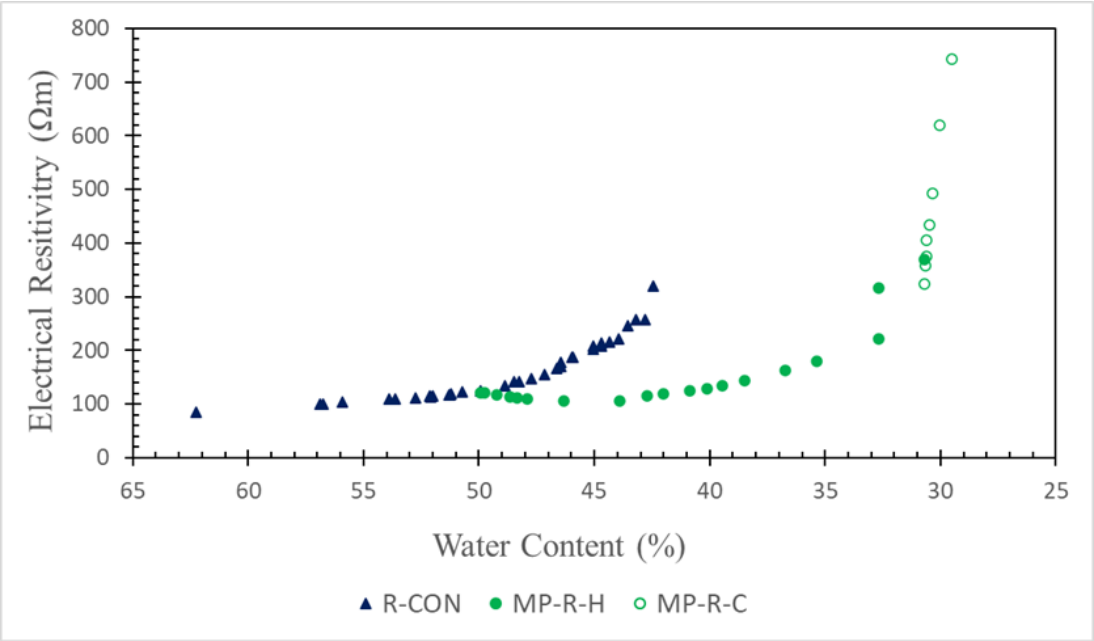

Figure 41: Electrical Resistivity vs. Water Content for Pure Kaolin and Kaolin + MP

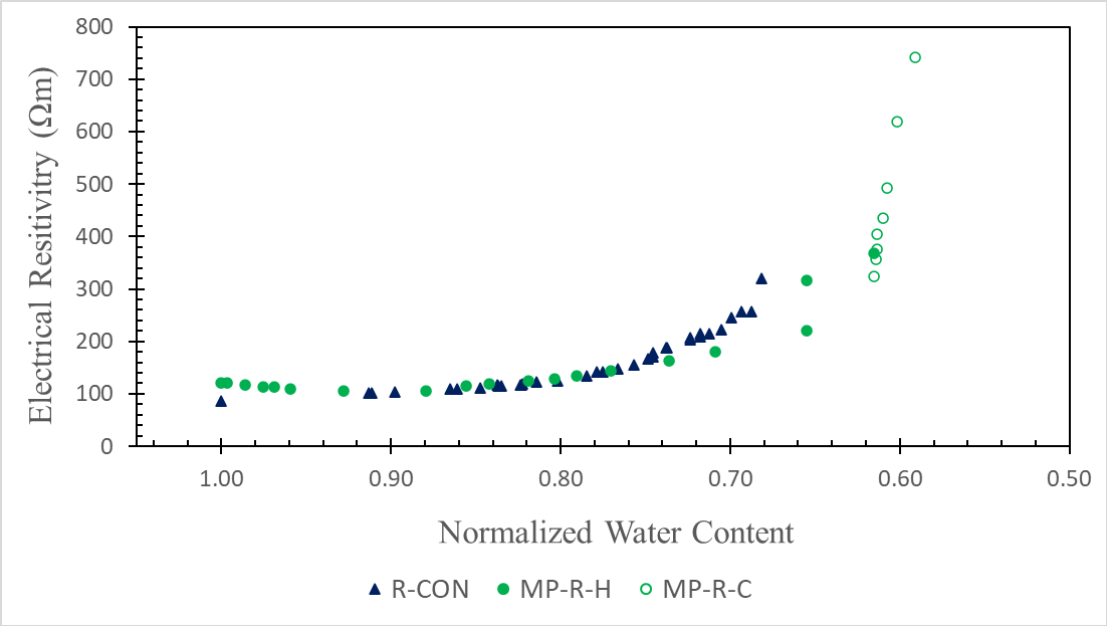

Figure 42: Electrical Resistivity vs. Normalized Water Content for Pure Kaolin and Kaolin + MP

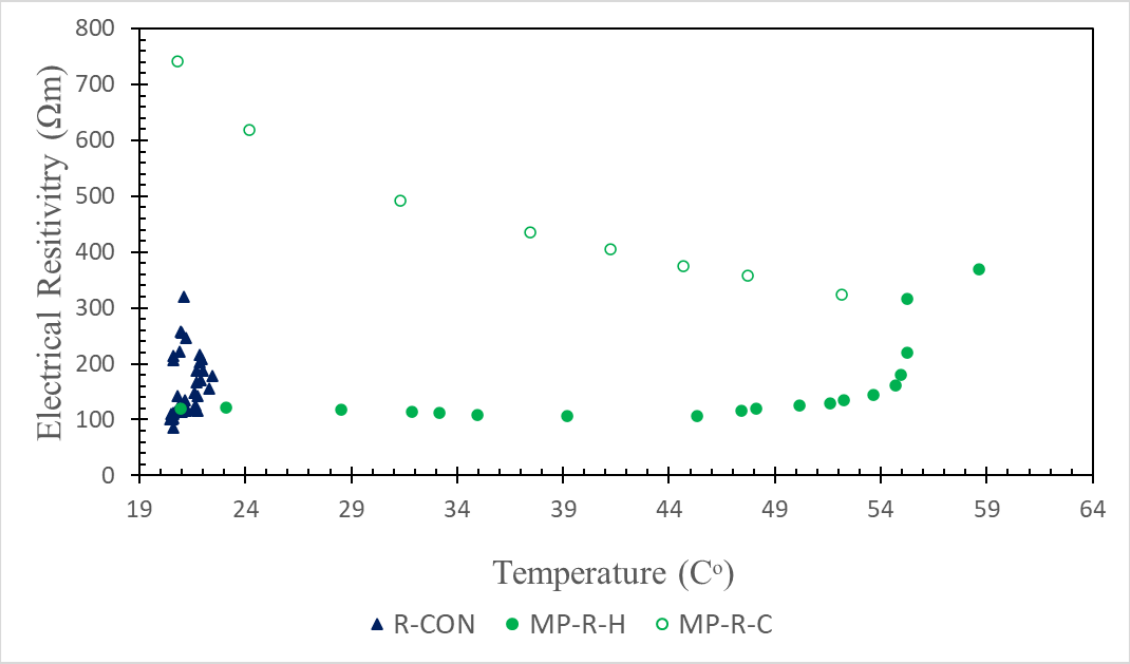

Figure 43: Electrical Resistivity vs. Temperature for Pure Kaolin and Kaolin + MP

Figures 44 and 45 show how the G_{max} changes in heated samples that have microplastics in respect to water content. For B-CON, MP-B-HC1, and MP-B-HC G_{max} decreases as the water content decreases, which can be expected. In Chapter 4, it was shown that heat decreases G_{max} and in Chapter 5 demonstrated that microplastics increased the G_{max}. However, when both are considered, it is apparent that the controlled sample (B-CON), for the most part, maintains a higher G_{max} than the two heated samples and can easier be shown in Figure 45. It is not until MP-B-HC1 reaches a water content of 35% where the G_{max} begins to increase significantly faster until it reaches a final value of 40 MPa. Whereas B-CON and MP-B-HC2 reached a final G_{max} of 36 MPa and 24 MPa respectively. It is to be noted that the ending behavior, of G_{max} in respect to water

content, for sample MP-B-HC1 is very different to all the other samples tested by the bender element. It could be possible that the caps were losing contact with the specimen due to the shrinkage of the sample. Which is why a second sample + MP was heated to confirm, and it was shown that it followed a similar path to all the other samples. However, it can also be that water content is a larger influence to G_{max} at lower percentages.

Figure 46 demonstrates the response of G_{max} in relation to temperature. For MP-B-HC1 and MP-B-HC2, the increase in G_{max} during the heating stage occurs at a rate similar to the cooling stage, differing from the trend observed when G_{max} was plotted against water content. At least for the heating stages, MP-B-CON was able to achieve higher G_{max} values than MP-B-HC1 and MP-B-HC2. However, at the end of the cooling stage, it is unclear whether microplastics and heat lower or increase G_{max} considering how the end behaviors of MP-B-HC1 and MP-B-HC2 differ.

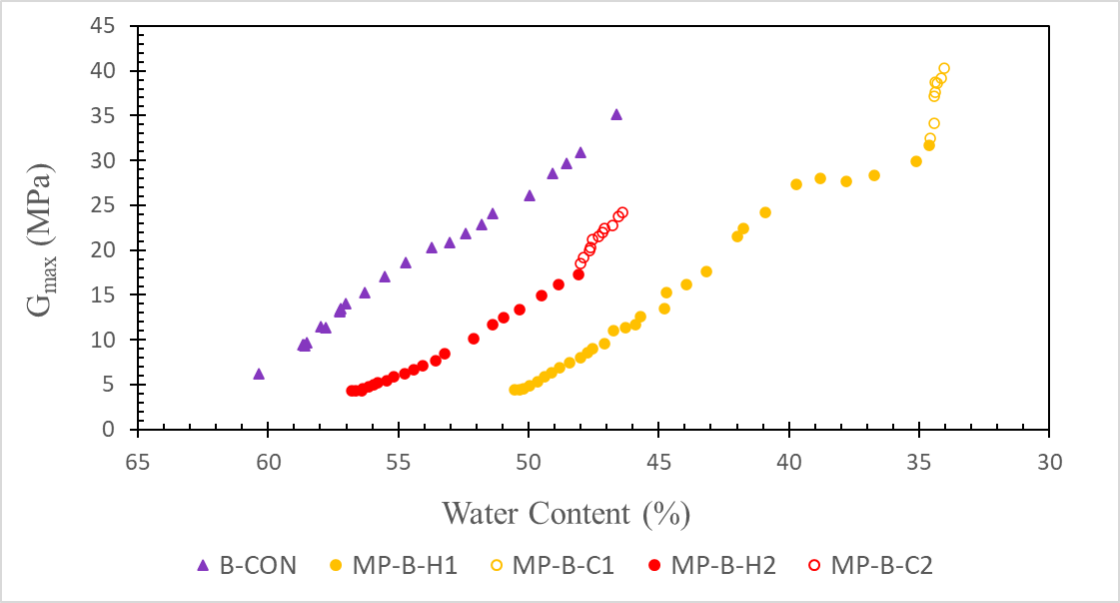

Figure 44: G_{max} vs. Water Content for Pure Kaolin and Kaolin + MP

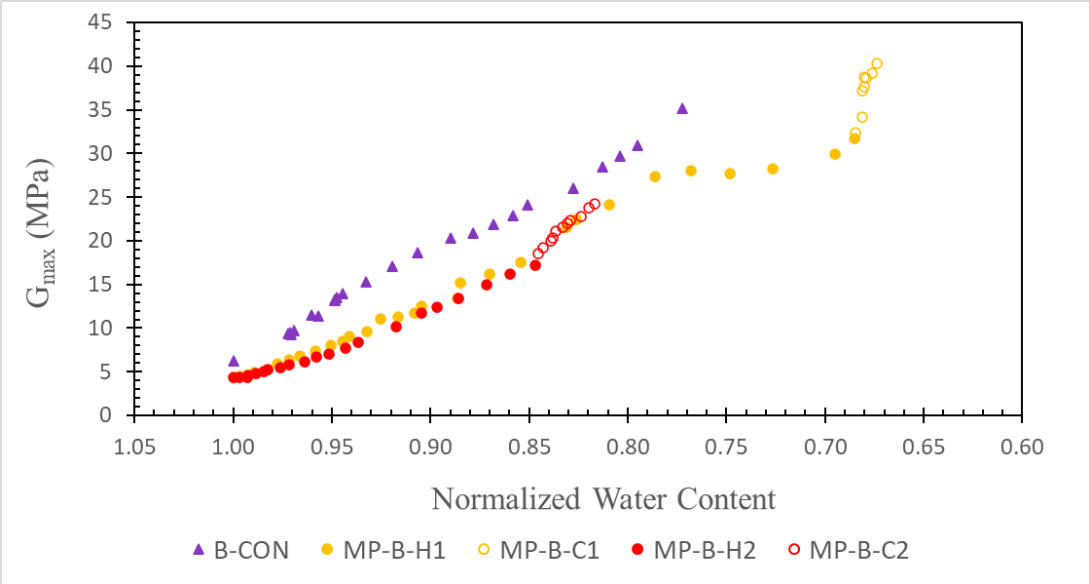

Figure 45: G_{max} vs. Normalized Water Content for Pure Kaolin and Kaolin + MP

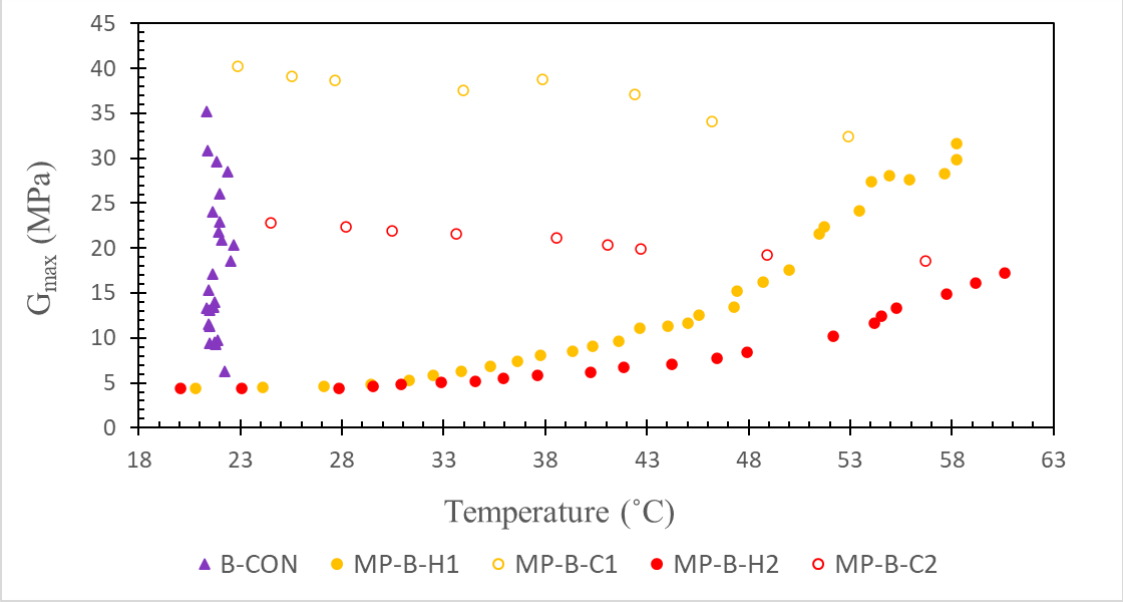

Figure 46: G_{max} vs. Temperature for Pure Kaolin and Kaolin + MP

Table 5: Summary of Tests

Test ID	$(w.c.)_i$ (%)	$(w.c.)_f$ (%)	$(mass)_i$ (g)	$(mass)_f$ (g)	Temp. (°C)	G_{max} (MPa)	Resistivity (Ω·m)
R-CON	62.28	42.23	737.8	646.9	20.5-22.5	-	85.8-319.2
R-HC1	49.67	42.29	732.0	696.2	21.7-58.9	-	59.89-117.1
R-HC2	50.74	37.49	740.1	674.5	21.3-61.0	-	61.0-166.6
B-CON	60.38	46.62	744.2	680.6	21.3-22.7	6.3-35.2	-
B-HC1	59.37	45.58	737.0	673.3	21.6-59.1	4.0-31.8	-
B-HC2	50.95	40.67	749.6	698.9	21.1-59.9	3.9-26.2	-
MP-R-CON	54.17	24.73	376.2	304.2	19.4-22.9	-	159.3-1363.7
MP-R-HC	49.92	29.5	371.1	321.7	21.0-58.7	-	106.0-742.5
MP-B-CON	53.47	27.35	371.8	307.5	22.0-23.6	4.6-73.7	-
MP-B-HC1	50.52	34.03	365.0	325.6	20.8-58.3	4.4-40.3	-
MP-B-HC2	56.81	46.39	357.7	333.9	20.1-60.6	4.4-24.3	-

CHAPTER 8

Cross-Test Examination of Enclosed Areas Analyses Between Two Selected Tests

To evaluate the mechanical behavior of Kaolin samples under the influence of heat and microplastics enclosed areas, G_{max} Vs. normalize water content between two selected tests, were created to analyze the different sample types. The enclosed areas were determined by plotting two tests at a time—each representing a specific investigation scenario (e.g., heat vs. non-heat or MP-contaminated vs. no contamination, and by using the area function in MATLAB to calculate the area created (MathWorks, 2024). However, for the data to be connected, one set of data was inversed so that when the data was combined, it started and ended at normalized water content of one. As shown below, samples made of the same material behaved relatively consistent, as they were prepared using the slurry-based consolidation box method (Ch. 3.2). This consistency is particularly evident after normalizing the water content shown in Figures 47-51. The shaded areas in the graph indicate the extent of damage sustained by the clay, as reflected in the observed stiffness degradation at the same normalized water content level.

Figure 47 plots B-CON against the two heated pure clay samples B-HC1 and B-HC2 to see the effects of heat on pure Kaolin which results in areas of 1.4 and 1.2 MPa respectively. Heat alone results in the second largest area (on average) showing further evidence of stiffness degradation in Kaolin.

Figure 48 B-CON was plotted with MP-B-CON to see how microplastics change the behavior of Kaolin as. The area of the full loop is 5.3 MPa which is the largest area. Introducing microplastics to the Kaolin samples lead to the largest decrease in G_{max}

meaning that microplastics alone degrades the stiffness of Kaolin clay the most. However, it is important to note that because MP-B-CON was able to lose a lot more water during testing, the normalized water content range was larger than the range for B-CON against B-HC1 and B-HC2. Which is why Figure 48 also shows a smaller area (shown in orange) that trims the x-axis to match the range for the pure Kaolin samples resulting in the area being lowered to 1.5 MPa. Indicating that most of the stiffness degradation occurs at lower water content levels, however, the effects of microplastics can still be shown at even high-water content levels.

Figure 49 plots both pure Kaolin heated samples (B-HC1 and B-HC-2) against the heated Kaolin + MP samples (MP-B-HC1) and (MP-B-HC2). It is shown that all four plots show a significantly small area (all areas under 0.4 MPa and even smaller at normalized W.C. > 0.76) compared to all the other plots. It is apparent that the addition to microplastics to heated samples has very little effect on the soil's stiffness.

Figure 50 plots MP-B-CON against MP-B-HC1 and MP-B-HC2 to determine how heat affects contaminated samples. If the full loops are considered, the areas are 2.2 and 3.7 MPa receptively, which are relatively high. However, if the trimmed areas are considered there is a drastic decrease resulting in areas of both 0.2 MPa. Showcasing that most of the soil's degradation occurs at lower water content levels.

Lastly, Figure 51 plots B-CON against MP-B-HC1 and against MP-B-HC2 to see how both heat and microplastics affect Kaolin. As a result, the areas created are 1.9 and 1.0 MPa respectively. The plot for B-CON and MP-B-HC1 also includes a trimmed area of 1.1 MPa. Indicating that the same amount of stiffness degradation occurs at low and high-water content levels.

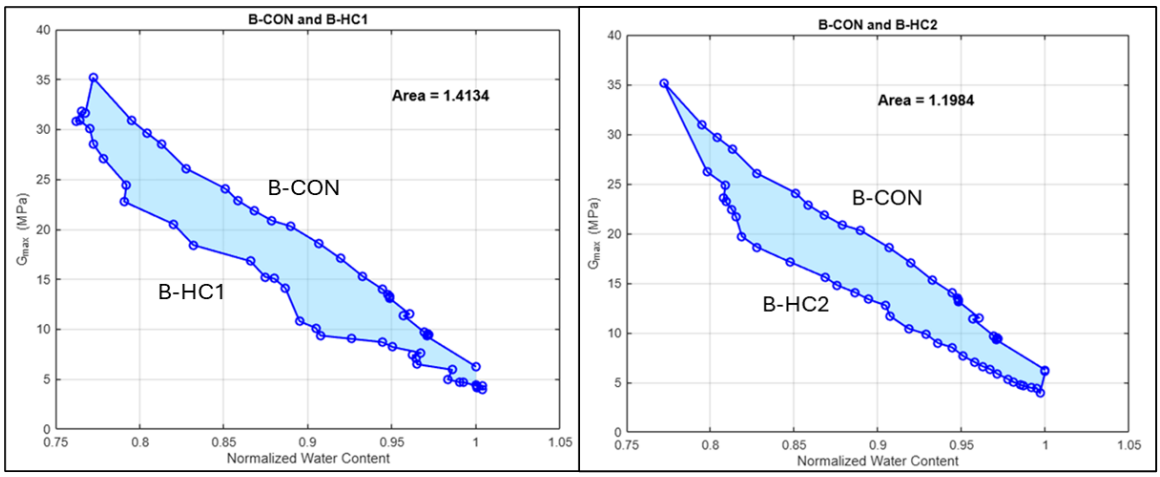

Figure 47: Enclosed Areas for the Effects of Heat Only

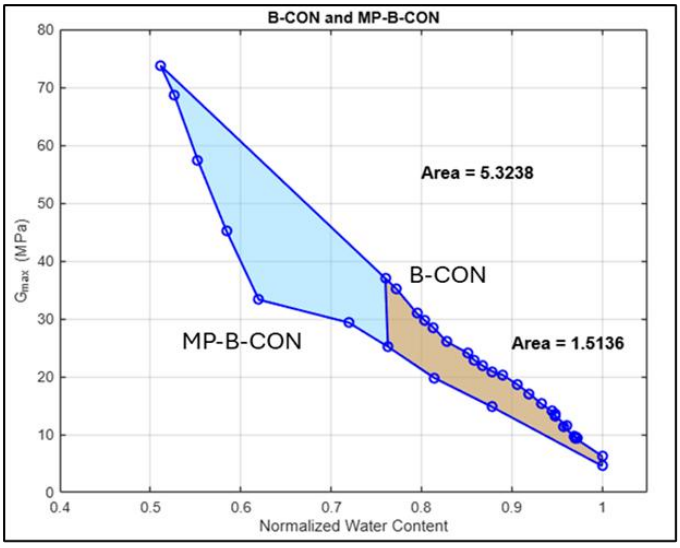

Figure 48: Enclosed Areas for the Effects of Microplastics

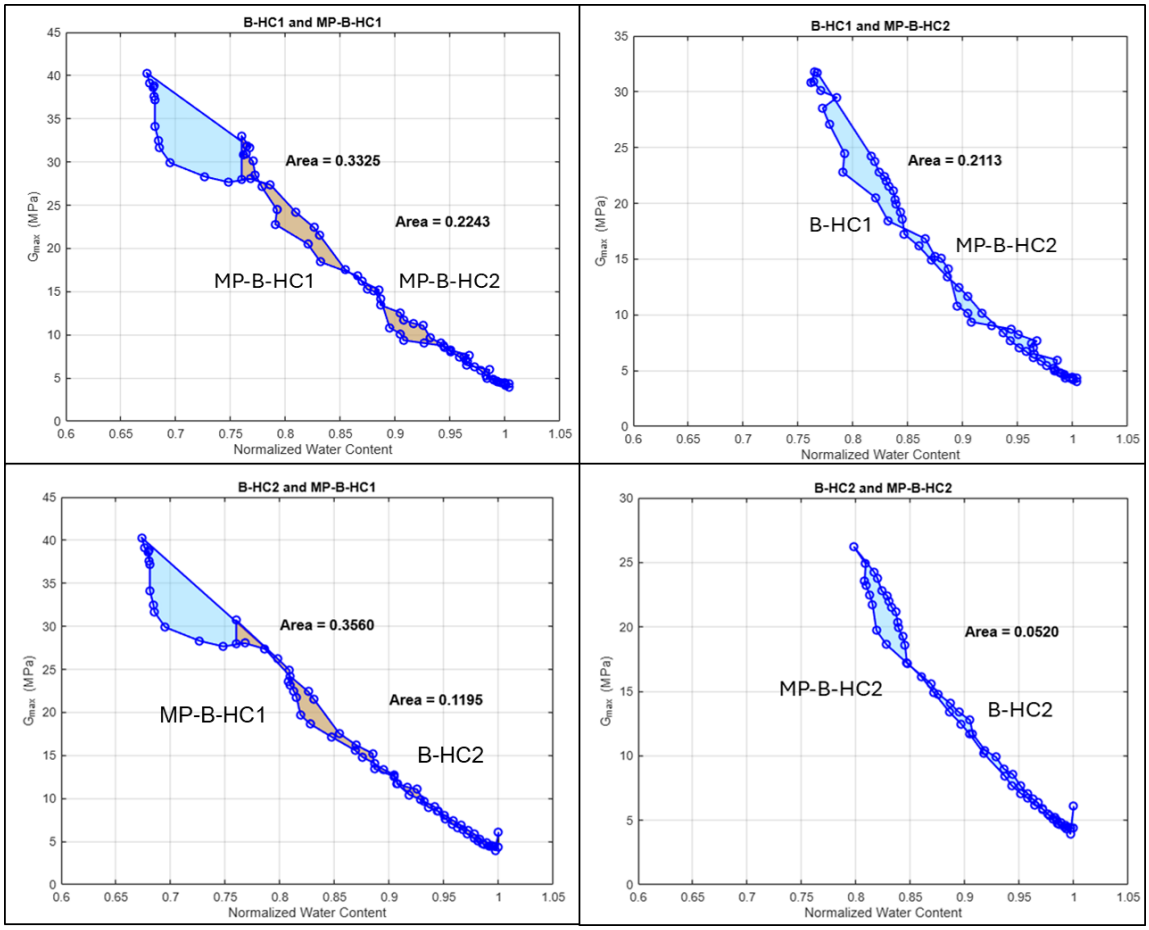

Figure 49: Enclosed Areas for the Effects of Microplastics on Heated Samples

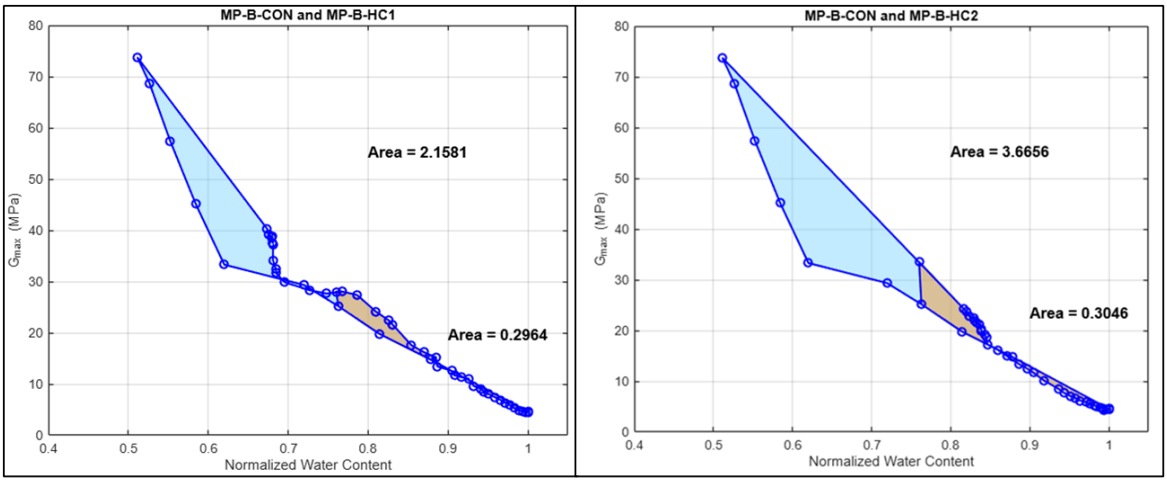

Figure 50: Enclosed Areas for the Effects of Heat on Contaminated Samples

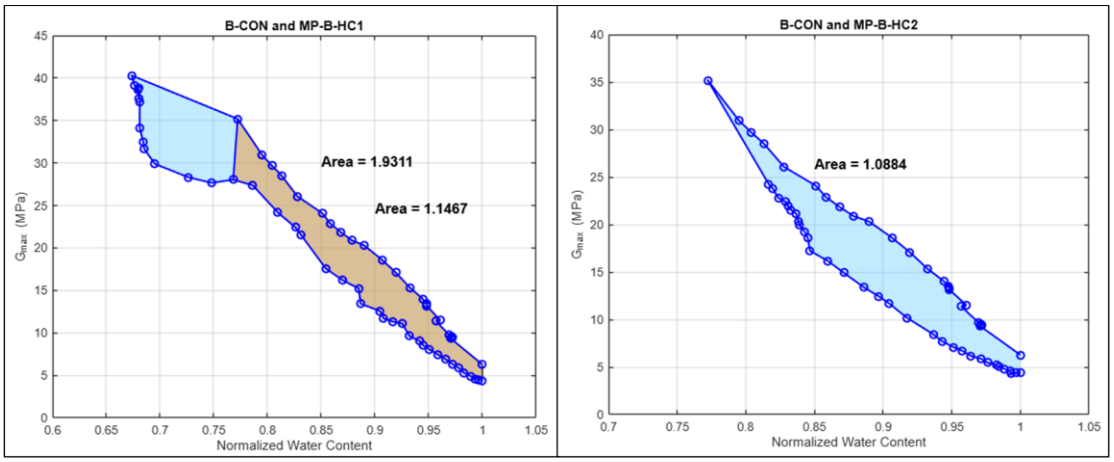

Figure 51: Enclosed Areas for the Effects of Heat and Microplastics

Table 5 summarizes the enclosed area analysis and shows the different scenarios the pair of tests represent. As a result, when there was only microplastic contamination it yielded the largest full and trimmed areas of 5.3 and 1.5 MPa respectively. Indicating that microplastics alone caused the most soil stiffness degradation in Kaolin clay. Whereas when microplastics were added to heated samples, it resulted in the lowest average full and trimmed areas od 0.2 and 0.15 MPa respectively. Showcasing that microplastics have minimal effect to the stiffness of the soil when soil has experienced heat, meaning that microplastics have a much larger effect on their own.

Table 6: Summary of Enclosed Areas

Pair	Full Area (MPa)	Considered Area (MPa) (Normalized W.C. >0.76)	Description	Scenario
B-CON & B-HC1	1.4134	1.4134	Kaolin vs. Kaolin + heat	The effect of heat only
B-CON & B-HC2	1.1984	1.1984		
B-CON & MP-B-CON	5.3238	1.5136	Kaolin vs. Kaolin + MP	The effect of MP contamination
B-HC1 &	0.3326	0.2243		

MP-B-HC1			Kaolin + heat vs. Kaolin + MP + heat	Effects of MP on heated samples
B-HC1 & MP-B-HC2	0.2113	0.2113		
B-HC2 & MP-B-HC1	0.3560	0.1195		
B-HC2 & MP-B-HC2	0.0520	0.0520		
MP-B-CON & MP-B-HC1	2.1581	0.2964	Kaolin + MP vs. Kaolin + MP + heat	The effect of heat on MP contaminated soil
MP-B-CON & MP-B-HC2	3.6656	0.3046		
B-CON & MP-B-HC1	1.9311	1.1467	Kaolin vs Kaolin + MP + heat	The combined effect of MP and heat on soil
B-CON & MP-B-HC2	1.0884	1.0884		

CHAPTER 9

CONCLUSION

This research aimed to explore the effects of heat and microplastic contamination individually and simultaneously in Kaolin clay. By using geophysical methods, it allowed for multiple measurements to be taken in real time in one Shelby tube sample as samples were being heated. Unfortunately, due to the resistivity and bender element caps not being heat-proof, temperatures of samples were only able to reach 60 degrees Celsius. However, the results of heat were still visible in the samples which can be related to soils experiencing extreme heat rather (~60 ˚C) than wildfires (> 200 ˚C).,

As a result of this research, it was shown that heat decreases both the stiffness and electrical resistivity in the pure Kaolin samples. As for the effect of microplastic contamination alone, it had the largest impact on Kaolin's stiffness degradation, based on the enclosed area analysis, and it significantly increased the electrical resistivity. However, it was learned that the electrical resistivity measurements from the resistance meter are material dependent, so no direct conclusions can be made from comparing the results from pure Kaolin samples to the contaminated samples. Lastly, with the combination of heat and microplastics, the stiffness of Kaolin decreases as well. However, as shown in Chapter 8, microplastics have a much larger effect alone rather when there is both heat and microplastic contamination. With heat and microplastic contamination electrical resistivity still increased but was not as extreme in magnitude compared to the sample with just 10% microplastics. After a heat wave in an area contaminated with microplastics, it can be expected that the soil will lose strength, potentially increasing the risk of soil detachment and slope instability. Additionally, if

soil is exposed to heat alone, a decrease in hydraulic conductivity may occur, raising concerns about reduced groundwater recharge and long-term impacts on aquifer sustainability. However, if there was also microplastic contamination it is still inconclusive what it will do the hydraulic conductivity.

It is hoped that this work encourages further studies combining geophysical techniques with heat and microplastic contamination, with future experiments with temperatures going beyond 60 degrees Celsius to look at the potential effects of wildfires rather than extreme heat.

REFERENCES

American Society for Testing and Materials (ASTM) International. (2018). *Standard Test Method for Field Measurement of Soil Resistivity Using the Wenner Four-Electrode Method* (GTJ20180354). https://store.astm.org/gtj20180354.html (accessed February 2, 2025).

ASTM. (2019). *Standard test method for determination of shear wave velocity and initial shear modulus in soil specimens using bender elements (ASTM D8295-19)*. ASTM International, West Conshohocken, PA. https://www.astm.org/d8295-19.html (accessed May 16, 2025).

Ashton, P. J., Hardisty, J. W., & Lewin, J. (2005). Physical and chemical changes in river sediments after wildfire. *Marine Pollution Bulletin*, 50(10), 1025–1033. https://doi.org/10.1016/j.marpolbul.2005.04.031

DeBano, L. F. (2003). The role of fire and soil heating on water repellency in wildland environments: A review. *International Journal of Wildland Fire*, 12(2), 95–101. https://doi.org/10.1071/WF03051

Dike, S., and Apte, S. D. (2024). "Impact of microplastics on strength parameters of clayey, sandy, silty soil: A comparative assessment." *Science of the Total Environment*, 946, 174161. https://doi.org/10.1016/j.scitotenv.2024.174161Geocomp Corporation. (n.d.). *PS-Wave Measurement System*. Retrieved from https://www.geocomp.com/products/ps-wave-measurement-system/ (accessed February 2, 2025).

Humboldt Mfg. Co. (n.d.). *Resistivity Meter*. Retrieved from https://www.humboldtmfg.com/resistivity-meter.html (accessed February 2, 2025).

Kam, T., Kwan, W. S., Tufenkjian, M., & Fuentes, J. (2020). Predicting Soil Strength using Electrical Resistivity Measurements in Clays. GeoVirtual - Resilience and Innovation

Kwan, W. S., Tufenkjian, M., Tuazon, J., Peralta, N., Khov, K., & Garcia, F. (2019). Electrical Resistivity Measurements in Advanced Triaxial Tests. *Geo-Congress 2019: Eighth International Conference on Case Histories in Geotechnical Engineering*. https://doi.org/https://doi.org/10.1061/9780784482124.058Lu, X., Wang, Z., Wang, L., & Wang, Y. (2024). Microplastics in soils: Sources, impacts, and remediation technologies. *Science of The Total Environment*, 924, 171231. https://doi.org/10.1016/j.scitotenv.2024.171231

MathWorks. (2024). MATLAB (Version R2024a) [Software]. The MathWorks, Inc. https://www.mathworks.com (accessed February 9, 2025).

Nanochemazone. (n.d.). *Polyethylene Terephthalate Powder*. Retrieved from https://www.nanochemazone.com/product/polyethylene-terephthalate-powder/ (accessed May 4, 2025).

National Park Service. (n.d.). Weather and climate – Death Valley National Park. U.S. Department of the Interior. https://www.nps.gov/deva/learn/nature/weather-and-climate.htm (accessed May 16, 2025).

Natural History Museum of Utah. *Wildfire FAQs*. Salt Lake City, UT: Natural History Museum of Utah. [Online]. Available: https://nhmu.utah.edu/sites/default/files/attachments/Wildfire%20FAQs.pdf

NOAA. 2024. "Heat wave in Southern California and the Southwest in early September 2024." NOAA Climate.gov.

Nunez, E., Kwan, W. S., & Leal, C. (2025). Laboratory Investigations into the Effects of Heating on Clay's Mechanical and Hydraulic Changes Using Geophysical Methods. *Geo-EnvironMeet 2025*, 47–56. https://doi.org/10.1061/9780784485705.006

Rodríguez, M., González, A., Carranza, A., García, J., & González, J. (2023). Fire-related impacts on soils and vegetation recovery in Mediterranean ecosystems: A review. *Eco-Environment & Health*, 2(2), 99–113. https://doi.org/10.1016/j.eehl.2023.01.004

Suzuki, Y., & Dyvik, R. (2017). Comparisons of Two Reconstitution Methods for Clay Specimens. *Geotechnical Frontiers 2017: Geotechnical Materials, Modeling, and Testing (GSP 280)*, 347–357. https://doi.org/10.1061/9780784480472.037

U.S. Environmental Protection Agency. (2023). *Climate Change Indicators: Wildfires*. Retrieved from https://www.epa.gov/climate-indicators/climate-change-indicators-wildfires

APPENDIX A

All Raw and Calculated Data

This page intentionally left blank

Table 7: All Data for B-CON

Time	Travel Time	Temperature		Scale Reading	Dial Gauge Reading	Sample Height	Sample Volume	Sample Mass	Density	Travel Distance	Shear Wave Velocity	Gmax	AVG Temp	Water Content
		Top	Bottom											
[min]	[ms]	[°C]		[g]	[in]	[mm]	[cm^3]	[g]	[g/cm^3]	[mm]	[m/s]	MPa	[°C]	[%]
0	2.25	22.4	22.1	4754.32	0.568	152.3	452.54	744.21	1.64	141.21	62.76	6.48	22.25	60.38
1131	1.83	21.4	21.3	4746.1	0.541	151.6	450.51	735.99	1.63	140.52	76.79	9.63	21.80	58.60
1275	1.82	21.6	21.7	4746.5	0.538	151.5	450.28	736.39	1.64	140.44	77.17	9.74	21.50	58.69
1346	1.81	21.9	21.8	4746.3	0.536	151.5	450.13	736.19	1.64	140.39	77.56	9.84	21.75	58.64
1570	1.79	21.9	22	4745.7	0.534	151.4	449.98	735.59	1.63	140.34	78.40	10.05	21.90	58.51
2585	1.65	21	21.1	4742.3	0.524	151.2	449.22	732.19	1.63	140.09	84.90	11.75	21.50	57.78
2772	1.64	21.8	21.8	4743.3	0.522	151.1	449.07	733.19	1.63	140.04	85.39	11.90	21.43	57.99
4000	1.53	21.1	21.2	4739.9	0.5085	150.8	448.05	729.79	1.63	139.69	91.30	13.58	21.48	57.26
4086	1.52	21.5	21.5	4739.9	0.5075	150.8	447.98	729.79	1.63	139.67	91.89	13.75	21.33	57.26
4212	1.51	21.8	21.9	4739.7	0.506	150.7	447.86	729.59	1.63	139.63	92.47	13.93	21.68	57.22
4389	1.48	21.6	21.6	4738.8	0.505	150.7	447.79	728.69	1.63	139.60	94.33	14.48	21.73	57.02
5666	1.41	21.3	21.3	4735.5	0.488	150.3	446.51	725.39	1.62	139.17	98.70	15.83	21.45	56.31
7126	1.33	22	22	4731.8	0.4795	150.1	445.86	721.69	1.62	138.96	104.48	17.67	21.65	55.51
8334	1.27	23.2	22.8	4728.2	0.469	149.8	445.07	718.09	1.61	138.69	109.21	19.24	22.50	54.73
10025	1.21	22.2	22.4	4723.5	0.458	149.5	444.24	713.39	1.61	138.41	114.39	21.01	22.65	53.71
11389	1.19	21.8	21.9	4720.4	0.45	149.3	443.64	710.29	1.60	138.21	116.14	21.60	22.08	53.04
12886	1.16	22	22	4717.5	0.443	149.1	443.11	707.39	1.60	138.03	118.99	22.60	21.93	52.42
14326	1.13	22	22	4714.7	0.436	149.0	442.58	704.59	1.59	137.85	121.99	23.69	22.00	51.81
15426	1.1	21.2	21.3	4712.7	0.431	148.8	442.20	702.59	1.59	137.73	125.20	24.91	21.63	51.38
17946	1.05	22.7	22.8	4706.2	0.411	148.3	440.69	696.09	1.58	137.22	130.68	26.98	22.00	49.98
21500	1	21.9	22	4702.1	0.4015	148.1	439.98	691.99	1.57	136.98	136.98	29.51	22.35	49.09
22930	0.98	21.6	21.8	4699.6	0.3935	147.9	439.37	689.49	1.57	136.77	69.94	7.68	21.83	48.55
24166	0.96	21.1	21.1	4697.1	0.386	147.7	438.81	686.99	1.57	136.58	71.47	8.00	21.40	48.01
28709	0.89	21.6	21.6	4690.7	0.357	146.9	436.62	680.59	1.56	135.85	76.41	9.10	21.35	46.62

Table 8: All Data for B-HC1

Time	Travel Time	Temperature		Scale Reading	Dial Gauge Reading	Sample Height	Sample Volume	Sample Mass	Density	Travel Distance	Shear Wave Velocity	Gmax	AVG Temp	Water Content
		Top	Bottom											
[min]	[ms]	[°C]		[g]	[in]	[mm]	[cm^3]	[g]	[g/cm^3]	[mm]	[m/s]	MPa	[°C]	[%]
0	2.67	21.6	21.6	3804.4	0.653	152.31	452.54	737	1.63	141.21	52.89	4.55	21.60	59.37
0.17	2.81	22.5	22.9	3805.5	0.653	152.25	452.37	738.1	1.63	141.15	50.23	4.12	22.15	59.61
7	2.69	25.3	25.8	3805.5	0.650	152.21	452.25	738.1	1.63	141.11	52.46	4.49	24.13	59.61
9	2.75	26.1	26.6	3804.6	0.649	152.18	452.16	737.2	1.63	141.08	51.30	4.29	25.95	59.41
17	2.69	28.1	28.4	3804.6	0.648	152.03	451.71	737.2	1.63	140.93	52.39	4.48	27.30	59.41
23	2.58	29.2	29.7	3802.4	0.642	151.84	451.15	735	1.63	140.74	54.55	4.85	28.85	58.94
33	2.57	30.3	30.6	3801.7	0.634	151.51	450.17	734.3	1.63	140.41	54.63	4.87	29.95	58.79
40	2.49	31.2	31.4	3799.8	0.621	151.12	449.01	732.4	1.63	140.02	56.23	5.16	30.88	58.38
60	2.28	31.7	31.8	3800.5	0.606	150.98	448.59	733.1	1.63	139.88	61.35	6.15	31.53	58.53
85	2.17	34.4	35.2	3794.8	0.600	150.66	447.64	727.4	1.62	139.56	64.31	6.72	33.28	57.29
94	2.08	35.1	36	3794.6	0.588	150.54	447.28	727.2	1.63	139.44	67.04	7.31	35.18	57.25
103	2.03	36.3	37.5	3794.1	0.583	150.40	446.87	726.7	1.63	139.30	68.62	7.66	36.23	57.14
109	2	37.1	38.6	3795.4	0.578	150.31	446.60	728	1.63	139.21	69.60	7.90	37.38	57.42
123	1.92	38	39.6	3790.8	0.574	150.07	445.89	723.4	1.62	138.97	72.38	8.50	38.33	56.43
135	1.86	38.1	39.8	3789.1	0.565	149.84	445.20	721.7	1.62	138.74	74.59	9.02	38.88	56.06
142	1.82	39.2	42.5	3784.1	0.556	149.82	445.14	716.7	1.61	138.72	76.22	9.35	39.90	54.98
150	1.78	41.1	44.8	3779	0.555	149.61	444.52	711.6	1.60	138.51	77.81	9.69	41.90	53.87
164	1.71	42.9	46.7	3778.3	0.546	149.32	443.66	710.9	1.60	138.22	80.83	10.47	43.88	53.72
177	1.65	43.7	47.5	3775.6	0.535	149.10	443.01	708.2	1.60	138.00	83.63	11.18	45.20	53.14
185	1.44	44	47.9	3773.3	0.526	148.91	442.44	705.9	1.60	137.81	95.70	14.61	45.78	52.64
204	1.39	46.7	54.4	3771.5	0.519	148.52	441.28	704.1	1.60	137.42	98.86	15.59	48.25	52.25
212	1.38	48	55.7	3770	0.504	148.34	440.75	702.6	1.59	137.24	99.45	15.76	51.20	51.92
221	1.31	49.1	56.6	3767.6	0.496	148.10	440.03	700.2	1.59	137.00	104.58	17.40	52.35	51.40

246	1.24	52.1	59.3	3758.3	0.487	147.46	438.13	690.9	1.58	136.36	109.96	19.07	54.28	49.39
264	1.17	56.6	57	3755.1	0.462	146.93	436.56	687.7	1.58	135.83	116.09	21.23	56.25	48.70
279	1.1	61.4	57.2	3747	0.441	146.09	434.06	679.6	1.57	134.99	122.71	23.58	58.05	46.94
286	1.06	52.8	64.8	3747.4	0.408	145.72	432.96	680	1.57	134.62	127.00	25.33	59.05	47.03
302	1	57.5	56.7	3743.6	0.393	144.74	430.05	676.2	1.57	133.64	133.64	28.08	57.95	46.21
314	0.97	53	49.8	3742	0.355	144.36	428.92	674.6	1.57	133.26	68.53	7.39	54.25	45.86
322	0.96	50	45.7	3745.5	0.340	144.20	428.45	678.1	1.58	133.10	69.44	7.63	49.63	46.62
341	0.94	40.6	38.6	3741.4	0.333	143.89	427.53	674	1.58	132.79	70.30	7.79	43.73	45.73
355	0.93	36.7	34.9	3739.8	0.321	143.76	427.14	672.4	1.57	132.66	71.28	8.00	37.70	45.39
366	0.93	34.1	32.7	3739.1	0.316	143.69	426.93	671.7	1.57	132.59	71.24	7.98	34.60	45.23
382	0.92	31.5	30.3	3740	0.313	143.64	426.78	672.6	1.58	132.54	72.29	8.24	32.15	45.43
428	0.92	26.6	26.2	3740.7	0.311	142.98	424.82	673.3	1.58	131.88	71.93	8.20	28.65	45.58

Table 9: All Data for B-HC2

Time	Travel Time	Temperature		Scale Reading	Dial Gauge Reading	Sample Height	Sample Volume	Sample Mass	Density	Travel Distance	Shear Wave Velocity	Gmax	AVG Temp	Water Content
		Top	Bottom											
[min]	[ms]	[°C]		[g]	[in]	[mm]	[cm^3]	[g]	[g/cm^3]	[mm]	[m/s]	MPa	[°C]	[%]
0	2.29	22.3	22.3	4642	0.797	152.31	452.54	749.61	1.66	141.21	61.66	6.30	22.30	50.95
3	2.85	25.7	26.7	4641.2	0.796	152.28	452.47	748.81	1.65	141.18	49.54	4.06	26.20	50.79
6	2.68	27.4	28.5	4640.7	0.796	152.28	452.47	748.31	1.65	141.18	52.68	4.59	27.95	50.69
14	2.67	30.1	31.1	4639.9	0.7955	152.27	452.43	747.51	1.65	141.17	52.87	4.62	30.60	50.53
22	2.61	32	32.9	4638.7	0.791	152.15	452.09	746.31	1.65	141.05	54.04	4.82	32.45	50.29
26	2.58	32.5	33.5	4638.3	0.789	152.10	451.94	745.91	1.65	141.00	54.65	4.93	33.00	50.20
34	2.5	33.3	34.3	4637.2	0.7815	151.91	451.37	744.81	1.65	140.81	56.32	5.23	33.80	49.98
42	2.43	33.8	34.8	4636.4	0.774	151.72	450.81	744.01	1.65	140.62	57.87	5.53	34.30	49.82
54	2.31	34.2	35.4	4634.8	0.761	151.39	449.83	742.41	1.65	140.29	60.73	6.09	34.80	49.49
63	2.22	34.4	36.2	4633.7	0.752	151.16	449.15	741.31	1.65	140.06	63.09	6.57	35.30	49.27
72	2.17	37	38.9	4632.6	0.745	150.98	448.62	740.21	1.65	139.88	64.46	6.86	37.95	49.05
83	2.1	38.2	40	4631.4	0.734	150.70	447.79	739.01	1.65	139.60	66.48	7.29	39.10	48.80
95	2.01	39	41	4629.7	0.72	150.35	446.73	737.31	1.65	139.25	69.28	7.92	40.00	48.46
107	1.9	39.3	43.8	4628	0.714	150.20	446.28	735.61	1.65	139.10	73.21	8.83	41.55	48.11
123	1.85	39.8	43.8	4625.9	0.71	150.10	445.98	733.51	1.64	139.00	75.13	9.28	41.80	47.69
135	1.76	41.9	47.2	4624.1	0.707	150.02	445.75	731.71	1.64	138.92	78.93	10.23	44.55	47.32
152	1.71	37.6	46.9	4621.5	0.701	149.87	445.30	729.11	1.64	138.77	81.15	10.78	42.25	46.79
170	1.61	46.4	46.7	4618.7	0.693	149.66	444.69	726.31	1.63	138.56	86.06	12.10	46.55	46.23
184	1.54	52.3	47.4	4618.1	0.685	149.46	444.09	725.71	1.63	138.36	89.84	13.19	49.85	46.10
197	1.5	50.7	50.3	4615.5	0.679	149.31	443.64	723.11	1.63	138.21	92.14	13.84	50.50	45.58
208	1.46	50.8	51.8	4613.5	0.673	149.16	443.18	721.11	1.63	138.06	94.56	14.55	51.30	45.17
225	1.42	53.4	51.7	4610.8	0.6655	148.96	442.62	718.41	1.62	137.86	97.09	15.30	52.55	44.62

236	1.38	53.5	53.5	4609	0.66	148.83	442.20	716.61	1.62	137.73	99.80	16.14	53.50	44.26
261	1.31	53.3	58.1	4603.7	0.646	148.47	441.15	711.31	1.61	137.37	104.86	17.73	55.70	43.18
287	1.25	54.3	61	4598.8	0.628	148.01	439.79	706.41	1.61	136.91	109.53	19.27	57.65	42.19
311	1.21	57.2	62.6	4596.5	0.602	147.35	437.83	704.11	1.61	136.25	112.60	20.39	59.90	41.72
323	1.15	58.3	57.7	4595.6	0.587	146.97	436.69	703.21	1.61	135.87	118.15	22.48	58.00	41.54
337	1.13	51.8	49.8	4595	0.5795	146.78	436.13	702.61	1.61	135.68	120.07	23.23	50.80	41.42
361	1.11	43.8	41.7	4594.1	0.571	146.56	435.49	701.71	1.61	135.46	122.04	24.00	42.75	41.23
379	1.1	39.9	37.8	4593.8	0.568	146.49	435.26	701.41	1.61	135.39	123.08	24.41	38.85	41.17
467	1.07	28.3	27.4	4594	0.56	146.29	434.66	701.61	1.61	135.19	126.34	25.77	27.85	41.21
1352	1.04	21	21.1	4591.3	0.552	146.08	434.05	698.91	1.61	134.98	129.79	27.12	21.05	40.67

Table 10: All Data for R-CON

Time	Temperature		Meter Reading	Multiplier	Scale Reading	Dial Gauge Reading	Sample Height	Sample Volume	Sample Mass	Density	Resistivity	AVG Temp	Water Content
	Top	Bottom											
[min]	[°C]		[ohms]	[-]	[g]	[in]	[mm]	[cm^3]	[g]	[g/cm^3]	[Ωm]	[°C]	[%]
0	20.3	20.9	4.4	1000	7567	0.078	152.31	452.54	737.8	1.63	85.84	20.6	62.28
2614	20.6	20.5	5.05	1000	7542.3	0.0393	148.78	442.08	713.1	1.61	100.85	20.55	56.89
2702	20.6	20.3	5.1	1000	7541.7	0.091	150.10	445.98	712.5	1.60	100.96	20.45	56.76
3712	20.7	20.5	5.2	1000	7537.8	0.076	149.71	444.85	708.6	1.59	103.20	20.6	55.91
6678	20.7	20.5	5.5	1000	7528.5	0.042	148.85	442.28	699.3	1.58	109.79	20.6	53.87
7068	20.6	20.4	5.5	1000	7527.4	0.039	148.77	442.05	698.2	1.58	109.85	20.5	53.63
8418	20.7	20.5	5.6	1000	7523.4	0.028	148.50	441.22	694.2	1.57	112.05	20.6	52.76
9542	20.9	20.5	5.7	1000	7520.4	0.019	148.27	440.54	691.2	1.57	114.23	20.7	52.11
9752	20.9	21.1	5.7	1000	7520	0.085	147.40	437.98	690.8	1.58	114.90	21	52.02
9825	21.3	21.1	5.7	1000	7520.6	0.0175	145.69	432.88	691.4	1.60	116.25	21.2	52.15
11325	21.7	21.8	5.7	1000	7516.8	0.006	145.40	432.02	687.6	1.59	116.48	21.75	51.32
11413	21.7	21.4	5.75	1000	7516.6	0.005	145.37	431.94	687.4	1.59	117.53	21.55	51.28
11501	21.1	21.4	5.8	1000	7516.3	0.004	145.35	431.86	687.1	1.59	118.57	21.25	51.21
12419	21	20.7	6	1000	7514	0.097	145.17	431.34	684.8	1.59	122.81	20.85	50.71
14073	21.8	21.5	6.1	1000	7510.4	0.0845	144.85	430.39	681.2	1.58	125.13	21.65	49.92
16837	21.3	21	6.55	1000	7505.6	0.07	144.48	429.30	676.4	1.58	134.70	21.15	48.87
18182	20.9	20.7	6.9	1000	7503.8	0.064	144.33	428.85	674.6	1.57	142.05	20.8	48.48
18474	21.8	21.7	6.9	1000	7502.8	0.0625	144.29	428.73	673.6	1.57	142.09	21.75	48.26
19669	21.6	21.6	7.2	1000	7500.3	0.0565	144.14	428.28	671.1	1.57	148.42	21.6	47.72
21362	22.3	22.3	7.55	1000	7497.7	0.048	143.92	427.64	668.5	1.56	155.87	22.3	47.15
22502	21.8	21.6	8.1	1000	7495.3	0.042	143.77	427.19	666.1	1.56	167.40	21.7	46.63
22949	22	21.8	8.25	1000	7494.5	0.04	143.72	427.03	665.3	1.56	170.56	21.9	46.45
24310	22.4	22.5	8.6	1000	7494.5	0.034	143.57	426.58	665.3	1.56	177.99	22.45	46.45

25542	21.6	21.8	9.05	1000	7492.3	0.029	143.44	426.20	663.1	1.56	187.47	21.7	45.97
25649	21.9	22.1	9.05	1000	7492.1	0.0285	143.43	426.17	662.9	1.56	187.48	22	45.93
28262	20.7	20.5	10	1000	7488.1	0.018	143.16	425.37	658.9	1.55	207.55	20.6	45.05
28641	21.9	21.8	9.75	1000	7488.1	0.0165	143.12	425.26	658.9	1.55	202.41	21.85	45.05
29702	20.7	20.5	10.3	1000	7486.5	0.0125	143.02	424.96	657.3	1.55	213.98	20.6	44.70
30149	21.9	22	10.05	1000	7486.5	0.011	142.98	424.85	657.3	1.55	208.85	21.95	44.70
31495	21.9	21.8	10.35	1000	7484.9	0.005	142.83	424.39	655.7	1.55	215.31	21.85	44.35
32780	20.8	21	10.85	1000	7483	0.098	145.19	431.41	653.8	1.52	222.04	20.9	43.94
34022	21.3	21.1	1.2	10000	7481.3	0.091	145.02	430.88	652.1	1.51	245.87	21.2	43.57
35372	21.1	20.9	1.25	10000	7479.6	0.078	144.69	429.90	650.4	1.51	256.70	21	43.20
36827	21	20.9	1.25	10000	7477.8	0.065	144.35	428.92	648.6	1.51	257.29	20.95	42.80
38342	21.1	21.1	1.55	10000	7476.1	0.062	144.28	428.69	646.9	1.51	319.21	21.1	42.43

Table 11: All Data for R-HC1

Time	Temperature		Meter Reading	Multiplier	Scale Reading	Dial Gauge Reading	Sample Height	Sample Volume	Sample Mass	Density	Resistivity	AVG Temp	Water Content
	Top	Bottom											
[min]	[°C]		[ohms]	[-]	[g]	[in]	[mm]	[cm^3]	[g]	[g/cm^3]	[Ωm]	[°C]	[%]
0	21.6	21.8	3.95	1000	7306.6	0.607	152.31	452.54	732	1.62	77.06	21.7	49.67
1	22.6	25.5	3.85	1000	7306.6	0.602	152.18	452.17	732	1.62	75.17	24.05	49.67
6	25.4	29.6	3.7	1000	7306.6	0.603	152.20	452.24	732	1.62	72.23	27.5	49.67
17	29.4	34	3.55	1000	7306.6	0.598	152.08	451.86	732	1.62	69.36	31.7	49.67
24	31	35.4	3.5	1000	7305.9	0.588	151.82	451.11	731.3	1.62	68.50	33.2	49.52
38	33	37.1	3.35	1000	7301.3	0.5635	151.20	449.26	726.7	1.62	65.83	35.05	48.58
54	37	44.1	3.15	1000	7299	0.541	150.63	447.56	724.4	1.62	62.14	40.55	48.10
62	39.3	46.4	3.05	1000	7297.7	0.526	150.25	446.43	723.1	1.62	60.32	42.85	47.83
76	41.5	48.4	3	1000	7295.3	0.5	149.59	444.47	720.7	1.62	59.59	44.95	47.34
100	43.9	50.3	3.05	1000	7290.3	0.446	148.22	440.39	715.7	1.63	61.14	47.1	46.31
113	44.2	50.4	3.1	1000	7288.1	0.419	147.53	438.35	713.5	1.63	62.43	47.3	45.86
123	48.4	57.5	3.05	1000	7286.2	0.408	147.25	437.52	711.6	1.63	61.54	52.95	45.47
145	58.2	56.9	3.1	1000	7282.2	0.396	146.95	436.62	707.6	1.62	62.68	57.55	44.64
156	59.2	57.4	3.25	1000	7279.5	0.3945	146.91	436.51	704.9	1.61	65.73	58.3	44.09
165	59.5	57.6	3.3	1000	7277.1	0.39	146.79	436.17	702.5	1.61	66.80	58.55	43.59
184	59.8	57.9	3.4	1000	7272.9	0.381	146.56	435.49	698.3	1.60	68.93	58.85	42.73
200	53.5	53	3.45	1000	7271.9	0.374	146.39	434.96	697.3	1.60	70.03	53.25	42.52
209	50.1	50	3.55	1000	7271.4	0.37	146.29	434.66	696.8	1.60	72.11	50.05	42.42
218	47.3	47.2	3.7	1000	7271	0.368	146.23	434.51	696.4	1.60	75.18	47.25	42.34
228	44.9	44.8	3.9	1000	7270.8	0.366	146.18	434.35	696.2	1.60	79.27	44.85	42.29
237	42.6	42.7	4	1000	7270.6	0.3645	146.15	434.24	696	1.60	81.32	42.65	42.25
244	40.9	40.8	4.2	1000	7270.4	0.363	146.11	434.13	695.8	1.60	85.41	40.85	42.21

258	38.4	38.3	4.4	1000	7270.4	0.3615	146.07	434.02	695.8	1.60	89.50	38.35	42.21
266	37.4	37.2	4.5	1000	7270.3	0.36	146.03	433.90	695.7	1.60	91.56	37.3	42.19
278	35.3	35.1	4.65	1000	7270.9	0.359	146.01	433.83	696.3	1.61	94.63	35.2	42.32
291	33.7	33.5	4.75	1000	7270.8	0.358	145.98	433.75	696.2	1.61	96.68	33.6	42.29
305	32.1	32	4.95	1000	7270.7	0.357	145.96	433.68	696.1	1.61	100.77	32.05	42.27
318	31	30.7	5	1000	7270.8	0.3356	145.41	432.06	696.2	1.61	102.17	30.85	42.29
330	29.9	29.7	5.1	1000	7270.7	0.3555	145.92	433.56	696.1	1.61	103.85	29.8	42.27
341	29.1	29	5.75	1000	7270.8	0.355	145.90	433.52	696.2	1.61	117.10	29.05	42.29
357	28.2	28	5.3	1000	7270.8	0.354	145.88	433.45	696.2	1.61	107.95	28.1	42.29
369	27.5	27.3	5.4	1000	7270.8	0.353	145.85	433.37	696.2	1.61	110.01	27.4	42.29
383	26.8	26.7	5.5	1000	7270.8	0.353	145.85	433.37	696.2	1.61	112.04	26.75	42.29

Table 12: All Data for R-HC2

Time	Temperature		Meter Reading	Multiplier	Scale Reading	Dial Gauge Reading	Sample Height	Sample Volume	Sample Mass	Density	Resistivity	AVG Temp	Water Content
	Top	Bottom											
[min]	[°C]		[ohms]	[-]	[g]	[in]	[mm]	[cm^3]	[g]	[g/cm^3]	[Ωm]	[°C]	[%]
0	22	22	3.9	1000	8055	0.587	152.31	452.54	740.14	1.64	76.08	22.00	50.74
2	24.2	26	3.8	1000	8055	0.587	149.77	445.00	740.14	1.66	75.39	25.10	50.74
9	26.8	28.8	3.7	1000	8054.2	0.5865	149.75	444.96	739.34	1.66	73.41	27.80	50.58
14	29	31.1	3.6	1000	8053.7	0.585	149.71	444.85	738.84	1.66	71.45	30.05	50.48
20	30.6	32.6	3.5	1000	8052.9	0.5805	149.60	444.51	738.04	1.66	69.52	31.60	50.32
30	32.3	34.3	3.4	1000	8051.6	0.569	149.31	443.64	736.74	1.66	67.66	33.30	50.06
39	33.2	35.2	3.35	1000	8050.6	0.557	149.00	442.73	735.74	1.66	66.80	34.20	49.85
62	36.5	40.1	3.25	1000	8047	0.527	148.24	440.47	732.14	1.66	65.14	38.30	49.13
72	38.1	41.8	3.15	1000	8045.3	0.513	145.35	431.86	730.44	1.69	64.40	39.95	48.78
90	41.7	46	3.05	1000	8042.1	0.492	144.81	430.28	727.24	1.69	62.58	43.85	48.14
110	43.8	48.4	3	1000	8037.6	0.478	144.46	429.22	722.74	1.68	61.71	46.10	47.23
153	48.2	53.9	2.95	1000	8028.7	0.445	143.62	426.73	713.84	1.67	61.03	51.05	45.43
164	48.8	54.6	3	1000	8026.7	0.437	143.42	426.13	711.84	1.67	62.15	51.70	45.03
180	50.5	51.3	3.05	1000	8023.1	0.426	140.60	417.75	708.24	1.70	64.46	50.90	44.30
230	56.9	57.3	3.1	1000	8011.5	0.391	139.71	415.11	696.64	1.68	65.93	57.10	41.96
236	57	57.6	3.15	1000	8009.4	0.385	139.55	414.66	694.54	1.67	67.07	57.30	41.53
248	57	57.9	3.25	1000	8006.9	0.374	139.27	413.83	692.04	1.67	69.34	57.45	41.03
261	58.6	59.6	3.3	1000	8003.5	0.364	139.02	413.07	688.64	1.67	70.53	59.10	40.34
279	60.1	61.9	3.4	1000	7998.8	0.349	138.64	411.94	683.94	1.66	72.87	61.00	39.39
286	59.9	60.9	3.25	1000	7997.9	0.345	138.54	411.64	683.04	1.66	69.70	60.40	39.21
297	56.6	56.4	3.3	1000	7997.6	0.341	138.44	411.34	682.74	1.66	70.83	56.50	39.15
304	53.8	53.3	3.45	1000	7997.5	0.338	138.36	411.11	682.64	1.66	74.09	53.55	39.13
312	51.1	50.6	3.6	1000	7997.4	0.3355	138.30	410.92	682.54	1.66	77.35	50.85	39.11
317	49.4	48.7	3.7	1000	7997.3	0.333	138.23	410.73	682.44	1.66	79.53	49.05	39.09

330	45.8	44.8	4.05	1000	7996.9	0.331	138.18	410.58	682.04	1.66	87.09	45.30	39.01
339	43.6	42.6	4.25	1000	7996.8	0.329	138.13	410.43	681.94	1.66	91.42	43.10	38.99
345	42.4	41.3	4.4	1000	7996.7	0.328	138.11	410.36	681.84	1.66	94.66	41.85	38.97
355	40.2	39.2	4.5	1000	7996.6	0.326	138.06	410.20	681.74	1.66	96.85	39.70	38.95
368	37.8	36.9	4.7	1000	7996.5	0.324	138.00	410.05	681.64	1.66	101.19	37.35	38.93
378	36.3	35.3	4.95	1000	7996.3	0.323	137.98	409.98	681.44	1.66	106.60	35.80	38.89
393	34.3	33.4	5.15	1000	7996.3	0.322	137.95	409.90	681.44	1.66	110.92	33.85	38.89
416	31.6	30.9	5.45	1000	7996.2	0.3215	137.94	409.86	681.34	1.66	117.39	31.25	38.87
1376	21.3	21.3	7.7	1000	7989.4	0.2985	137.36	408.13	674.54	1.65	166.57	21.30	37.49

Table 13: All Data for MP-B-CON

Time	Travel Time	Temperature		Scale Reading	Dial Gauge Reading	Sample Height	Sample Volume	Sample Mass	Density	Travel Distance	Shear Wave Velocity	Gmax	AVG Temp	Water Content
		Top	Bottom											
[min]	[ms]	[°C]		[g]	[in]	[mm]	[cm^3]	[g]	[g/cm^3]	[mm]	[m/s]	MPa	[°C]	[%]
0	1.24	22.9	22.9	5780.3	0.66	76.50	227.30	371.8	1.64	65.40	52.74	4.55	22.90	53.47
3600	0.65556	22.2	22.2	5764.3	0.539	73.43	218.17	355.8	1.63	62.33	95.07	14.74	22.20	46.97
7200	0.55	22.2	22.3	5755.8	0.473	71.75	213.19	347.3	1.63	60.65	110.27	19.81	22.25	43.52
10800	0.48	22	22	5749.1	0.445	71.04	211.08	340.6	1.61	59.94	124.87	25.16	22.00	40.80
14400	0.43889	22.1	22.1	5743.4	0.427	70.58	209.72	334.9	1.60	59.48	135.53	29.33	22.10	38.48
25200	0.39722	23	23	5730.3	0.361	68.91	204.74	321.8	1.57	57.81	145.52	33.29	23.00	33.16
28800	0.33611	23	23	5725.6	0.331	68.14	202.47	317.1	1.57	57.04	169.72	45.11	23.00	31.25
32400	0.29444	22.7	22.7	5721.4	0.311	67.64	200.96	312.9	1.56	56.54	192.01	57.40	22.70	29.54
36000	0.26667	22.5	22.6	5718	0.295	67.23	199.76	309.5	1.55	56.13	210.48	68.64	22.55	28.16
39600	0.25556	23.6	23.6	5716	0.2815	66.89	198.74	307.5	1.55	55.79	218.29	73.73	23.60	27.35

Table 14: All Data for MP-B-HC1

Time	Travel Time	Temperature		Scale Reading	Dial Gauge Reading	Sample Height	Sample Volume	Sample Mass	Density	Travel Distance	Shear Wave Velocity	Gmax	AVG Temp	Water Content
		Top	Bottom											
[min]	[ms]	[°C]		[g]	[in]	[mm]	[cm^3]	[g]	[g/cm^3]	[mm]	[m/s]	MPa	[°C]	[%]
0	1.25	20.6	21	5785	0.814	76.50	227.30	365	1.61	65.40	52.32	4.40	20.80	50.52
3	1.24	25.4	22.8	5784.6	0.8115	76.44	227.12	364.6	1.61	65.34	52.69	4.46	24.10	50.36
6	1.22	28.6	25.6	5784.2	0.808	76.35	226.85	364.2	1.61	65.25	53.48	4.59	27.10	50.19
10	1.18	30.9	28	5783.7	0.803	76.22	226.47	363.7	1.61	65.12	55.19	4.89	29.45	49.98
15	1.13	32.7	29.9	5782.9	0.795	76.02	225.87	362.9	1.61	64.92	57.45	5.30	31.30	49.64
20	1.07	33.8	31.2	5782.3	0.788	75.84	225.34	362.3	1.61	64.74	60.50	5.89	32.50	49.39
24	1.03	35.3	32.4	5781.6	0.781	75.66	224.81	361.6	1.61	64.56	62.68	6.32	33.85	49.10
30	0.99	36.7	33.9	5780.9	0.772	75.43	224.13	360.9	1.61	64.33	65.24	6.85	35.30	48.81
35	0.94	38.2	35.1	5780	0.7635	75.22	223.49	360	1.61	64.12	67.89	7.42	36.65	48.43
40	0.90	39.3	36.2	5779	0.755	75.00	222.85	359	1.61	63.90	70.78	8.07	37.75	48.01
45	0.88	41	37.7	5778.3	0.745	74.75	222.10	358.3	1.61	63.65	72.74	8.54	39.35	47.72
50	0.85	42.1	38.6	5777.9	0.7365	74.53	221.46	357.9	1.62	63.43	74.87	9.06	40.35	47.55
55	0.82	43.4	39.8	5776.8	0.728	74.32	220.81	356.8	1.62	63.22	77.14	9.62	41.60	47.09
60	0.76	44.5	40.8	5776	0.72	74.11	220.21	356	1.62	63.01	82.73	11.06	42.65	46.76
65	0.75	46.1	42	5774.9	0.711	73.88	219.53	354.9	1.62	62.78	83.71	11.33	44.05	46.30
70	0.74	47	43	5773.9	0.703	73.68	218.93	353.9	1.62	62.58	85.02	11.68	45.00	45.88
75	0.71	47.5	43.6	5773.5	0.695	73.48	218.32	353.5	1.62	62.38	88.06	12.56	45.55	45.71
85	0.68	49.4	45.2	5771.3	0.682	73.15	217.34	351.3	1.62	62.05	91.17	13.44	47.30	44.79
87	0.64	49.5	45.4	5771.1	0.68	73.10	217.19	351.1	1.62	62.00	97.04	15.22	47.45	44.70
95	0.62	51	46.4	5769.3	0.672	72.89	216.59	349.3	1.61	61.79	100.20	16.19	48.70	43.95
105	0.59	52.2	47.8	5767.4	0.661	72.61	215.76	347.4	1.61	61.51	104.46	17.57	50.00	43.16
116	0.53	53.9	49.1	5764.6	0.647	72.26	214.70	344.6	1.61	61.16	115.88	21.55	51.50	41.98

120	0.52	54	49.4	5764	0.643	72.16	214.40	344	1.60	61.06	118.17	22.40	51.70	41.73
130	0.49	56	50.9	5762	0.63	71.83	213.42	342	1.60	60.73	122.82	24.17	53.45	40.90
141	0.46	56.5	51.6	5759.2	0.615	71.45	212.29	339.2	1.60	60.35	130.87	27.37	54.05	39.72
150	0.45	57.5	52.4	5757	0.603	71.14	211.38	337	1.59	60.04	132.60	28.03	54.95	38.80
160	0.45	58.6	53.2	5754.6	0.59	70.81	210.40	334.6	1.59	59.71	131.88	27.66	55.90	37.80
170	0.44	60.3	55	5752	0.577	70.48	209.42	332	1.59	59.38	133.61	28.30	57.65	36.71
180	0.43	60.5	56	5748.2	0.556	69.95	207.83	328.2	1.58	58.85	137.56	29.88	58.25	35.12
186	0.41	60.3	56.2	5747	0.547	69.72	207.15	327	1.58	58.62	141.63	31.66	58.25	34.62
190	0.41	53.1	52.7	5746.9	0.542	69.59	206.78	326.9	1.58	58.49	143.24	32.44	52.90	34.58
198	0.40	46.7	45.7	5746.5	0.537	69.46	206.40	326.5	1.58	58.36	146.93	34.15	46.20	34.41
204	0.38	42.8	42	5746.5	0.534	69.39	206.17	326.5	1.58	58.29	153.16	37.15	42.40	34.41
214	0.37	38.1	37.6	5746.4	0.531	69.31	205.95	326.4	1.58	58.21	156.39	38.76	37.85	34.37
227	0.38	34.1	33.8	5746.4	0.529	69.26	205.79	326.4	1.59	58.16	153.95	37.59	33.95	34.37
264	0.37	27.6	27.7	5746.3	0.525	69.16	205.49	326.3	1.59	58.06	155.98	38.63	27.65	34.32
287	0.37	25.5	25.6	5745.9	0.524	69.13	205.42	325.9	1.59	58.03	157.09	39.15	25.55	34.16
349	0.36	22.8	22.9	5745.6	0.523	69.11	205.34	325.6	1.59	58.01	159.41	40.29	22.85	34.03

Table 15: All Data for MP-B-HC2

Time	Travel Time	Temperature		Scale Reading	Dial Gauge Reading	Sample Height	Sample Volume	Sample Mass	Density	Travel Distance	Shear Wave Velocity	Gmax	AVG Temp	Water Content
		Top	Bottom											
[min]	[ms]	[°C]		[g]	[in]	[mm]	[cm^3]	[g]	[g/cm^3]	[mm]	[m/s]	MPa	[°C]	[%]
0	1.24	20	20.1	5205.5	0.935	76.5	227.3042	357.7	1.57	65.40	52.74	4.38	20.05	56.81
1	1.24	23.4	22.7	5205.1	0.933	76.4492	227.1533	357.3	1.57	65.35	52.70	4.37	23.05	56.63
4	1.24	28.7	27	5204.6	0.931	76.3984	227.0023	356.8	1.57	65.30	52.66	4.36	27.85	56.41
6	1.21	30.3	28.8	5204.5	0.928	76.3222	226.7759	356.7	1.57	65.22	53.90	4.57	29.55	56.37
8	1.18	31.6	30.2	5204	0.925	76.246	226.5495	356.2	1.57	65.15	55.21	4.79	30.90	56.15
10	1.15	33.8	32	5203.5	0.921	76.1444	226.2476	355.7	1.57	65.04	56.56	5.03	32.90	55.93
12	1.13	35.4	33.7	5203.2	0.918	76.0682	226.0212	355.4	1.57	64.97	57.49	5.20	34.55	55.80
14	1.1	36.8	35.1	5202.4	0.911	75.8904	225.4929	354.6	1.57	64.79	58.90	5.46	35.95	55.45
17	1.06	38.3	36.9	5201.8	0.909	75.8396	225.342	354	1.57	64.74	61.08	5.86	37.60	55.19
20	1.03	41.3	39.2	5200.8	0.904	75.7126	224.9646	353	1.57	64.61	62.73	6.17	40.25	54.75
23	0.99	42.8	40.9	5200	0.899	75.5856	224.5872	352.2	1.57	64.49	65.39	6.71	41.85	54.40
25	0.96	45.5	43	5199.2	0.896	75.5094	224.3608	351.4	1.57	64.41	67.21	7.07	44.25	54.05
28	0.92	47.8	45.1	5198.1	0.892	75.4078	224.059	350.3	1.56	64.31	70.15	7.69	46.45	53.57
30	0.88	49.2	46.7	5197.3	0.89	75.357	223.908	349.5	1.56	64.26	73.44	8.42	47.95	53.22
36	0.79	53.5	50.8	5194.8	0.88	75.103	223.1533	347	1.55	64.00	80.85	10.16	52.15	52.12
41	0.74	55.5	52.9	5193.1	0.875	74.976	222.7759	345.3	1.55	63.88	86.78	11.67	54.20	51.38
44	0.71	55.8	53.3	5192.1	0.871	74.8744	222.4741	344.3	1.55	63.77	89.68	12.45	54.55	50.94
48	0.68	56.6	54	5190.7	0.864	74.6966	221.9458	342.9	1.54	63.60	93.07	13.38	55.30	50.33
52	0.64	59.4	56.1	5188.8	0.857	74.5188	221.4175	341	1.54	63.42	98.41	14.91	57.75	49.50
56	0.62	60.9	57.4	5187.3	0.849	74.3156	220.8137	339.5	1.54	63.22	102.51	16.16	59.15	48.84
60	0.59	62.5	58.7	5185.6	0.841	74.1124	220.2099	337.8	1.53	63.01	106.00	17.24	60.60	48.10
63	0.57	57.9	55.5	5185.4	0.838	74.0362	219.9835	337.6	1.53	62.94	109.99	18.56	56.70	48.01

69	0.56	49.5	48.3	5185.1	0.832	73.8838	219.5307	337.3	1.54	62.78	111.89	19.24	48.90	47.88
77	0.55	43.1	42.3	5184.6	0.826	73.7314	219.0779	336.8	1.54	62.63	113.88	19.94	42.70	47.66
80	0.54	41.4	40.7	5184.5	0.825	73.706	219.0024	336.7	1.54	62.61	114.99	20.33	41.05	47.61
85	0.53	38.9	38.2	5184.3	0.822	73.6298	218.776	336.5	1.54	62.53	117.24	21.14	38.55	47.53
99	0.53	33.8	33.4	5183.8	0.82	73.579	218.625	336	1.54	62.48	118.38	21.54	33.60	47.31
109	0.52	30.6	30.3	5183.5	0.818	73.5282	218.4741	335.7	1.54	62.43	119.54	21.96	30.45	47.18
122	0.52	28.4	28	5183.3	0.815	73.452	218.2477	335.5	1.54	62.35	120.68	22.39	28.20	47.09
153	0.51	24.5	24.5	5182.6	0.8125	73.3885	218.059	334.8	1.54	62.29	121.87	22.80	24.50	46.78
195	0.50	22.2	22.3	5182.1	0.81	73.325	217.8703	334.3	1.53	62.23	124.45	23.76	22.25	46.56
240	0.49	21.2	21.3	5181.7	0.808	73.2742	217.7194	333.9	1.53	62.17	125.75	24.25	21.25	46.39

Table 16: All Data for MP-R-CON

Time	Temperature		Meter Reading	Multiplier	Scale Reading	Dial Gauge Reading	Sample Height	Sample Volume	Sample Mass	Density	Resistivity	AVG Temp	Water Content
	Top	Bottom											
[min]	[°C]		[ohms]	[-]	[g]	[in]	[mm]	[cm^3]	[g]	[g/cm^3]	[Ωm]	[°C]	[%]
0	21.3	21.2	4.1	1000	1061.2	0.583	76.50	227.30	376.2	1.66	159.245971	21.25	54.17
3600	20.1	19.7	4.6	1000	1043.7	0.48	71.34	211.98	358.7	1.69	191.578878	19.90	47.02
10800	21.2	20.8	5.25	1000	1033.3	0.435	70.20	208.59	348.3	1.67	222.209834	21.00	42.76
14400	21.1	20.6	5.5	1000	1028.2	0.425	69.95	207.83	343.2	1.65	233.636596	20.85	40.68
25200	21.1	20.6	6.25	1000	1019.1	0.394	69.16	205.49	334.1	1.63	268.518883	20.85	36.96
28800	20.8	20.2	6.7	1000	1016.5	0.383	68.88	204.66	331.5	1.62	289.019867	20.50	35.90
32400	20.6	20.1	8	1000	1013.8	0.373	68.63	203.91	328.8	1.61	346.375633	20.35	34.79
36000	20.2	19.8	9.4	1000	1011.4	0.3675	65.95	195.95	326.4	1.67	423.529291	20.00	33.81
46800	23.2	21.7	1.4	10000	1006.4	0.349	65.48	194.55	321.4	1.65	635.315242	22.45	31.77
50400	20	20	1.6	10000	1004.7	0.343	65.32	194.10	319.7	1.65	727.768484	20.00	31.07
54000	19.7	19.7	1.7	10000	1003.4	0.34	65.25	193.87	318.4	1.64	774.157063	19.70	30.54
57600	20.1	20.1	1.8	10000	1002.2	0.337	65.17	193.64	317.2	1.64	820.654119	20.10	30.05
61200	19.9	19.9	1.95	10000	1001.1	0.335	62.58	185.95	316.1	1.70	925.847659	19.90	29.60
72000	19.6	19.6	2.2	10000	998.3	0.329	62.43	185.49	313.3	1.69	1047.09602	19.60	28.45
75600	19.4	19.4	2.3	10000	997.4	0.323	62.28	185.04	312.4	1.69	1097.37019	19.40	28.09
79200	20.2	20.2	2.35	10000	997.2	0.3215	62.24	184.93	312.2	1.69	1121.91244	20.20	28.00
86400	20.1	20.1	2.5	10000	995.6	0.319	62.17	184.74	312.2	1.69	1194.74284	20.10	28.00
93600	20.8	20.8	2.6	10000	994.4	0.317	62.12	184.59	311	1.68	1243.54861	20.80	27.51
104400	21.2	21.2	2.75	10000	992.6	0.316	62.10	184.51	309.2	1.68	1315.82979	21.20	26.78
122400	22.3	22.3	2.85	10000	989.1	0.3155	62.09	184.47	305.7	1.66	1363.95709	22.30	25.35
129600	22.9	22.9	2.85	10000	987.6	0.316	62.10	184.51	304.2	1.65	1363.67814	22.90	24.73

Table 17: All Data for MP-R-HC

Time	Temperature		Meter Reading	Multiplier	Scale Reading	Dial Gauge Reading	Sample Height	Sample Volume	Sample Mass	Density	Resistivity	AVG Temp	Water Content
	Top	Bottom											
[min]	[°C]		[ohms]	[-]	[g]	[in]	[mm]	[cm^3]	[g]	[g/cm^3]	[Ωm]	[°C]	[%]
0	21	20.9	3.1	1000	10140	0.7365	76.50	227.30	371.1	1.63	120.41	20.95	49.92
1	23	23.2	3	1000	10139.6	0.723	73.62	218.74	370.7	1.69	121.08	23.10	49.75
9	28.5	28.5	2.9	1000	10138.3	0.712	73.34	217.91	369.4	1.70	117.49	28.50	49.21
15.5	31.8	31.9	2.8	1000	10137	0.695	72.91	216.63	368.1	1.70	114.11	31.85	48.68
19	33.1	33.2	2.75	1000	10136.2	0.685	72.65	215.87	367.3	1.70	112.47	33.15	48.35
24	34.8	35.1	2.65	1000	10135.1	0.672	72.32	214.89	366.2	1.70	108.87	34.95	47.89
38	39.1	39.3	2.55	1000	10131.3	0.632	71.31	211.87	362.4	1.71	106.26	39.20	46.32
55	45.3	45.3	2.5	1000	10125.4	0.584	70.09	208.25	356.5	1.71	105.99	45.30	43.88
67	47.4	47.4	2.6	1000	10122.6	0.5655	67.08	199.30	353.7	1.77	115.17	47.40	42.73
73	48.1	48.1	2.7	1000	10120.9	0.561	66.96	198.96	352.0	1.77	119.81	48.10	42.02
81	50.2	50.1	2.8	1000	10118.1	0.552	66.73	198.29	349.2	1.76	124.67	50.15	40.87
86	51.8	51.4	2.9	1000	10116.3	0.546	66.58	197.83	347.4	1.76	129.42	51.60	40.12
91	52.5	52	3	1000	10114.7	0.5415	66.47	197.49	345.8	1.75	134.11	52.25	39.46
107	54.4	55	3.45	1000	10108.1	0.513	63.20	187.80	339.2	1.81	162.19	54.70	36.74
114	54.5	55.4	3.8	1000	10104.8	0.497	62.80	186.59	335.9	1.80	179.80	54.95	35.37
128	54.5	56	4.6	1000	10098.3	0.463	61.93	184.02	329.4	1.79	220.69	55.25	32.69
142	54.3	56.2	6.5	1000	10090.5	0.428	61.04	181.38	329.4	1.82	316.38	55.25	32.69
154	57.1	60.2	7.5	1000	10085.7	0.406	60.49	179.72	324.6	1.81	368.43	58.65	30.70
161	53	51.3	6.6	1000	10085.7	0.402	60.38	179.42	324.6	1.81	324.77	52.15	30.70
168	48.6	46.8	7.25	1000	10085.6	0.399	60.31	179.19	324.5	1.81	357.20	47.70	30.66
173	45.5	43.8	7.6	1000	10085.5	0.397	60.26	179.04	324.4	1.81	374.76	44.65	30.62
182	42	40.5	8.2	1000	10085.5	0.394	60.18	178.81	324.4	1.81	404.86	41.25	30.62

195	38.1	36.8	8.8	1000	10085.1	0.3925	60.14	178.70	324.0	1.81	434.76	37.45	30.45
226	31.5	31.1	9.95	1000	10084.8	0.389	60.05	178.44	323.7	1.81	492.30	31.30	30.33
306	24.2	24.2	1.25	10000	10084.1	0.388	60.03	178.36	323.0	1.81	618.73	24.20	30.04
3906	20.8	20.8	1.5	10000	10082.8	0.388	60.03	178.36	321.7	1.80	742.48	20.80	29.50

APPENDIX B

Graphs for All Resistivity Data Altogether

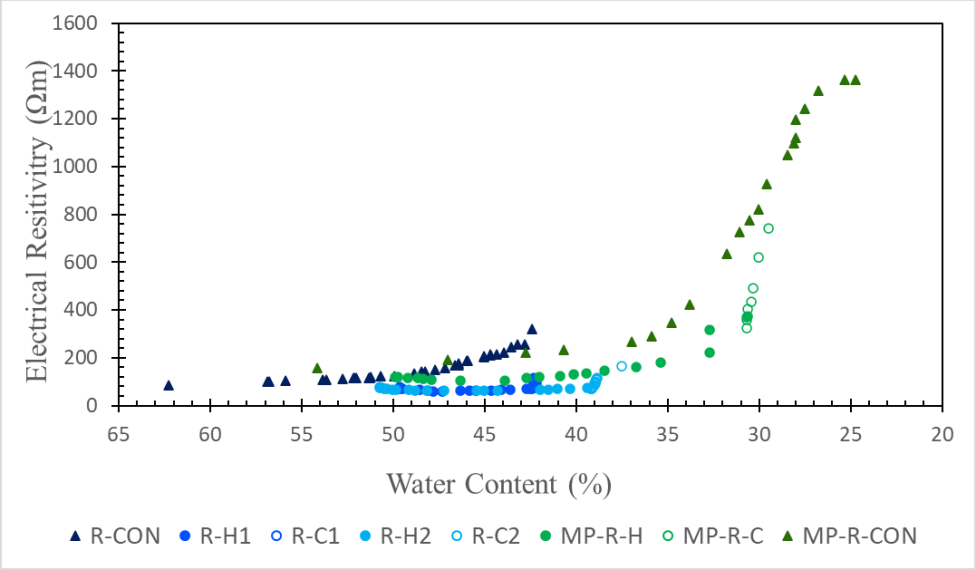

Figure 52: Electrical Resistivity vs. Water Content for All Samples Tested by the Resistance Meter

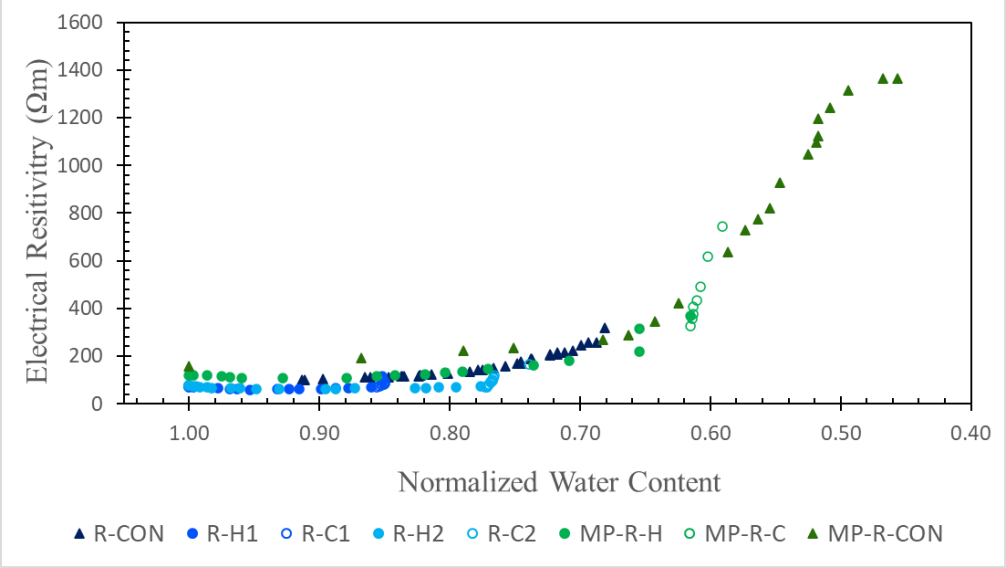

Figure 53: Electrical Resistivity vs. Normalized Water Content for All Samples Tested by the Resistance Meter

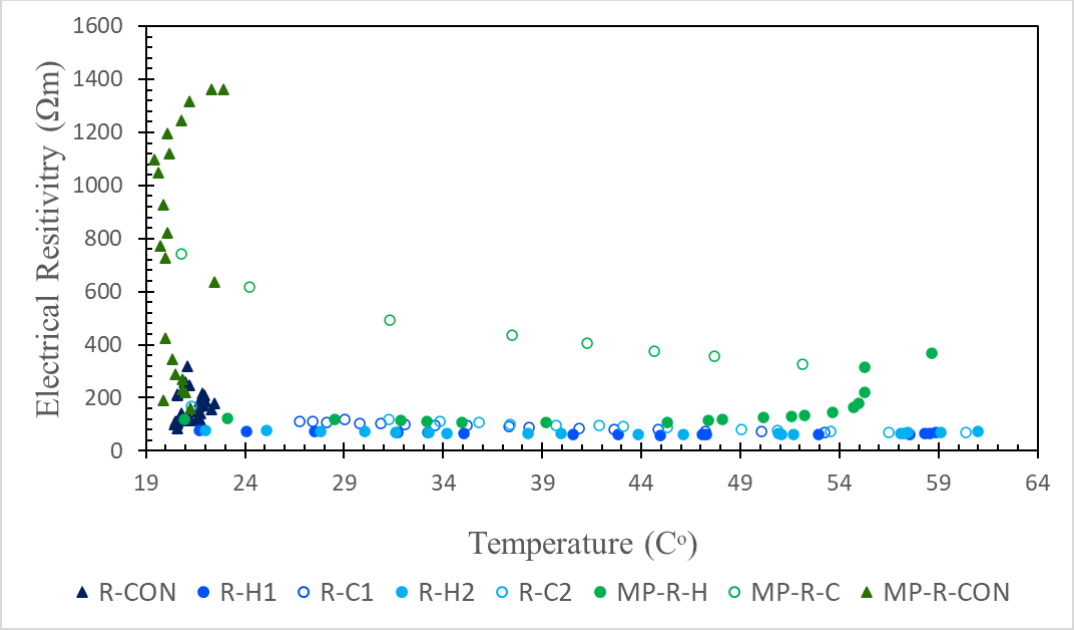

Figure 54: Electrical Resistivity vs. Temperature for All Samples Tested by the Resistance Meter

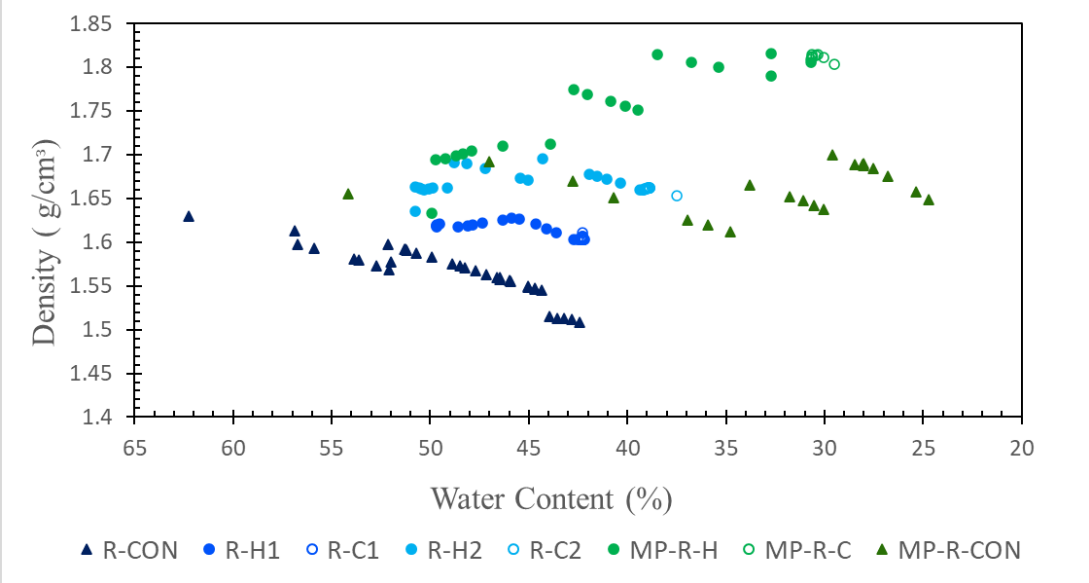

Figure 55: Density vs. Water Content for All Samples Tested by the Resistance Meter

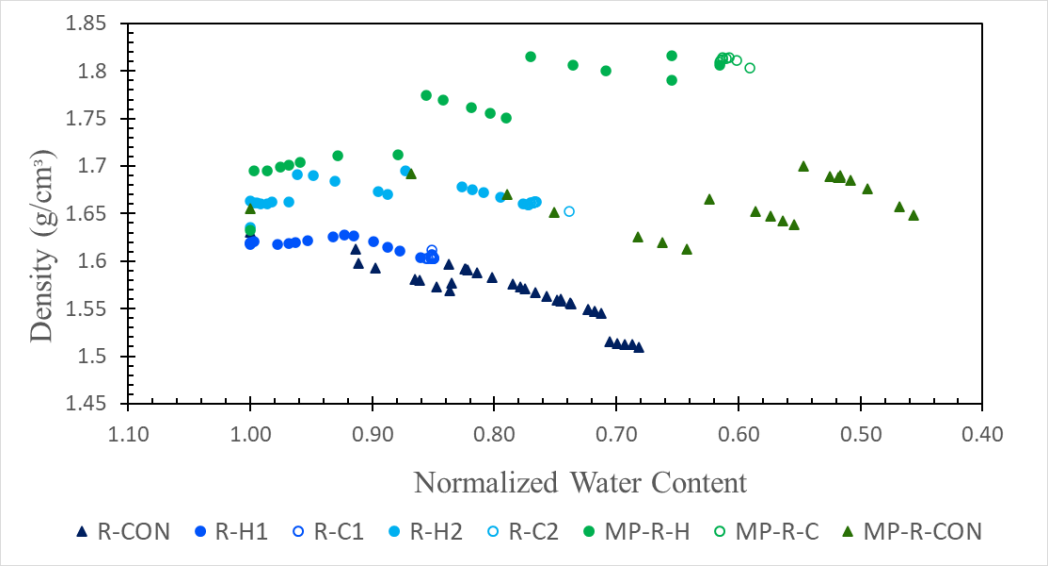

Figure 56: Density vs. Normalized Water Content for All Samples Tested by the Resistance Meter

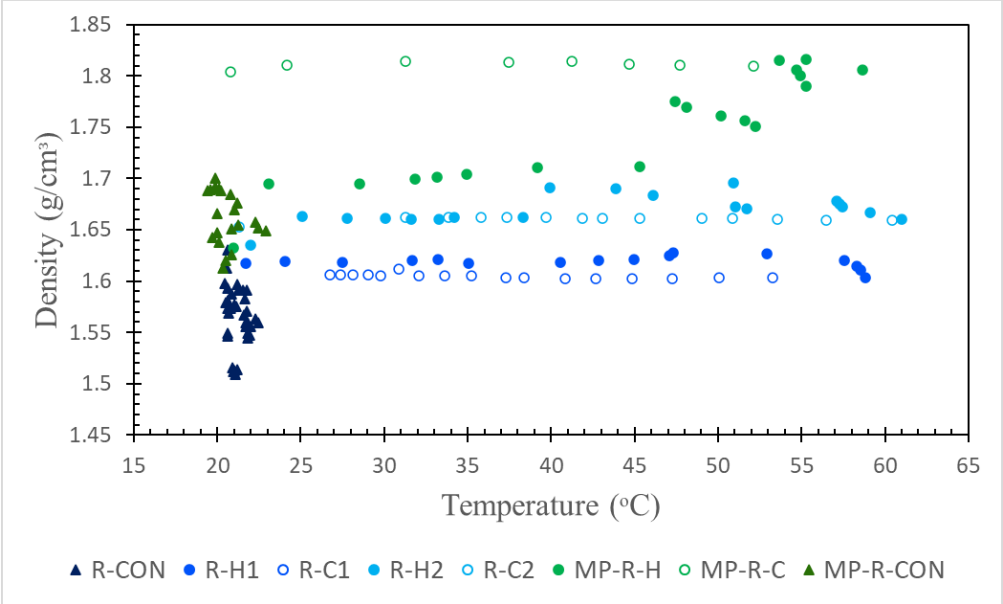

Figure 57: Density vs. Temperature for All Samples Tested by the Resistance Meter

APPENDIX C

Graphs for All Bender Element Data Altogether

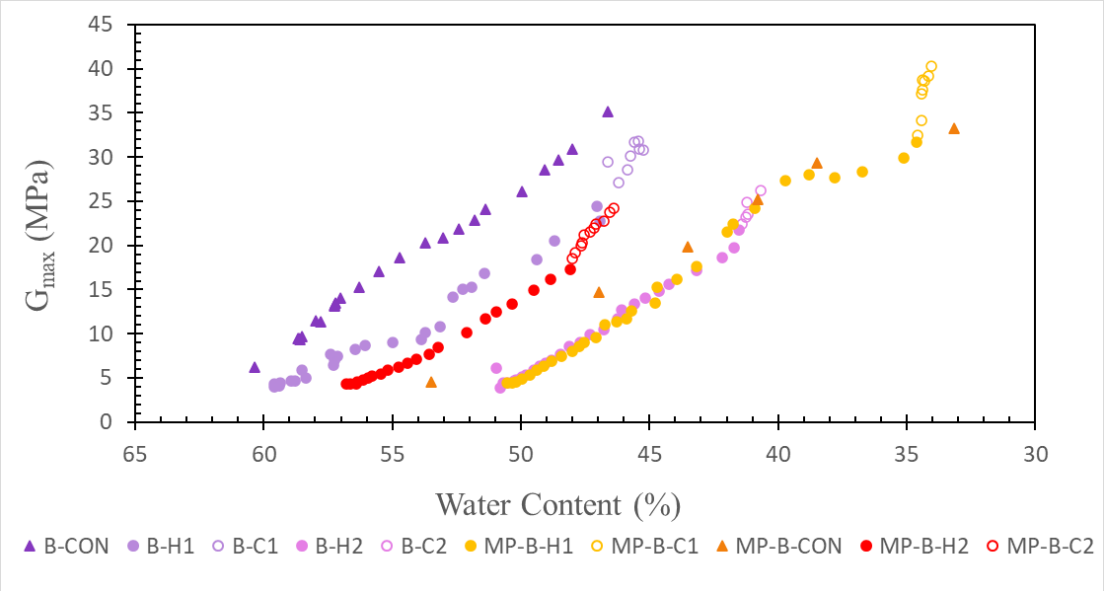

Figure 58: G_{max} vs. Water Content for All Samples Tested by the Bender Element

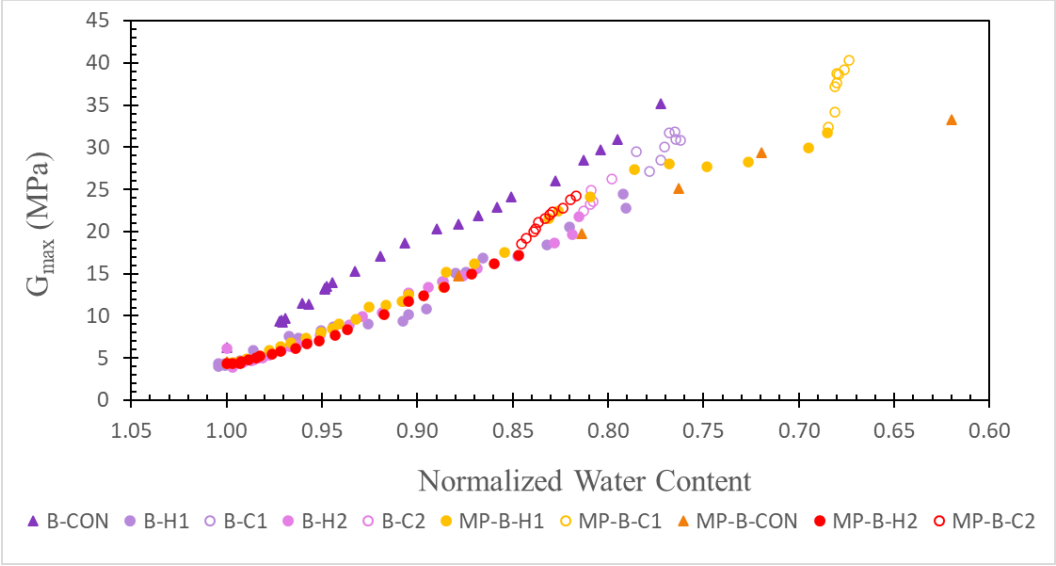

Figure 59: G_{max} vs. Normalized Water Content for All Samples Tested by the Bender Element

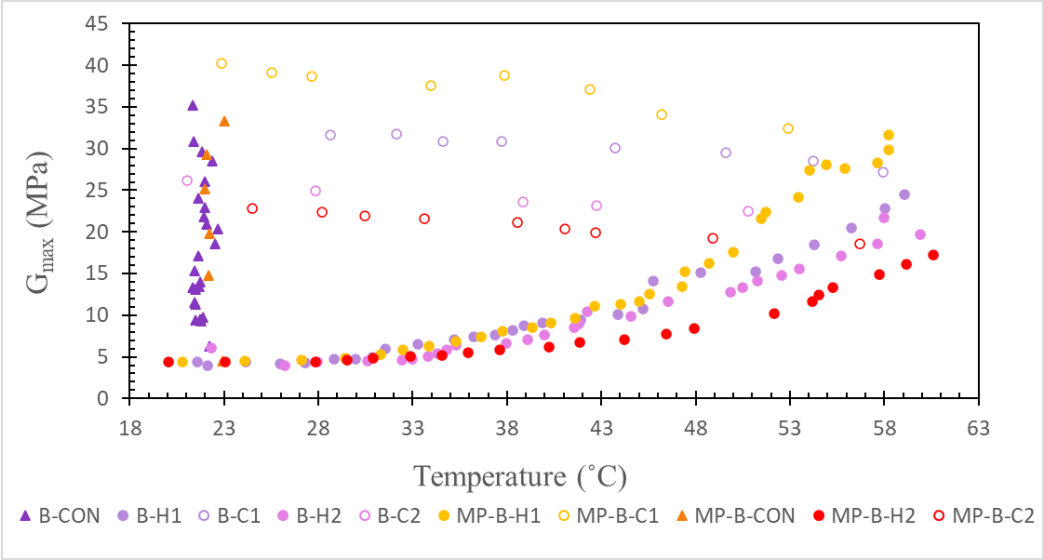

Figure 60: G_{max} vs. Temperature for All Samples Tested by the Bender Element

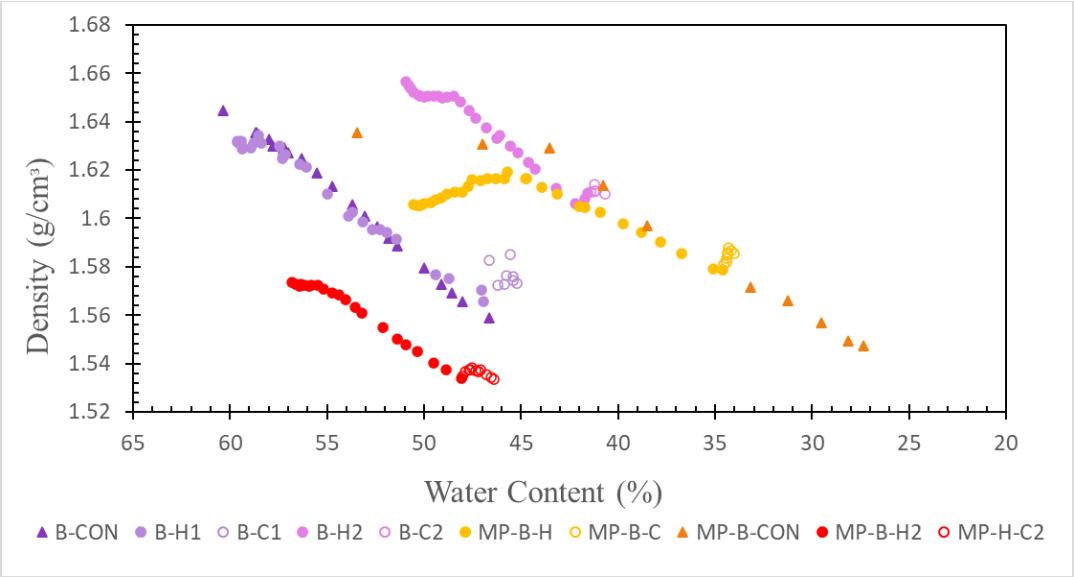

Figure 61: Density vs. Water Content for All Samples Tested by the Bender Element

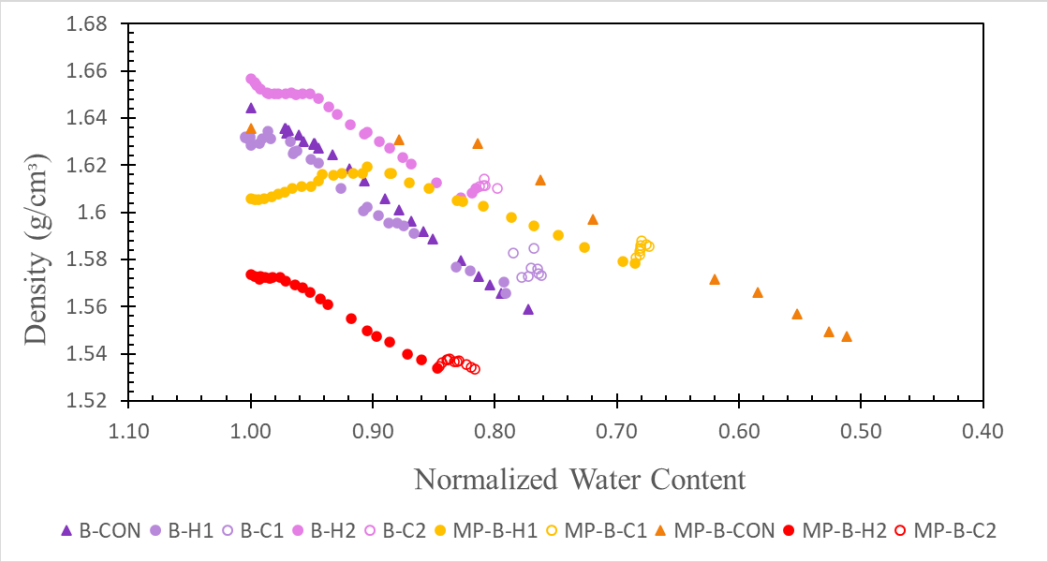

Figure 62: Density vs. Normalized Water Content for All Samples Tested by the Bender Element

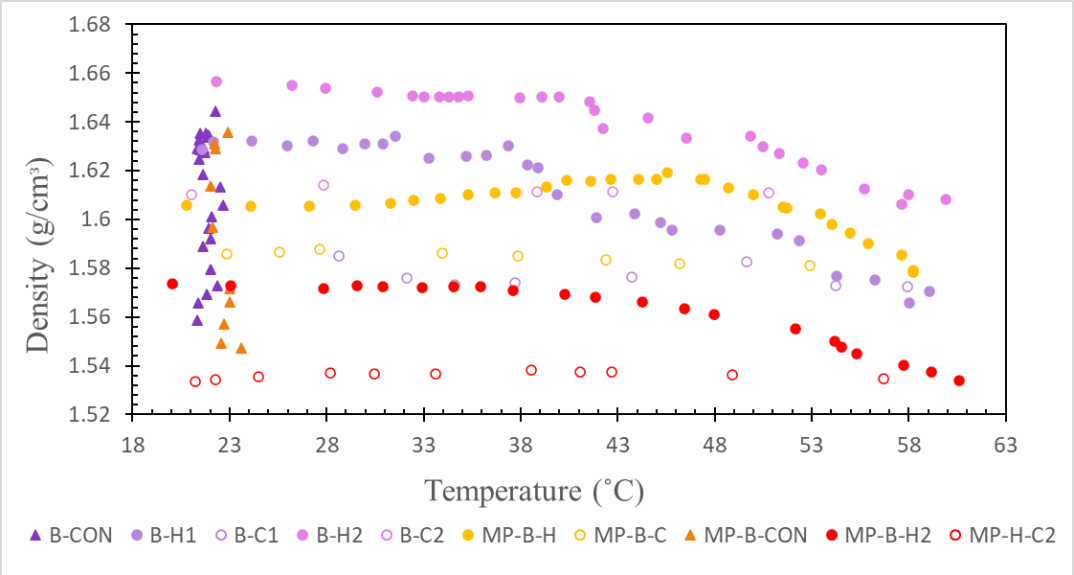

Figure 63: Density vs. Temperature for All Samples Tested by the Bender Element

APPENDIX D

Procedure to Find P-Wave/S-Wave Reading

1. Open CGR201 Program: Computer > OS (C:) > Data > WaVeMe.New > Software > CGR201

    if the shortcut is on the desktop, simply double click the icon

2. Connect to device (window will pop up, click green option and connect)

3. Set Waveform Generator Trigger Mode to Free-Running

4. Set Waveform Generator Output Mode to Continuous

5. Set Trigger Source to Manual

6. Set Trigger Cycles: On=1, Off=100 (large enough so signal does not repeat), Repeat=0

7. Set Trigger Mode to Normal

8. On the Oscilloscope window, slide A and B away from each other for easier readings (optional)

9. Slide the "X" at the top of the graph to the left side

9. On Waveform Generator window, Set Amplitude to 100

10. Slide Frequency Bar until the response is visible; the upper and lower limits on the Frequency slider can be changed for more precise tuning

    use the Channel A and B zoom functions until both signals are visible

    the response signal should look similar to the excitation signal

    click the buttons above and below the frequency bar to set the frequency range

        FOR S-WAVE: Use frequency ranges between 3000 and 10000

        FOR P-WAVE: Use frequency ranges between 10000 and 10000000

optimal frequencies may vary between each test, feel free to experiment with different values

11. Switch Waveform Generator Output Mode to Tone Burst

12. On Oscilloscope Window, go to: View > Digital Average > 256

13. Use zoom in/out functions as necessary until the graph produced is clear enough

14. Switch Waveform Generator Trigger Mode to "Triggered" to stop graph generation

THIS IS IMPORTANT!!! LEAVING WAVEFORM GENERATOR IN FREE RUNNING MODE MAY CAUSE COMPUTER TO FREEZE

WHEN SAVING CSV FILE

15. Right click on Oscilloscope graph, and click "toggle time cursors"

16. Align T1 with the first peak of the Excitation Wave and align T2 with the first peak of the response wave

17. Create a Powerpoint file with the naming convention "YY.MM.DD TESTID"

18. On the title slide, write the test ID, name of operator, and date of testing

19. Format the subsequent slides to have the "Two Content" layout

20. On the title of each slide, identify the Date, Time, stage of testing, p or s wave, and any important information to help identify the reading

21. Capture the two windows (oscilloscope and waveform generator) by clicking on the text box in the powerpoint slide, then clicking Insert > Screenshot > Click the Corresponding Window

22. On Oscilloscope window, go to Tools > Export Waveform (CSV), and save file to appropriate folder

Use naming convention: date_time_name_wavetype "YYMMDD_HHMM_TESTID_[P/S]"

Repeat steps 3 - 22 for both P-wave and S-wave readings.

Note that certain steps such as creation of the powerpoint slide need not be repeated

Turn the signal knob on the WaVeMe device to switch between P-Wave and S-Wave modes

Be sure to turn off or reset the Digital Average when taking another reading